HAROKOPIO UNIVERSITY

SCHOOL OF ENVIRONMENT, GEOGRAPHY AND APPLIED ECONOMICS
DEPARTMENT OF GEOGRAPHY
POSTGRADUATE PROGRAMME: "APPLIED GEOGRAPHY AND SPATIAL PLANNING"
COURSE OF GEO-INGORMATICS

Exploring the vegetation regeneration of a natural ecosystem in Greece after a wildfire using LANDSAT TM and OLI satellite imagery and GIS

Master Thesis

Ioannis Lemesios

Athens, 2022

ΧΑΡΟΚΟΠΕΙΟ ΠΑΝΕΠΙΣΤΗΜΙΟ

ΣΧΟΛΗ ΠΕΡΙΒΑΛΛΟΝΤΟΣ, ΓΕΩΓΡΑΦΙΑΣ ΚΑΙ ΕΦΑΡΜΟΣΜΕΝΩΝ ΟΙΚΟΝΟΜΙΚΩΝ
ΤΜΗΜΑ ΓΕΩΓΡΑΦΙΑΣ
ΠΡΟΓΡΑΜΜΑ ΜΕΤΑΠΤΥΧΙΑΚΩΝ ΣΠΟΥΔΩΝ: "ΕΦΑΡΜΟΣΜΕΝΗ ΓΕΩΓΡΑΦΙΑ ΚΑΙ ΔΙΑΧΕΙΡΙΣΗ ΤΟΥ ΧΩΡΟΥ
ΚΑΤΕΥΘΥΝΣΗ ΓΕΩΠΛΗΡΟΦΟΡΙΚΗ

Διερεύνηση της αναβλάστησης ενός φυσικού οικοσυστήματος στην Ελλάδα μετά από πυρκαγιά με χρήση δορυφορικών δεδομένων LANDSAT TM και OLI καθώς και Σ.Γ.Π.

Μεταπτυχιακή εργασία

Ιωάννης Λεμέσιος

Αθήνα, 2022

HAROKOPIO UNIVERSITY

SCHOOL OF ENVIRONMENT, GEOGRAPHY AND APPLIED ECONOMICS
DEPARTMENT OF GEOGRAPHY
POSTGRADUATE PROGRAMME: "APPLIED GEOGRAPHY AND SPATIAL PLANNING"
COURSE OF GEO-INGORMATICS

Examining Committee

Petropoulos George P. (Supervisor)
Assistant Professor, Department of Geography, Harokopio University

Chalkias Christos (Examiner)
Professor, Vice-Rector of Research, Development and Lifelong Education, Department of Geography, Harokopio University

Katsafados Petros (Examiner)
Assistant Professor, Department of Geography, Harokopio University

Ethics and Copyright Statement

I, Ioannis Lemesios, hereby declare that:

1) I am the owner of the intellectual rights of this original work and to the best of my knowledge, my work does not insult persons, nor does it offend the intellectual rights of third parties.

2) I accept that Library and Information Centre of Harokopio University may, without changing the content of my work, make it available in electronic form through its Digital Library, copy it in any medium and / or any format and hold more than one copy for maintenance and safety purposes.

3) I have obtained, where necessary, permission from the copyright owners to use any third-party copyright material reproduced in the master thesis while the corresponding material is visible in the submitted work.

Acknowledgements

As my course of study at Harokopio University has come to an end, I would like to sincerely thank the supervisor of my thesis, Associate Professor George P. Petropoulos, for his continuous help and constructive review of my thesis, as well as the other members of the examining committee, Professor Christos Chalkias and Associate Professor Petros Katsafados for the apt comments and suggestions on my work. Last but not least, I would like to thank all the lecturers of the post-graduate program for the valuable knowledge they imparted to me in the field of geoinformatics.

I will not fail to thank all my friends and especially my family members for their constant support and patience. Thank you all!

Table of Contents

List of Figures

List of Tables

Abstract

Analysis of satellite data, often combined with Geographical Information Systems (GIS), allows monitoring of changing land cover dynamics which may occur after a natural hazard such as a wildfire. In the present thesis, the vegetation recovery dynamics of a burnt area are investigated by exploiting freely distribute satellite data and GIS techniques. The relationships of regrowth dynamics to the burn severity levels as well as topographical characteristics such as aspect are also explored. As a case study, an area of northeastern Attica, Greece, where a wildfire occurred during August 2009, is used. Vegetation recovery dynamics within the study area were investigated based on chronosequence analysis of the normalized difference vegetation index (NDVI) as well as the Regeneration Index (RI) derived from anniversary Landsat TM and OLI images for the period 2009 (just after fire suppression) until 2020. The spatio-temporal patterns of NDVI on each post-fire image date were statistically compared to the pre-fire pattern to determine the extent to which the pre-fire spatial pattern was re-established. Additionally, using the regeneration index, it was investigated whether the level of vegetation in selected areas of various land uses within the burnt area recovered to the corresponding level of vegetation outside the burnt area. In addition, with the use of NDVI, the relationships between the regeneration dynamics with burn severity level as well as topography were also investigated.

The results revealed that two years after fire, vegetation of the study area shows the first steps of recovery, while eleven years after fire, the analysis showed that the majority of the burnt area (97%) recovered or improved in contrast to pre-fire levels. Regarding the analysis conducting with the use of RI, results presented similar regeneration trends as captured by NDVI regarding areas covered with more adaptable to fire vegetation such as scrubs, herbaceous vegetation, woodlands as well as agricultural, while forested areas although they presented a gradual increase in regrowth process, they didn't reach the NDVI levels of the unburned forested areas. In addition, areas with low to moderate-low burn severity presented high regeneration dynamics and recovered within two to five years after fire event whereas areas with moderate-high and high burn severity the regeneration process took approximately a decade to revert to pre-fire levels. Finally, analysis revealed that north facing aspects have a slightly higher regeneration rate compared to south facing exposures.

In conclusion, this thesis contributes to the understanding of Mediterranean vegetation dynamics, and supports the usefulness particularly of NDVI and RI in post-fire regeneration

assessment studies while the provided methodology could also be transferable to other regions. In addition, it provides further evidence that satellite data when combined with GIS techniques can offer a powerful tool for mapping the vegetation regeneration dynamics after wildfires.

Keywords

Vegetation regeneration; wildfires; burn severity assessment; burnt area delineation; Landsat TM; Landsat OLI; NVDI; Regeneration Index; Greece

1 Introduction

1.1 Background information

The natural role of forest fires in Mediterranean-type ecosystems is directly related to the evolutionary succession of vegetation, making fires an important ecological process, which affects the structure and function of the ecosystem over time (Tedim et al., 2015). Despite this "peculiar" relationship that Mediterranean plant communities have developed with fires, the latter are a direct threat to human life and one of the most important disturbances of natural ecosystems on a global scale (Dupuy et al., 2020). Indeed, due to the increase in their frequency and severity in recent years (Röder et al., 2008), and especially in the Mediterranean basin (Joint Research Centre, 2020), their negative effects, economic, ecological and social, have multiplied (Dupuy et al., 2020). Natural processes such as the intense soil erosion, the degradation of the productivity of forest ecosystems, the alteration of the aesthetics of the landscape, the changes in the microclimate, the changes in the form and composition of the vegetation are set of short-term and long-term effects that essentially characterize the magnitude of the destructiveness of fires (Pérez-Cabello et al., 2006; Pausas et al., 2008; Xanthopoulos et al., 2022).

The main factors of the high frequency of fires in recent decades in the Mediterranean region are considered to be the changes in land uses due to human interventions, as well as the abrupt and sometimes unpredictable climate fluctuations (Caldararo, 2002; Dimitrakopoulos et al., 2011; Pausas & Fernández-Muñoz, 2012; Moreira et al., 2020). As a consequence, despite the adaptability of many species to fire, especially sclerophyll shrub vegetation, there is a risk of inhibiting the natural succession and natural regeneration of Mediterranean forest species, especially in cases of multiple consecutive events (Ferran et al., 2005).

Forest fires handling and management are complex issues as they are influenced by a significant number of environmental, ecological, economic, social and political factors, which interact with each other (Tedim et al., 2018). Therefore, the strengthening of the existing political and strategic fire prevention plans as well as the design of new ones more effective for the protection of ecosystems is considered essential. But primarily, the timely collection and availability of information and reliable statistics related to the extent of the fire-affected areas as well as the immediate effects of the fire and the long-term dynamics of the vegetation in the post-fire environment are required (Lentile et al., 2006; Gitas et al., 2012).

Vegetation regeneration after fire in Mediterranean ecosystems is a complex process and as a result that it is difficult to generalize its post-fire dynamics due to a number of factors that influence it. Indicatively, it is mentioned the increased spatial heterogeneity, the ecotype, the duration and intensity of the fire, the pre-existing vegetation, and the local topographical, climatic and soil conditions (Moreira et al., 2009; Petropoulos et al., 2014; Veraverbeke et al., 2010). For example, in fire-adapted sclerophyll shrub communities their recovery occurs within a few years (Wittenberg et al., 2007), in contrast to pure forest species where several decades are required (Capitanio & Carcaillet, 2008). Also, due to better sunlight and evapotranspiration, south-facing slopes show a higher rate of vegetation regeneration than north-facing slopes (Petropoulos et al., 2014).

At the local level, for small-scale events, it is usually possible to assess the effects of fires in detail through extensive field work. On the contrary, in large-scale fire phenomena, the examination of both immediate and long-term interactions between the post-fire dynamics of vegetation, burn severity, climate and other parameters remains a laborious (in time and cost) process (Gouveia et al., 2010).

Satellite data and remote sensing techniques are now a widespread and reliable tool, commonly used alongside fieldwork, to assess the fire impacts and monitor affected ecosystems over time, at both large and small scales (Ireland & Petropoulos, 2015; Smith-Ramírez et al., 2022). Satellite remote sensing research and applications are now being carried out at all key stages of forest fire management, from mapping forest fuels and fire risk (Chuvieco et al., 2002), to mapping the affected areas' perimeters (Gitas et al., 2008), as well as to monitoring the long-term vegetation succession and regrowth (Röder et al., 2008). Main advantages of the satellite approach are the possibility of obtaining individual images or even time series of data without cost, and the large spatial coverage they offer.

The combination with Earth Observation data and GIS techniques, has provided promising potential for analyzing and extracting spatial information related to wildfires (Chen et al., 2005; Durduran, 2010; Chen et al., 2011; Kalivas et al., 2013). It presents an excellent way for data capture, storage, synthesis and analysis of acquired EO spatial data. Indeed, EO satellite data can be combined with GIS and can provide an efficient approach for analysing and extracting spatial information to support decision making reliably and consistently (Chen et al., 2005; Gens, 2010).

1.2 Aims and Objectives

The aim of this thesis is to assess the post-fire vegetation regeneration in a Mediterranean ecosystem using freely available high resolution satellite data from Landsat missions and Geographical Information Systems, and to examine the relationships between vegetation regrowth dynamics and burn severity as well as the topographical characteristics of the study area. The specific objectives are:

1. Use of high-end supervised classification techniques and tools for the burnt area delineation within the study area.
2. Assess burn severity within the burn scar using the Normalized Burn Ratio (NBR) and the Differenced Normalized Burn Ratio (dNBR).
3. Utilize multi-temporal analysis with the use of the Normalized Difference Vegetation Index (NDVI) as well as the Regeneration Index (RI) based on Landsat TM and OLI imagery for mapping and assessing the post-fire vegetation regrowth dynamics within the burn scar.
4. Assess the relationship of aspect on vegetation regrowth dynamics within the burnt area.

2 Literature review

2.1 The catastrophic effects of forest fires and the need to study the vegetation regeneration process

Fires have always been an integral part of forest ecosystems (Tedim et al., 2015), however, in recent decades they have been one of the most threatening natural disaster with adverse effects on both the environment and the economy, as well as human life (Dupuy et al., 2020). Europe is repeatedly affected by severe forest fires, with Mediterranean countries accounting for the majority of the total burnt area (Joint Research Centre (JRC), 2020). The characteristic climate, the heterogeneity of vegetation and human interventions and activities are the main factors that make the European Mediterranean region particularly vulnerable to forest fires (Keeley et al., 2011; Moreira et al., 2020).

Although recent statistical reports indicate a decrease in the number of fires and burnt areas in Mediterranean area (Turco et al., 2016), the increasing occurrence of unpredictable and extreme weather events, as a result of climate change, is expected to increase both the frequency and intensity of fires (IPCC, 2022). More specifically, climate change is estimated to cause more frequent and intense periods of droughts in the Mediterranean resulting in the increase of fire risk compared to current conditions (Joint Research Centre, 2018). In fact, the areas that will show strong drought phenomena are predicted to expand towards the northernmost regions of Europe which, until now, have not been prone to catastrophic fires (Joint Research Centre, 2018; Venäläinen et al., 2020). It is worth mentioning that recent intense fire events can be considered as indications of the impacts of climate change on forest fires in both Mediterranean and northern Europe. The most characteristic examples include the fires of 2018 in Greece and Portugal but also in unexpected areas above the Arctic Circle, such as Sweden, where incalculable environmental and economic disasters as well as human losses were caused (Varela et al., 2019; Ribeiro et al., 2020). Prolonged drought of the 2007 fire season was also characteristic, in which devastating fires occurred in previously no high-risk, high-altitude areas of the Peloponnese, Greece (Koutsias et al., 2012; EEA, 2017).

With regard to the spatio-temporal behavior of vegetation in the post-fire environment, the knowledge and understanding of its regeneration dynamics becomes necessary for:

• the assessing the short-term and long-term effects of fires and taking the corresponding recovery measures (Gouveia et al., 2010; I. Gitas et al., 2012);

• the understanding of the driving factors of the changes taking place, especially if climate change scenarios are taken into account (Casady et al., 2010);

• the effective management of post-fire ecosystems (Wittenberg et al., 2007);

• drawing up prevention policies and strategies (Petropoulos et al., 2014)

2.2 Use of earth observation in burnt area delineation and burn severity

The spectral behavior of burnt areas varies according to the ecosystem, the severity of the phenomenon and the time duration between the moment of the event and the reception of the spectral information. Immediately after the fire, the ash deposition determines the spectral signal of the burnt surface for a short period of time. Then, the spectral behavior is determined by the removal and the temporal regrowth of the vegetation in the post-fire environment (Chuvieco 1999). In general, the near (NIR) and mid-infrared (SWIR) parts of the electromagnetic spectrum are considered more suitable for distinguishing burnt areas and/or estimating burn severity, especially when considered simultaneously (Koutsias & Karteris, 2000). More specifically, in the near-infrared, a decrease in reflectance is observed after the fire due to the destruction of the leaf structure, while at the same time an increase in reflectance is observed in the mid-infrared (Lentile et al., 2006; Miller & Thode, 2007).

As far as burn severity is concerned, it describes the degree to which an area has been altered or disrupted by the fire and how the functioning of the ecosystem in the burn scar has been affected. The observed effects often vary within the area and between different ecosystems (Keeley, 2009). Burn severity determined by evaluating and classifying the regions with similar visible combustion attributes in the field (Soverel et al., 2010). Mapping of burn severity is a crucial part of the post-fire planning and monitoring, which is generally accomplished using earth observation data (Meng et al., 2017; Cai & Wang, 2022; Tonbul et al., 2022).

The following subsections present the sensors and the main techniques used in literature to determine the burnt area and to estimate the burn severity.

2.2.1 Overview of methods and techniques for burnt area mapping

Optical satellite data have been extensively used to detect and map burnt areas both locally/regionally/nationally (Chuvieco & Congalton, 1988; Duncan et al., 2009) and globally (Barbosa et al., 1999; Roy et al., 2008). Medium and low spatial resolution data (250 m to 1 km resolution) that have been used for these purposes come from sensors and systems such as the National Oceanic and Atmospheric Administration (NOAA)/Advanced Very High Resolution Radiometer (AVHRR) (Pereira, 1999; Fraser et al., 2000; Chuvieco et al., 2005), the Satellite Pour l'Observation de la Terre (SPOT) VEGETATION (VGT) (Stroppiana et al., 2002; Bartalev et al., 2007), the Along Track Scanning Radiometer (ATSR) (Eva & Lambin, 1998) and the Moderate Resolution Imaging Spectroradiometer (MODIS) (T. Loboda et al., 2007; Giglio et al., 2009).

High spatial resolution data, which have been used to delineate and map burnt areas, mainly come from Landsat satellites (resolution 30-80 m) (Koutsias & Karteris, 2000; Kontoes et al., 2009; Petropoulos et al., 2010; Bastarrika et al., 2011; Oliveira et al., 2011; Petropoulos et al., 2011, 2012), Sentinel 2 (Lazzeri et al., 2021; Llorens et al., 2021), Earth Observing-1 (EO-1) and the Advanced Land Imager (ALI) radiometer (30 m resolution) (Petropoulos et al., 2012), PRISMA (Hyperspectral sensor) (Lazzeri et al., 2021), SPOT 4 HRVIR (High-Resolution Visible and InfraRed) (Kontoes et al., 2009). Also, very high-resolution images of the IKONOS satellite (1 m) (Mitri & Gitas, 2013; Dragozi et al., 2014) and the AVIRIS sensor (Airborne Visible and Infrared Imaging Spectrometer), with resolution 2.4 m, have also been analyzed (Kokaly et al., 2007). Finally, in addition to satellite data, UAVs (unmanned aerial vehicles) have also been used to map burnt areas (Lazzeri et al., 2021).

In addition to the abundance of different types of satellite data, a large number of techniques and methods have been developed to detect and map burnt areas, such as the vegetation index differencing (Chuvieco et al., 2002; T. Loboda et al., 2007; Lazzeri et al., 2021; Llorens et al., 2021); the Principal Component Analysis (PCA) (Alexandris et al., 2017); the Spectral Mixture Analysis (SMA) (Quintano et al., 2006) and the Object-based image classification (I. Z. Gitas et al., 2004; Polychronaki & Gitas, 2012). Also, supervised image classification techniques such as the Maximum Likelihood (Petropoulos et al., 2012), the Spectral Angle Mapper (Petropoulos et al., 2010), the Artificial Neural Networks (Al-Rawi et al., 2001; Petropoulos et al., 2010, 2012) and the Support Vector Machines (Cao et al., 2009; Petropoulos et al., 2011, 2012; Dragozi et al., 2014) have also been utilized.

2.2.2 Overview of methods and techniques for burn severity assessment

Regarding burn severity assessment, data from various satellites, mainly Landsat (French et al., 2008; Hall et al., 2008; Whitman et al., 2018; Quintano et al., 2020; Whitman et al., 2020; Chen et al., 2021; Rupasinghe & Chow-Fraser, 2021; Smith-Ramírez et al., 2022) and Sentinel 2 (Quintano et al., 2020; Llorens et al., 2021; Morresi et al., 2022; Tonbul et al., 2022) have been used. Additionally, Deimos-1 satellite (García-Llamas et al., 2019), WorldView-3 (Warner et al., 2017) as well as hyperspectral data from the Earth Observing-1 (EO-1) satellite (Fernandez-Manso et al., 2019) have also been utilized.

There are also a lot of methods and approaches that have used for burn severity estimation such as the multitemporal change detection analysis based on the use of pre-fire and post-fire images (Warner et al., 2017; Zheng et al., 2018; He et al., 2019), image analysis techniques including the Tasseled Cap Transformation (Loboda et al., 2013), the Principal Components Transformation (Brewer et al., 2005) and the Spectral Mixture Analysis (Quintano et al., 2013, 2017). Furthermore, Support Vector Regression (SVR) analysis has also been used for burn severity assessment (Hultquist et al., 2014; Zheng et al., 2018). However, the majority of studies have employed spectral indices for the burn severity assessment such as the Normalized Difference Vegetation Index (Escuin et al., 2008; Fornacca et al., 2018), the Relativized Burn Ratio (Parks et al., 2014), the Normalized Burn Ratio (NBR) (Veraverbeke et al., 2012; Gibson et al., 2020) and the differenced Normalized Burn Ratio (dNBR) (Quintano et al., 2018; Chen et al., 2020; Gibson et al., 2020; Chen et al., 2021; Llorens et al., 2021; Picotte et al., 2021; Giddey et al., 2022; Tonbul et al., 2022) which has been the most commonly used index for the classification of burn severity within multitemporal (pre-fire/post-fire images) approaches. Additionally, based on NBR and dNBR, many authors have developed new spectral indices for the burn severity assessment such as the relative differenced Normalized Burn Ration (RdNBR) (Miller & Thode, 2007; Miller et al., 2009; Morresi et al., 2022) as well as the Relativized Burn Ratio (RBR) (Parks et al., 2014; Simone et al., 2020; Morresi et al., 2022).

2.3 Earth observation in post-fire vegetation regeneration assessment

A wealth of satellite data has been used to monitor vegetation regeneration after fire, and several satellite image analysis methods have been applied. Regarding the methods, the majority of them are based on the use of spectral vegetation indices, with NDVI (Normalized Difference Vegetation Index) being the most used. Other methods, less used, are the Spectral Mixture

Analysis (SMA), the Fractional Vegetation Cover (FVC) and the classification methods. The following table (Table 2-1) presents the bibliographic review of the studies that have been carried out in recent years regarding the post-fire vegetation regrowth. More specifically, Table 2-1 presents the sensor, the resolution of the satellite images utilized, the type of ecosystem and the location as well as the method used to study the vegetation regeneration process and the respective reference.

Table 2-1: Indicative literature on investigating vegetation regeneration after wildfire

Sensor/Resolution	Ecosystem	Method/Index	Reference
Landsat-5 TM (30 m)	Shrubs and Pine Forest Mediterranean - Greece	NDVI and other various vegetation indices (VIs)	Veraverbeke et al., 2012
Landsat-5 TM Landsat-7 ETM+ (30 m)	Shrubs and Pine Forest Mediterranean - Spain	NDVI in combination with fire severity and geographical data	Viana-Soto et al., 2017
Landsat-5 TM (30 m)	Pine and Fir forests Grasses and shrubs Farmlands Suburban housing Mediterranean - Greece	NDVI	Petropoulos et al., 2014
Landsat-5 TM (30 m)	Coniferous forests Montane Cordillera Ecozone-Canada	NDVI RI	Ireland & Petropoulos, 2015
Landsat-5 TM Landsat-8 OLI (30 m)	Mediterranean sclerophyllous vegetation – Chile	NDVI NDWI (Normalized Difference Water Index) Field Data	Smith-Ramírez et al., 2022
Landsat-5 TM Landsat-7 ETM+ Landsat-8 OLI (30 m)	Boreal Forest – China	NDVI	Wang et al., 2022

Landsat-5 TM Landsat-7 ETM+ Landsat-8 OLI (30 m)	Pine plantation forest - Taiwan	Normalized Burn Ratio (NBR) Difference Normalized Burn Ratio (dNBR) Based on NBR new spectral index BRR (Burn Recovery Ratio)	Chompuchan & Lin, 2017
Landsat-5 TM Landsat-7 ETM + (30 m)	Canadian boreal forests	Spectral recovery metrics based on NBR: Relative Recovery Indicator (RRI) Ratio of Eighty Percent (R80P) Year on Year Average (YrYr)	Frazier et al., 2018
Landsat-5 TM Landsat-7 ETM+ Landsat-8 OLI (30 m)	Siberian Larch Forest	NDVI based index called Fractional Vegetation Cover (FVC)	Chu et al., 2017
Landsat-5 TM Landsat-7 ETM+ (30 m)	Scrubs, Pines, Quercus Forest Mediterranean - Spain	Multiple Endmember Spectral Mixture Analysis (MESMA)	Fernandez-Manso et al., 2016
Airborne Visible/Infrared Imaging Spectrometer (AVIRIS) (20 m)	Sclerophyllous California chaparral	Spectral mixture analysis (SMA) NDVI Regeneration Index (RI) Normalized Regeneration Index (NRI)	Riaño et al., 2002
CORONA KH-4B (1,9 m)	Alpine treeline ecotone, Coniferous forest	Supervised classification	Stueve et al., 2009

	Washington State, USA		
QuickBird (2,4 m) EO-1 Hyperion (30 m)	Shrubs and Pine Forest Mediterranean - Greece	Object-based image classification Field data	Mitri & Gitas, 2013

2.4 Topography and vegetation regrowth dynamics

Topography is an important physiographic factor which affects vegetation regeneration. Studies have shown that aspect is a key control on an area's microclimate influencing the fire proneness of an area due to the effect it has on insolation and evapotranspiration rates (Ireland & Petropoulos, 2015). More precisely, south-facing slopes experience higher insolation and evapotranspiration rates than in north-facing slopes. In addition, soil moisture content is remarkably lower on south- than on north-facing slopes in the northern hemisphere, due to the fact that south-facing slopes receiving as much as six times more solar radiation than north-facing slopes (Gong et al., 2008) which is not conducive to vegetation growth. This results in higher vegetation growth or regrowth dynamics in north-facing slopes where moisture conditions are more favourable (Petropoulos et al., 2014, Ireland & Petropoulos, 2015, Louhaichi et al., 2021). Accordingly, south-facing slopes present higher values of burn severity, as a consequence of their exposure in higher values of solar radiation. The increased solar radiation rises the likelihood of ignition due to lower soil moisture content and drier environment leading in higher severity in those south-facing slopes (Ozelkan et al., 2011)

2.5 Summary

In summary, classification techniques are widely used for burn area delineation while Vis are an effective tool in mapping vegetation regeneration as well as burn severity. NDVI is the most widely adopted index for analysing vegetation regeneration it has the advantage of highlighting areas and patterns of regeneration across landscapes that would require substantial investments of time and money to survey directly. The use of RI in vegetation regeneration analysis has been found to be very prominent method in current literature mainly due to its high correlation with crown closure, leaf area index (LAI), and other vegetation parameters, as well as detecting change in canopy cover or vegetation biomass. Additionally, very few works in the literature related to

vegetation regeneration have used the combined study of NDVI and RI indices, a fact that was taken in account in defining the objectives of this work. Knowledge is also limited regarding the effect of topographic features combined with burn severity on vegetation regeneration in burned areas, something that this thesis covers.

3 Experimental set up

3.1 Study area

The region of interest comprises the area of northeastern Attica, located approximately 30 km north-east from Athens, Greece, extending approximately from 23°8' to 24°03' East and from 38° to 38°3' North (Figure 3-1). The area borders the mountain range of Parnitha (highest peak 1,413 m) to the west and mountain range of Penteli (highest peak 1,110 m) to the north, forming a rugged terrain which varies from sea level to approximately 980m. Regarding climatic conditions of the studied area, the average annual temperature ranges from 17.5°C at low altitudes to 12.5°C at high altitudes (about 1000 m). During summer, the average temperature reaches the 27°C at low altitudes and 22-23°C at 1000m height. As far as precipitation is concerned, its average annual value reaches 550-650mm. During summer, precipitation drops at 10-15mm. Concerning vegetation, at lower altitudes, land is covered mainly by schlerophyllous vegetation, sparse vegetation areas and some agricultural land. At higher altitudes, areas are covered mainly by forest of different types (coniferous and/or broadleaf forests) as well as transitional woodland/scrubland areas.

On August, 2009 the study area experienced a severe damage from a wildfire outbreak. The fire started on the night of August, 21st from the area near the coastal settlement of Sesi Grammatikou (northeastern Attica). It quickly grew in size and on the morning of August 22nd, began to threaten the areas of Grammatikos, Varnavas, Marathon, and Lake of Marathon (approximately 40 km from Athens). Highly supported by the strong winds, the fire moved further south and reached the borders of the areas of Agios Stefanos, Anixi, Stamata, Rodopolis and Dionysos during night of August 22nd, while from August 23rd the fire spread to the south side of Penteli mountain and started burning houses in Drafi, Palea Penteli, Anthousa, Pikermi and Pallini.

The EU civil protection mechanism came into force on Saturday night of August 23rd, following the relevant decision of the EU. Italy, France, Cyprus, Austria and Bulgaria offered assistance with aircraft, helicopters, personnel and other technical means and the fire was brought under control on Monday, August 24th. It is considered one of the most devastating wildfires in Attica.

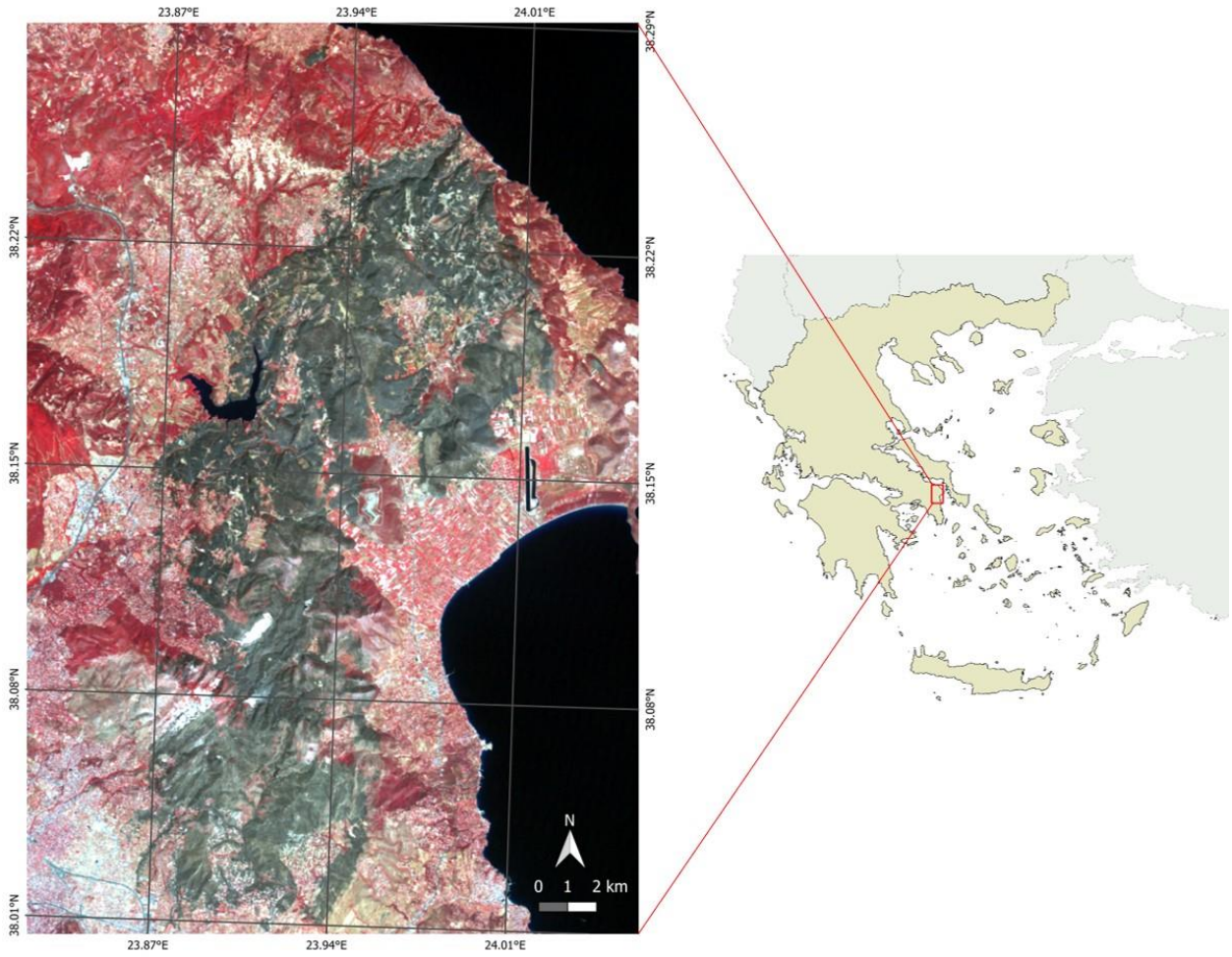

Figure 3-1: Location of study area. The satellite image shows the false color composite of the first post-fire LANDSAT TM used, which was captured few days after the fire suppression (3/9/2009), and illustrates clearly the burn scar (dark grey color).

3.2 Datasets

For the exploration of the vegetation regeneration dynamics of the burn scar in the selected study region over a period of 11 years, six Landsat images were analyzed. More precisely, from 2009 to 2020, three Landsat 5 Thematic Mapper (TM) and three Landsat 8 Operational Land Imager (OLI) images, around the same dates ("anniversary dates"; Lillesand et al., 2015), every three years, were selected to avoid the influence of seasonal dissimilarities in both spectral radiation (e.g., meteorological conditions, distance between Sun & Earth and Sun elevation angle) and surface reflection. Dates of acquisition as well as basic metadata of the images are presented in Table 3-1.

All images were obtained from the U.S. Geological Survey (USGS) with the use of Google Earth Engine (GEE). Due to the lack of images, mainly from earlier years, on the desired "anniversary" date in EarthExplorer (https://earthexplorer.usgs.gov/), GEE was used to access all LANDSAT image collections. For the implementation of the present thesis, the Level 2, Collection 2, Tier 1 datasets from Earth Engine Data Catalog were used for both LANDSAT 5 and 8 images. These

datasets contain atmospherically corrected surface reflectance derived from the data produced by the Landsat 5 TM sensor for the period 1984-2012 and by Landsat 8 OLI sensor for the period 2013 until today. Images from LANDSAT 5 collection, contain 3 visible (B1-B3), 1 near infrared (NIR) (B4) and 2 short-wave infrared (SWIR) (B5, B7) bands processed to orthorectified surface reflectance as well as a thermal infrared (TIR) band (B6) which didn't used in the framework of this study (USGS, 2021). On the other hand, images from LANDSAT 8 collection, contain 4 visible (B1-B4), 1 near infrared (NIR) (B5) and 2 shortwave infrared (SWIR) (B6-B7) bands processed to orthorectified surface reflectance (USGS, 2022). Similarly, thermal infrared (TIR) band (B10) didn't used.

Table 3-1: Basic metadata of the images used for the investigation of vegetation regeneraton within the study area under burn scar

	Dates	Satellite	Path/row	Resolution	Projection
Pre-fire image	18/8/2009	Landsat 5 TM	182/34	30m	WGS 84 / UTM zone 35N EPSG:32635
Post-fire images	3/9/2009				
	24/8/2011				
	23/8/2014	Landsat 8 OLI	183/33		WGS 84 / UTM zone 34N EPSG:32634
	8/8/2017		182/34		WGS 84 / UTM zone 35N EPSG:32635
	23/8/2020		183/33		WGS 84 / UTM zone 34N EPSG:32634

In addition, the Shuttle Radar Topography Mission (SRTM) 1 arc-second (30 meters) elevation data (version 3) was used for obtaining topographical information about the area of interest. The SRTM is a joint project between the National Geospatial-Intelligence Agency (NGA) and the National Aeronautics and Space Administration (NASA). For the calculation of surface elevation, SRTM made use of the radar interferometry technique. In Version 3 SRTM products gaps or voids were filled with elevation data primarily form the Terra Advanced Spaceborne Thermal Emission and Reflection Radiometer (ASTER) Global Digital Elevation Model Version 2.0 (GDEM2) and

secondarily from the USGS GMTED2010 elevation model or the USGS National Elevation Dataset (NED) (SRTM, 2015). The dataset was downloaded from EarthExplorer (https://earthexplorer.usgs.gov/) in geotiff format, in geographic lat/lon projection and WGS84 horizontal and EGM96 vertical datum. To cover the study area, two tiles were downloaded namely N38, E023 and N38, E024.

Finally, the CORINE Land Cover (CLC) inventory of 2006 was used to identify the types of land cover in the study area before the fire occurrence. CORINE Land Cover dataset was downloaded from the Copernicus Land Monitoring Service (CLMS - https://land.copernicus.eu/pan-european/corine-land-cover) in geotiff format.

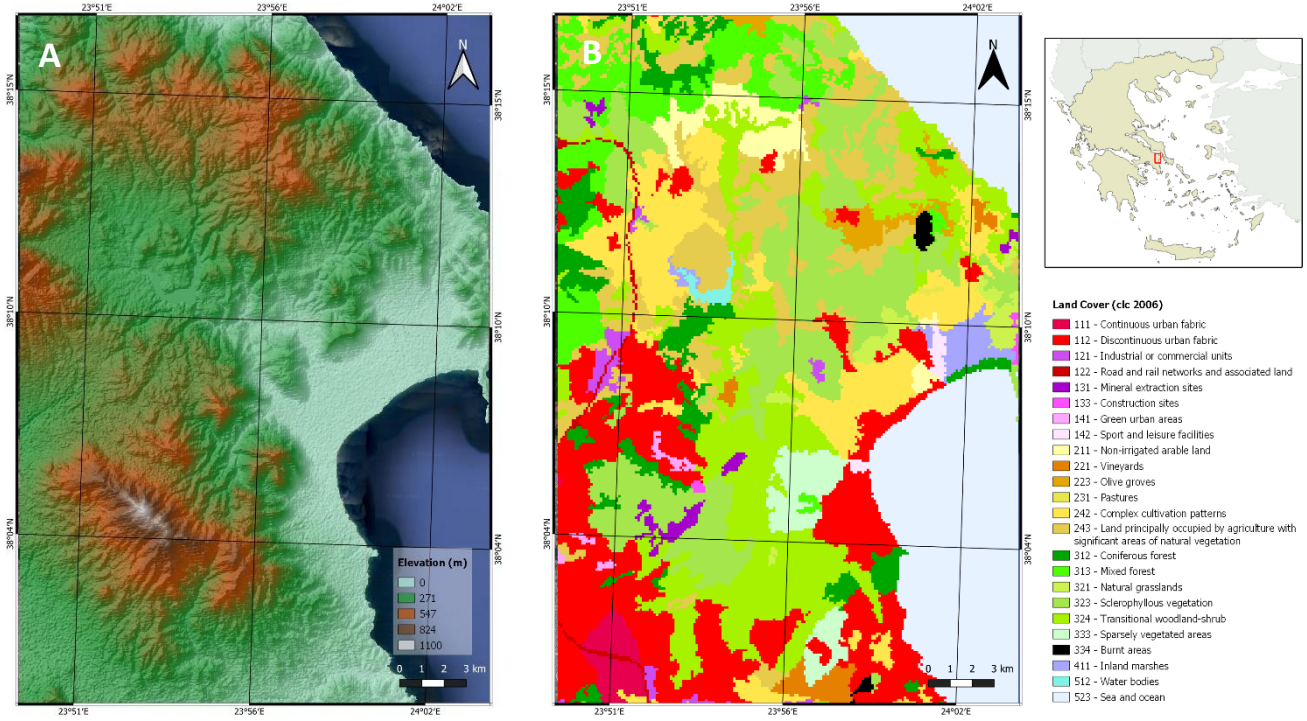

Figure 3-2: Digital Elevation Model – DEM (A) and Corine Land Cover 2006 map (B) of the study area

4 Methodology

All vegetation regrowth spatial analysis of the studied area under burn scar was carried out using ENVI (v. 5.3, L3HARRIS GEOSPATIAL), QGIS (v. 3.16.14) and Google Earth Engine (GEE), while statistical analysis was carried out with the use of Excel (v. 2019, Microsoft) as well as Matlab (R2019a, MathWorks). An overview of the methodology implemented herein to satisfy the study objectives is illustrated in Figure 4-1.

4.1 Image pre-processing

All pre-processing of satellite images used was carried out in GEE as well as in ENVI. As stated earlier all images were downloaded using the GEE. During this, all pre-processing was also applied to images using the appropriate commands. Firstly, a polygon of the broader study area was constructed and used for masking the area of interest from the entire Landsat image. For the latter the command clip (ee.Image.clip) was used. After that, the selection of preferable Bands was carried out. Using the "select" command (ee.Image.select) the blue, green, red and near infrared bands was selected in both Landsat 5 TM and 8 OLI images. In addition, the scaling factor was applied to all the selected bands. Landsat Collection 2 surface reflectance has a scale factor of 0.0000275 and an additional offset of -0.2 per pixel. To apply that, all bands was multiplied with the 0.0000275 (ee.Image.multiply) and the -0.2 was added to them (ee.Image.add) to take the real value of surface reflectance. Finally, images were downloaded in geotiff format with all preferred spectral bands stacked in a single image using the command Export.image.toDrive.

The above clearly shows the advantage of using GEE over EarthExplorer. In addition to the lack of the full archive of images, as mentioned above, EarthExplorer neither give the option to mask the study area nor to layer stack in a single image all spectral bands. As a result, the entire available image is downloaded from each acquisition date and each band separately leading to downloading large image files as well as extra time for clipping the study area and layer stacking.

No atmospheric or topographic correction was carried out as LANDSAT images were already atmospherically and terrain corrected.

The next pre-processing of images was the co-registration since all images did not have the same projection (Table 3-1). In order to analyze images from different dates, there must be spatially

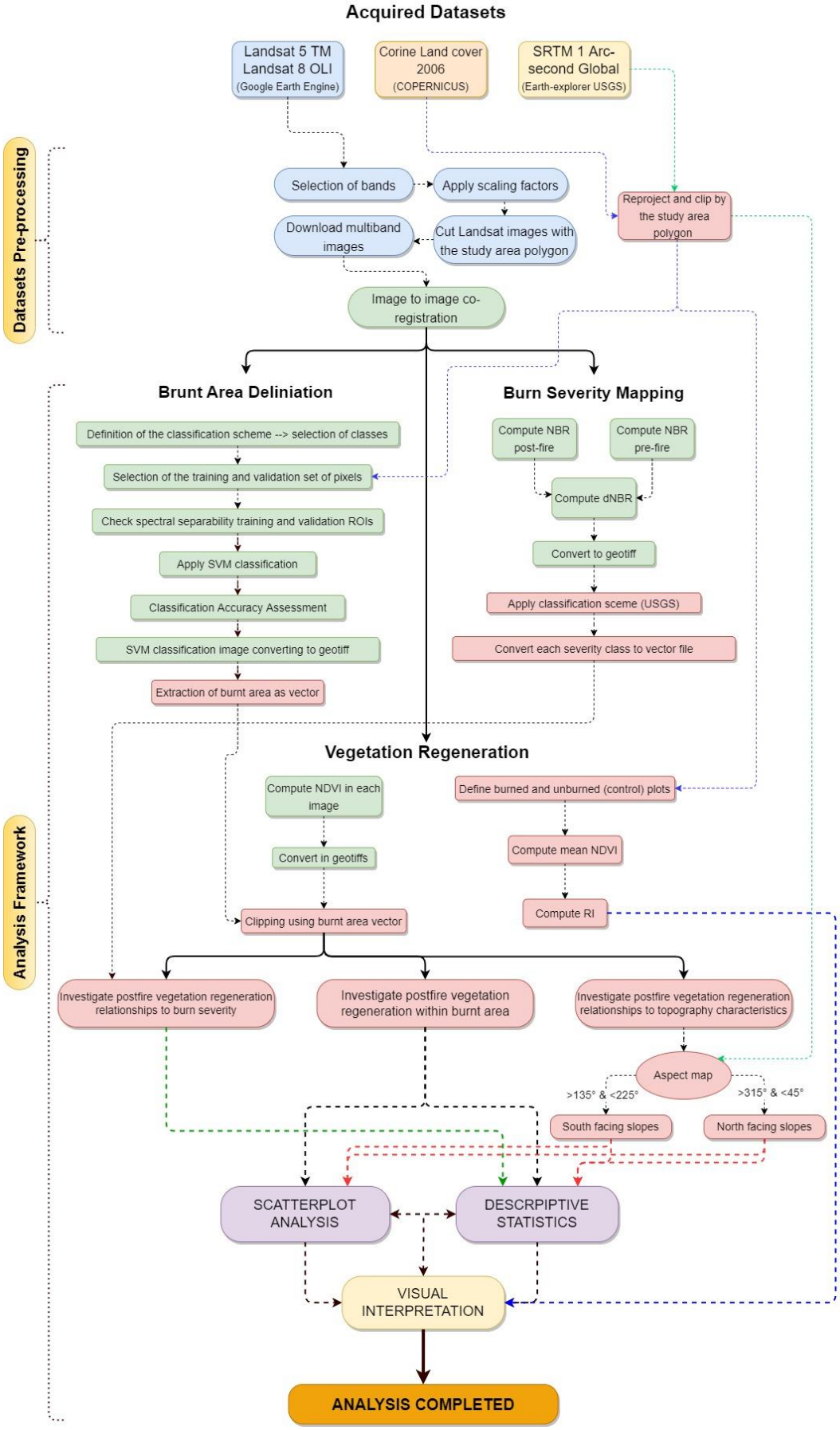

Figure 4-1:Overall methodological framework which was implemented for the assessment of vegetation regeneration dynamics within the study area. Processes filled with green color implemented in ENVI, with red implemented in GIS software, with blue in GEE and with purple in Excel and Matlab

co-registered so that satellite data are in the same spatial reference frame (Schmidt & Glaesser, 1998). The TM pre-fire image was used as a base image to which images of 2014 and 2020 were co-registered. Almost 12 commonly identified ground control points (GCPs) were selected randomly from easily detectable corner points (e.g. road junctions). Image warping was performed using ENVI by applying the nearest neighbor resampling method, allowing a co-registration of the two images into a common UTM 35N projection under a WGS84 ellipsoid (EPSG: 32635). The nearest neighbor resampling method was used to better preserve the reflectance values of the original images to the new registered images (Petropoulos et al., 2014).

Co-registration was also implemented for Digital Elevation Model (DEM) as well as Corine Land Cover (CLC) rasters used. More specifically, with the use of QGIS, both rasters were reprojected into the common coordinate reference system i.e. WGS 84 / UTM zone 35N. In addition, DEM and CLC were clipped by the study area's polygon.

4.2 Burnt area delineation

For the burnt area delineation, the Support Vector Machine (SVM) supervised classification was applied using ENVI image processing environment. SVM was implemented at the original sensor spatial resolution (i.e. 30m) using the image just after the fire occurrence (September 9, 2009). The first step was the definition of the classification scheme, namely the selection of a number of classes to be used for SVM implementation. To this end, five classes were selected, namely: burnt area, agricultural areas, forested areas, urban areas and water bodies. Apart from burnt area, the remaining classes were defined using the CLC 2006 classes of the study area. Table 4-1 shows the classes of CLC 2006 included in each of the five classes of SVM classification.

The next step involved the selection of the training and validation sets of pixels (ROIs) from the image just after the fire occurrence for the SVM performance and validation of the produced thematic map, respectively. Usually, it is proposed that a minimum of 10-30p pixels per class can be used for training the algorithm, where p is the number of image bands used (Piper, 1992; Mather & Koch, 2011; Van Niel et al., 2005; Petropoulos et al., 2011). Additionally, previous studies have also shown that SVM is able to provide very satisfactory classification results when small training sets are used (Pal & Mather, 2006). In this study, approximately 900 representative training pixels for each class were selected from the Landsat TM imagery based on a random distribution. An extra set of approximately 300 pixels (about 1/3 of the training pixels), was also selected to be used in the accuracy assessment of the produced classification map. Selection of

the most spectrally pure pixels for each class was mainly based on both visual observation of the satellite image and the land cover raster (CLC2006) of the studied area. As a further test of the

Table 4-1: Sub-classes of CLC2006 included in main five classes of SVM classification

Classes of SVM Classification	Sub-Categories of Land Cover (CLC 2006)
Agricultural areas	Non-irrigated arable land Vineyards Olive groves Pastures Complex cultivation patterns Land principally occupied by agriculture, with significant areas of natural vegetation
Forested areas	Broad-leaved forest Coniferous forest Mixed forest Natural grasslands Sclerophyllous vegetation Transitional woodland-shrub Sparsely vegetated areas Burnt areas
Urban areas	Continuous urban fabric Discontinuous urban fabric Industrial or commercial units Road and rail networks and associated land Airports Mineral extraction sites Construction sites Green urban areas Sport and leisure facilities
Water bodies	Inland marshes Salt marshes Water bodies Sea and ocean
Burnt area	*The spatial distribution of this class was based on visual observation of the image*

appropriateness of the training and validation ROIs for each class, the Jeffries – Matusita and the Transformed Divergence statistical measures were also used in ENVI to measure their spectral separability. In both measurements, their values range from 0 to 2 and indicate how well the selected ROIs are statistically separate. Values higher than 1.9 indicate that ROI pairs have sufficient separability. Separability values lower than 1.9 indicate the need of improvement by editing ROIs or by selecting of new ones. If separability values for ROI pairs is less than 1, then these ROIs are might belong in the same class and have to unified (ENVI, 2009). Separability values of the selected ROIs of all classes used for the training and validation of the SVM classification implemented in the study area, are shown in Table 4-2 and Table 4-3 respectively. From these results, it becomes clear the sufficient separability of the burnt area as well as water bodies among all the other classes. Also, forested areas have high separability among burnt areas, water bodies as well as urban areas, however, it is lower between agricultural areas. Finally, the lowest separability was observed in the separation between the urban and the agricultural classes. Despite this low separability, no attempt was made to improve the ROIs of these two classes, as the purpose of the SVM classification was to determine the burnt area and not to implement an accurate classification of all land uses of the study area. The separability of the selected ROIs, is also provided in Figure 4-2 which depicts the average spectral signatures of the selected training sites for all the classes used in the SVM classifier implementation.

Table 4-2: Spectral separability between training ROIs with the use of Jeffries – Matusita (left) and Transformed Divergence (right) separability measures

	Burnt area	Water bodies		Forested areas		Agricultural areas		Urban areas	
Burnt area		1.99	2	1.99	2	1.99	2	1.99	2
Water bodies				1.99	2	1.99	2	1.99	2
Forested areas						1.7	1.99	1.96	1.99
Agricultural areas								1.51	1.79

Table 4-3: Spectral separability between validation ROIs with the use of Jeffries – Matusita (left) and Transformed Divergence (right) separability measures

	Burnt area	Water bodies		Forested areas		Agricultural areas		Urban areas	
Burnt area		1.99	2	1.99	2	1.99	2	1.99	1.99
Water bodies				1.99	2	2	2	1.99	2
Forested areas						1.95	1.99	1.93	1.99
Agricultural areas								1.72	1.89

As far as SVM configuration is concerned, the kernel type of Radial Basis Function (RBF) was used. The parameters which were set were the penalty, the pyramid levels, the classification probability threshold as well as the Gamma in kernel function (γ). To force all pixels in the training data to converge to a class, the penalty parameter was set to its maximum values, i.e., 100. In addition, the pyramid levels as well as the classification probability threshold were set to zero causing the satellite image to be processed at full spatial resolution as well as restricting all image pixels to get exactly one class label so as no pixels remain unclassified, respectively. Finally, the γ parameter is a value equal to the inverse of the number of the spectral bands used in the classification. Consequently, in this case, the γ parameter was set to 0.167 because all spectral bands (six in total) were used for the implementation of SVM classification.

The produced image from SVM supervised classification process was converted to geotiff and the burnt area was extracted as vector file, with the use of QGIS software, to be used further in the detection of the vegetation recovery rate of the fire-affected area.

4.2.1 Accuracy assessment

Accuracy assessment of the thematic classification map was carried out constructing the error matrix. With this process, the overall accuracy (OA), the user's (UA) and producer's (PA)

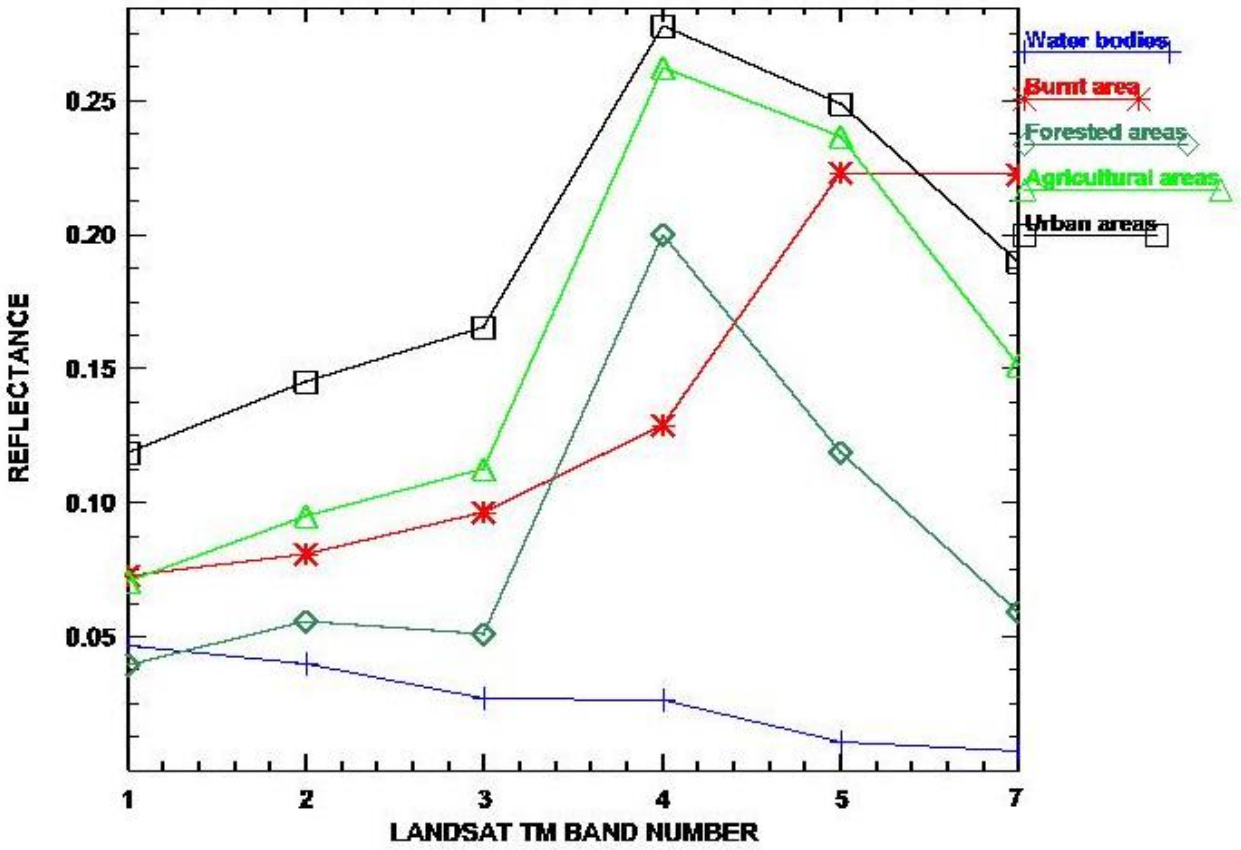

Figure 4-2: Average spectral signatures of the selected training sites for all the classes used in the SVM classifier implementation with post-fire Landsat TM imagery just after fire suppression (September 2009)

accuracies as well as the Kappa (K) statistic were estimated (Congalton & Green, 2019). Overall accuracy computed by dividing the total number of correctly classified pixels by the total number of reference pixels. Expressed as percentage (%), OA is a measure of the overall classification accuracy as it shows the probability that a pixel is classified correctly. PA is resulting from dividing the number of correctly classified pixels in each category by the total reference pixels of the category. PA expresses what percentage of a category on the ground is correctly classified in the right category as well as measures the pixels omitted from its reference class (omission error). In addition, UA is computed by dividing the number of correctly classified pixels in each category by the total number of pixels that were classified in that category. It represents the probability that a pixel classified into a given class actually represents that category on the ground as well as the percentage of pixels that have committed to other ground truth classes (commission error). As far as K coefficient is concerned, it measures the actual agreement between the reference data and the classified versus the chance of agreement between the reference data and a random classifier. The mathematical formulas for all the previous parameters are presented below (Liu et al., 2007; Congalton & Green, 2019):

$$OA = \frac{1}{N}\sum_{i=1}^{r} n_{ii} \quad (1)$$

$$PA = \frac{n_{ii}}{n_{icol}} \quad (2)$$

$$UA = \frac{n_{ii}}{n_{irow}} \quad (3)$$

$$K_c = N\sum_{i=1}^{r} n_{ii} - \sum_{i=1}^{r} \frac{n_{icol} n_{irow}}{N^2} - \sum_{i=1}^{r} n_{icol}\, n_{irow} \quad (4)$$

where n_{ii} is the number of pixels correctly classified in a category; N is the total number of pixels in the confusion matrix; r is the number of rows; and n_{icol} and n_{irow} are the column (reference data) and row (predicted classes) total, respectively.

4.3 Burn Severity Mapping

Burnt severity was mapped using the Normalized Burn Ratio (NBR) index which was defined to highlight not only the burnt areas but also to index the severity of the fire. For the computation of NBR, its formula combines both near infrared (NIR) and shortwave infrared (SWIR) wavelengths. Healthy vegetation shows high reflectance in the NIR and low reflectance in the SWIR portion of the EM spectrum while the opposite is seen in burnt areas. To benefit from this difference in reflectances, NBR uses the ratio between NIR and SWIR bands according the formula below:

$$NBR = \frac{NIR - SWIR}{NIR + SWIR} \quad (5)$$

High NBR values indicate healthy vegetation while low values indicate bare ground and recently burnt areas. Non-burnt areas are normally attributed to values close to zero. For the study area, the calculation of NBR was implemented using the Band 4 (NIR) and Band 7 (SWIR) of the Landsat TM images.

For the burn severity assessment, the differenced NBR scaled index (dNBR) was estimated which is, in general, the difference between the pre-fire and post-fire NBR obtained from the respective images. The mathematical expression is provided below:

$$dNBR = NBR_{post} - NBR_{pre} \quad (6)$$

High values of dNBR indicate more severe damage, while areas with negative dNBR value indicate vegetation regeneration following a fire devastation. Severity classification, from low to high, based on dNBR is shown in Table 4-4. This classification scheme has been proposed by the United States Geological Survey (USGS) (UN-SPYDER Knowledge Portal, 2022).

Table 4-4: USGS classification of burn severity based on dNBR ranges

Severity level	dNBR range
High post-fire regrowth	< -0.251
Low post-fire regrowth	-0.250 to -0.101
Unburnt	-0.1 to 0.99
Low Severity	0.1 to 0.269
Moderate-low Severity	0.270 to 0.439
Moderate-high Severity	0.44 to 0.659
High Severity	< 0.66

Both pre-fire and post-fire NBR as well as dNBR were calculated in ENVI using the Band Math tool. dNBR image was converted to geotiff for further processing in GIS environment. In GIS, dNBR classes from low to high severity were separated and converted as vector layers while the remaining classes were excluded for further analysis.

4.4 Vegetation re-growth assessment

Vegetation regeneration of the study area after the fire was evaluated through multi-temporal analysis of the Normalized Difference Vegetation Index (NDVI) as well as the Regeneration Index (RI). The methodology followed for the calculation of the two indexes is presented as follows.

4.4.1 Normalized Difference Vegetation Index

As mention earlier, NDVI is an index commonly used in the assessment of post-fire vegetation regeneration dynamics (ref to – section 2.3). It is calculated as a ratio between the red (R) and near infrared (NIR) bands. NDVI is calculated using the formula originally proposed by Rouse et al. (1973):

$$NDVI = \frac{\rho_{NIR} - \rho_R}{\rho_{NIR} + \rho_R} \quad (7)$$

where ρ_{NIR} and ρ_R referred to near-infrared and red surface reflectance respectively.

The rationale behind the NDVI formulation lies in the fact that healthy vegetation absorbs more red and blue bands while reflects strongly the NIR and green bands of the EM spectrum. The result of this formula generates a value that in theory is ranged between -1 and +1. Values approaching +1, which means that the reflectance of NIR is much higher than red, register the healthy vegetation with strong photosynthetic activity. As a result, NDVI is an expression closed related to the amount of photosynthetically active vegetation exposed to the sensor within each pixel. However, NDVI values for vegetated areas are in general well above 0.1 (Jensen, 2000; Petropoulos & Kalaitzidis, 2011). More precisely, NDVI values between 0.2-0.6 reflect the semi-arid vegetation and healthy green grass while values between 0.6-0.9 reflect the forested areas (coniferous, deciduous forest) (Jensen, 2016).

For the case of Landsat TM images of the study area, NDVI was calculated in ENVI using Band 3 (red) and Band 4 (near-infrared) while for Landsat OLI images NDVI was estimated using Band 4 (red) and Band 5 (near-infrared) surface reflectances. The Band Math tool was utilized for the computation of NDVI. All NDVI images were converted to geotiff format and then clipped using the burnt area vector layer derived from the SVM classification in the GIS environment.

The dynamics of the regrowth process were subsequently analyzed by comparing post-fire NDVI spatial patterns to the pre-fire pattern within the burnt area. With this procedure, it was determined the extent to which the pre-fire pattern was re-established as well as the rate of this recovery. In addition, descriptive statistics of NDVI within the studied region were calculated from each TM image, which together with scatter plots and non-parametric correlation analysis were used to assess the NDVI variability under the burn scar (Petropoulos et al., 2014).

In the next step, relationships between vegetation regrowth dynamics and aspect as well as burn severity level were explored. In the first case, it was investigated the variation in vegetation recovery dynamics between the north and south facing slopes. To that end, the aspect layer was derived from the SRTM DEM in QGIS and the north and south facing slopes were separated in two difference vector layers. As north facing slopes were classified the pixels with an orientation between NW (315°) and NE (45°) whereas south facing slopes were classified those that had an orientation SE (135°) and SW (225°) (Petropoulos et al., 2014). Pixels non falling within this

orientation were excluded from this analysis. Regarding burn severity and regrowth relationship, it was explored the different regeneration patterns in each burn severity class. For this purpose, separated severity classes were used as masked layer for clipping the initial NDVI layers. Finally, it was also investigated how aspect may differentiate regrowth rate within each burn severity class. To this end, the layers of north and south facing slopes as well as those of burn severity classes and NDVI layers were combined into the GIS environment.

4.4.2 Regeneration Index

Further analysis of the vegetation regrowth dynamics was carried out by investigating the ratio referred as the Regeneration Index (RI) (Riaño, Chuvieco, Salas, et al., 2002; Riaño, Chuvieco, Ustin, et al., 2002), where, in general, NDVI values of specific areas within burn scar are compared with respective ones outside burnt area (control areas). To this end, with pre-fire image as well as the CLC 2006 layer used as based map, there were selected vegetated areas, and more precisely, forested, scrub and agricultural areas inside and outside burn scar. It is noted that areas, inside and outside the burnt area, were selected with the same vegetation type. For example, since only coniferous forests existed inside the burn scar, it was also selected coniferous areas outside despite the fact that there were also broadleaf forests. Next, mean NDVI was computed for common land use areas, inside and outside burnt area, in all satellite images and RI was estimated using the following formula:

$$RI_i = \frac{NDVI_{fire(i)}}{NDVI_{control(i)}} \quad (8)$$

where *i* is the different type of land cover, in this case, forest, scrubs and agriculture and $NDVI_{fire}$ as well as $NDVI_{control}$ are the mean NDVI of the selected areas inside and outside burn scar of the common land cover respectively.

5 Results

5.1 Burnt area delineation and accuracy assessment

Classification map derived from the implementation of the Support Vector Machine supervised classification methodology is illustrated in Figure 5-1. Table 5-1 summarizes the various statistical parameters computed for the assessment of the classification map accuracy based on the error matrix. According to the accuracy results, the OA reaches approximately 93% while K_c approaches 0,91. Regarding burnt area delineation, which was the initial scope of the SVM implementation, the accuracy results show PA and UA of the burnt area class reach approximately 100% and 94% respectively. However, from the visual inspection of the derived thematic map, there are some areas that have false classified as burnt. This is evident mainly along the coastline as well as on roads west of the burnt area. These false classified areas are perhaps related to artefacts produced from the SVM implementation and excluded from the analysis of the regrowth regeneration. Regarding the total area of the burn scar, it was estimated about 147 km^2.

Regarding the type of land cover burnt, Figure 5-2 illustrates the pre-fire land cover map of the burnt area, while Table 5-2 presents for each type of land cover the area in km^2 which is burnt. It is recalled that the land cover information under the burn scar, was derived from the CORINE Land Cover (CLC) inventory of 2006. The results show that the largest burnt area was covered with transitional woodland-shrub (36%) as well as sclerophyllous vegetation (33%) which is the typical vegetation of Mediterranean landscapes. In addition, the cover type of land principally occupied by agriculture, with significant areas of natural vegetation was the third in the ranking of the highest burnt land types (about 14%) in the area of interest. Also, forested areas with coniferous and mixed forests were about 4.5%. Of special interest are the results about the burnt artificial surfaces and more precisely the discontinuous urban fabric which, although small in extent (4%), are shown the destructive impacts of fire on residential areas. In total, forest and semi natural areas cover about 115km^2 (78%), agricultural areas cover 25km^2 (17%) and artificial surfaces cover approximately 6 km^2 (4%).

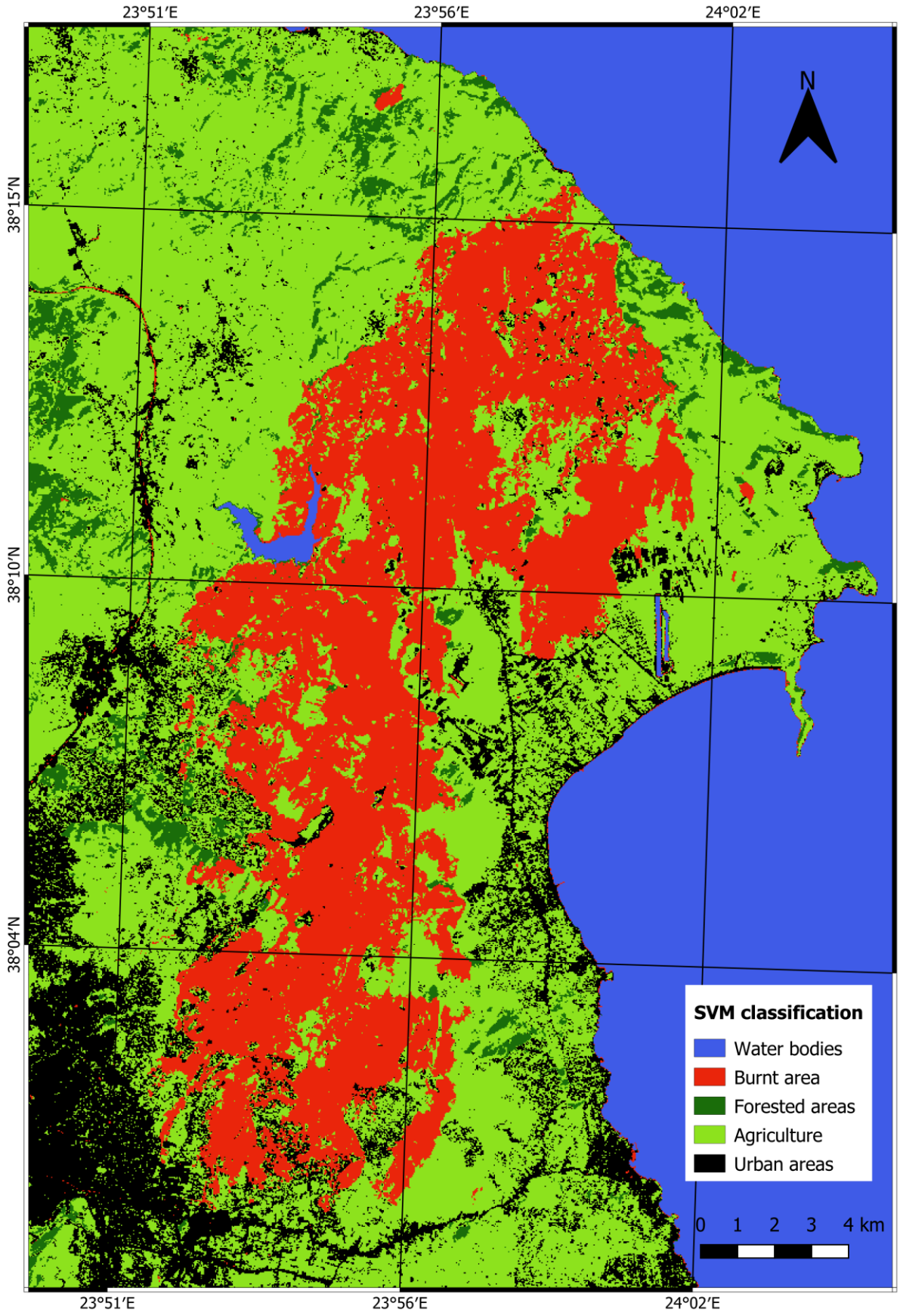

Figure 5-1: SVM classification of the studied area – burnt area delineation, with the use of the post-fire LANDSAT TM image (3/9/2009) just after fire suppression.

Table 5-1: Classification results obtained from the SVM implementation with the post-fire Landsat TM imagery.

	Producer's accuracy (%)	User's accuracy (%)
Water bodies	100.00	100.00
Burnt area	100.00	94.32
Forested areas	81.05	89.53
Agricultural areas	96.73	90.10
Urban areas	84.95	98.31
Overall accuracy	**93.22%**	
Kappa coefficient (K_c)	**0.906**	

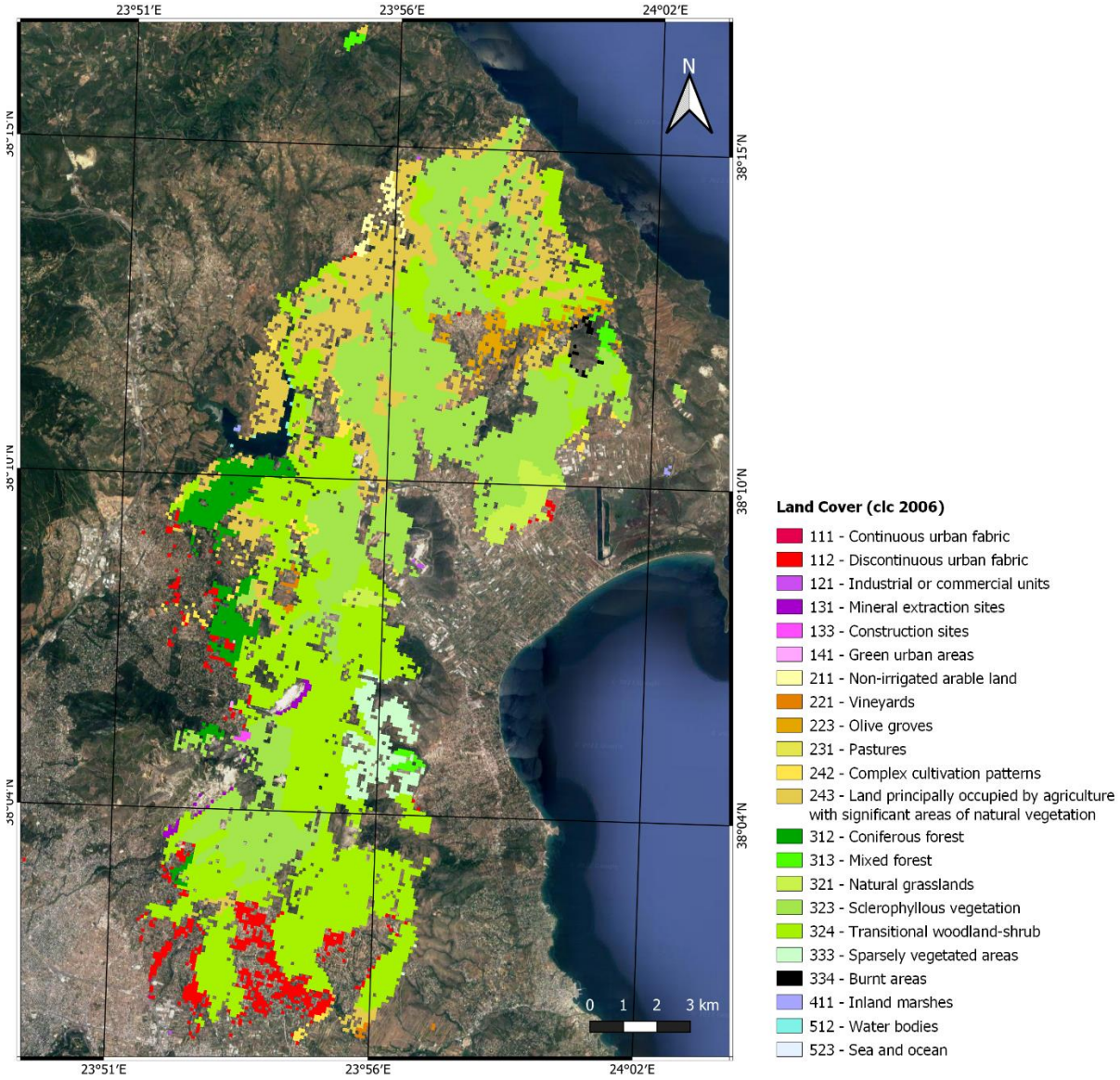

Figure 5-2: Pre-fire land cover map of the study area under burn scar

Table 5-2: Type and extent (in km²) of land cover burnt in the area of interest based on CLC 2006

	Land cover type	Area (*km²*)
FOREST AND SEMI NATURAL AREAS	Transitional woodland-shrub	53.33
	Sclerophyllous vegetation	48.14
	Coniferous forest	5.64
	Sparsely vegetated areas	3.96
	Natural grasslands	2.89
	Mixed forest	0.94
	Burnt areas	0.23
AGRICULTURAL AREAS	Land principally occupied by agriculture, with significant areas of natural vegetation	20.90
	Olive groves	1.84
	Complex cultivation patterns	1.42
	Non-irrigated arable land	0.79
	Vineyards	0.32
	Pastures	0.05
ARTIFICIAL SURFACES	Discontinuous urban fabric	5.8
	Mineral extraction sites	0.41
	Construction sites	0.1
	Industrial or commercial units	0.06
	Continuous urban fabric	0.02
	Green urban areas	0.02

5.2 Burn severity mapping

Spatial distribution of the various burn severity classes within the burn scar is presented in Figure 5-3, while Table 5-3 shows the area of each class (in km²) as well as the percentage of each of them in relation to the total area. From these results, it is clear that the majority of the study

area experienced moderate to high severity burn (about 43%) followed by moderate to low (about 31%). Additionally, 16% of the area faced high severity burn while a small percentage of the burnt area of interest experienced low levels of burn severity (about 10%). Concerning the type of land cover burned in each severity class, Figure 5-4 and Table 5-4 show the area of each land cover type which burned in relation to the severity level.

Table 5-3: The area (km^2) and percentage of each burn severity class within the burn scar

Burn Severity classes	**Area (km^2)**	**Percentage (%)**
Low	14	9.9
Moderate-low	45	31.3
Moderate-high	63	43.1
High	23	16.0
Total	**146**	**100**

Results show that the highest burnt land types i.e., transitional woodland-shrub and sclerophyllous vegetation faced mainly moderate to high severity burn, about 47% and 53% respectively following by moderate to low severity, about 30% and 25% respectively and finally high severity, about 17% both. Similar severity pattern presents also the land principally occupied by agriculture, with significant areas of natural vegetation. On the contrary, coniferous forested areas, faced mainly high severity burn (about 54%), following by moderate to high severity burn (about 30%) and moderate to low (about 13%).

5.3 Spatio-temporal patterns of vegetation re-growth dynamics using NDVI

The results regarding the assessment of spatio-temporal patterns of vegetation regeneration within the burn scar using the NDVI are presented in Figures 5-5 – 5-10. In addition, Table 5-5 provides the corresponding descriptive statistics. Moreover, several NDVI difference maps were constructed for the further evaluation of the spatio-temporal changes in NDVI between the pre-fire as well as the post-fire (just after fire suppression) conditions and all subsequent dates (Figure 5-11 & Figure 5-12). It is noted that while Figures 5-5 – 5-10 were created with a common

colorbar for the best visual comparison between them as the same color tones correspond to the same values, in Figures 5-11 & 5-12 the same was not presented due to the fact that in some images the spatial distribution of the index was not provided (the same color tone for the entire map)

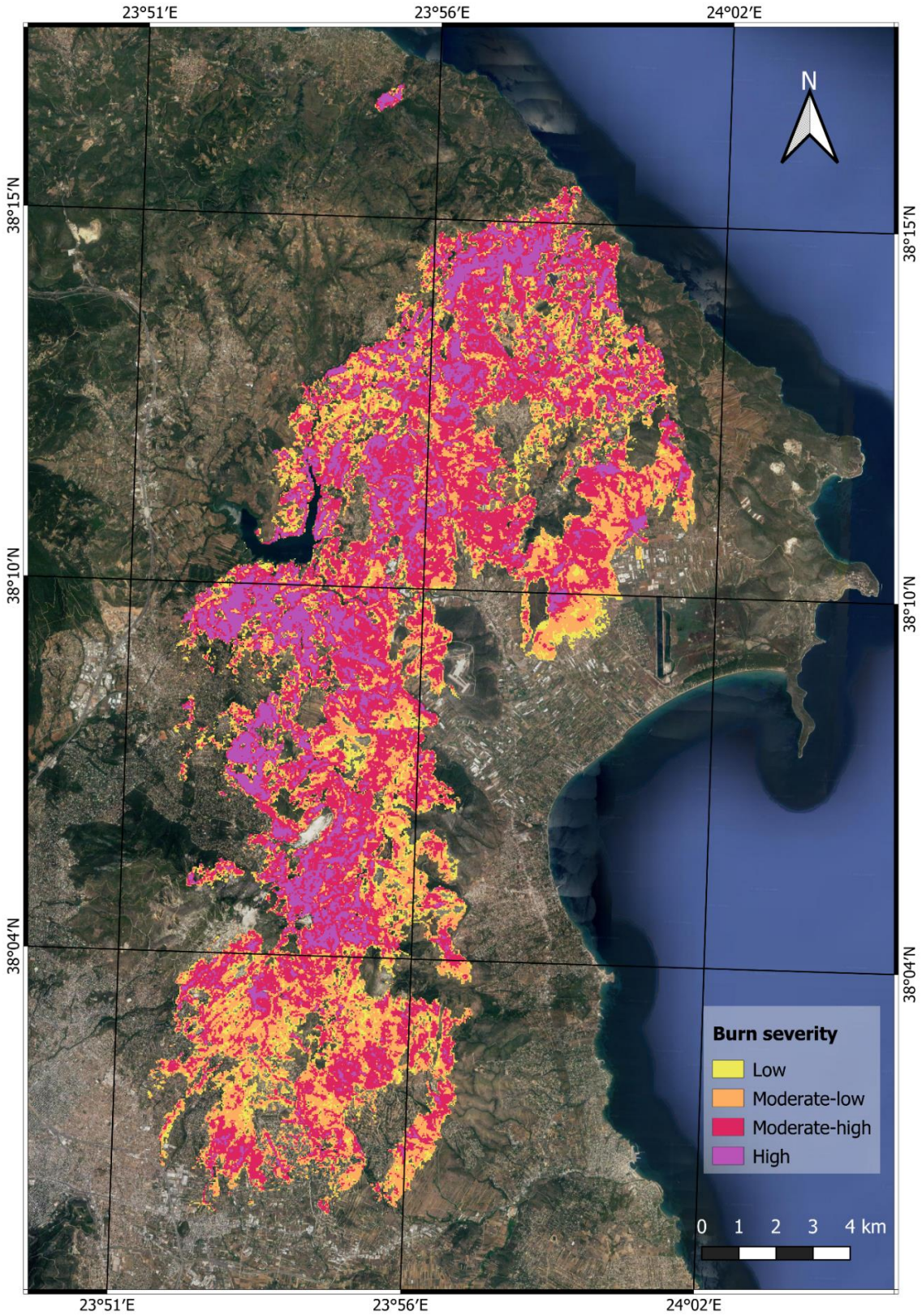

Figure 5-3: Burn severity classification within the area of interest

Table 5-4: Type and extent (in km²) of land cover burnt per burn severity class in the area of interest based on CLC 2006

		Severity classes			
		Low	Moderate-low	Moderate-high	High
	Land cover	**Area (km²)**			
Artificial Surfaces	Discontinuous urban fabric	0.61	2.30	1.16	0.13
	Mineral extraction sites	0.04	0.17	0.10	0.03
	Construction sites	0.00	0.04	0.05	0.00
	Green urban areas	0.00	0.01	0.01	0.00
Agricultural Areas	Non-irrigated arable land	0.09	0.33	0.15	0.04
	Vineyards	0.02	0.11	0.03	0.00
	Olive groves	0.38	0.65	0.30	0.04
	Pastures	0.01	0.00	0.02	0.00
	Complex cultivation patterns	0.22	0.43	0.27	0.11
	Land principally occupied by agriculture, with significant areas of natural vegetation	2.66	6.01	6.92	2.84
Forest and semi natural areas	Coniferous forest	0.18	0.70	1.54	2.84
	Mixed forest	0.10	0.18	0.35	0.18
	Natural grasslands	0.66	1.58	0.45	0.00
	Sclerophyllous vegetation	1.86	11.45	24.25	7.79
	Transitional woodland-shrub	3.00	14.96	23.77	8.83
	Sparsely vegetated areas	0.68	2.05	0.68	0.02
	Burnt areas	0.05	0.09	0.02	0.00
Wetlands	Inland marhses	0.00	0.01	0.01	0.00

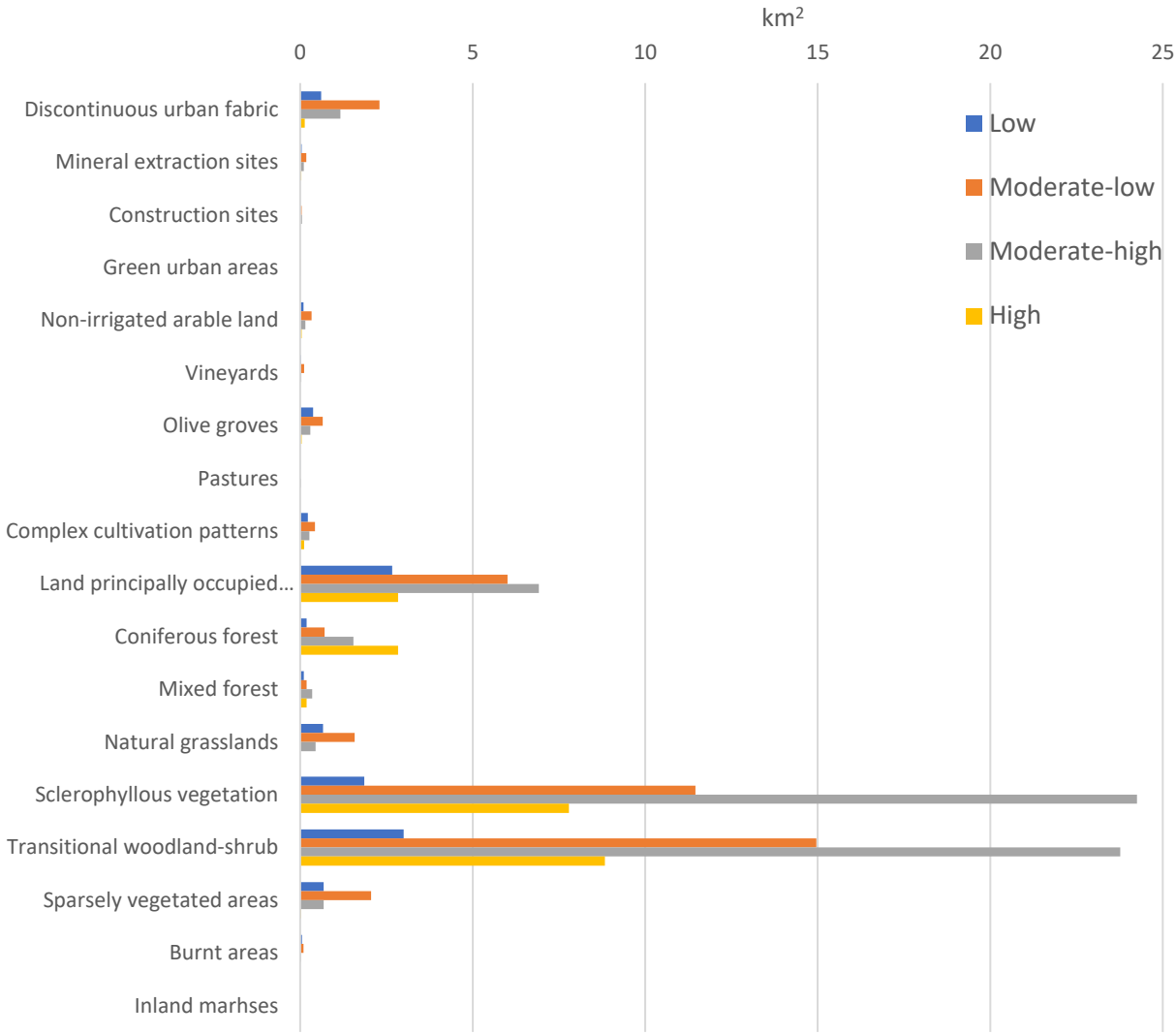

Figure 5-4: Chart showing the comparison of the different land cover burnt in relation to the burn severity classes

Firstly, from the visual comparison of the pre-fire NDVI map with the respective first post-fire NDVI map, it becomes clear the extent of vegetation destruction caused by the fire. Also, these negative effects of fire on the area of interest's vegetation are further evident by the changes in the descriptive statistics of NDVI between the pre-fire and the first post-fire image (Table 5-5). More precisely, the mean NDVI within the study area before the fire occurrence is about 0.39 while after the fire suppression the respective NDVI reaches the value of 0.15. As regards the maximum NDVI, it decreases from 0.79 before the fire to 0.42 after the fire. The latter shows that some of the vegetation inside the burn scar was only partially destroyed by the fire.

Regarding the dynamics of the vegetation regeneration within the burn scar, a visual inspection of post-fire NDVI maps in combination with the respective NDVI descriptive statistics (Table 5-5)

show a gradual regrowth progress withing the fire-affected region. More precisely, mean and max NDVI of post-fire images present a gradual increase which is indicative of vegetation regeneration in the area. This increase of mean and max NDVI is more intense during the first five years after the fire event (period 2009-2014) showing a higher rate of regeneration in contrast with the next six years, from 2014 until 2020, where mean and max NDVI are increasing at a slower rate. In addition, spatial distribution of post-fire NDVI, from 2011 onwards, as illustrated in Figures 5-5 – 5-10 as well as in difference NDVI maps (Figure 5-11), reveal disparate regeneration dynamics within the study area. Clearly, stronger dynamics in regeneration process are more apparent at the center as well as at west and north of the fire-affected area in comparison to the rest of it.

As for the regeneration progress through years towards the recovery of pre-fire conditions of vegetation in the affected study area, Figure 5-12 as well as descriptive statistics (Table 5-5) show that from 2014 and beyond the condition of vegetation of the burnt area shows the first steps of recovery to the pre-fire levels. In addition, difference maps between pre-fire images with the respective of 2017 and 2020 show NDVI has even increased, from 0.14-0.18 (light green areas) to 0.23-0.27 (dark green areas), compared to pre-fire conditions.

Table 5-5: Descriptive statistics of NDVI in different "anniversary" dates withing the burn scar

Landsat image date	NDVI			
	Min	**Max**	**Mean**	**Std dev**
18/8/2009	-0.016	0.794	0.394	0.103
3/9/2009	-0.069	0.417	0.151	0.038
24/8/2011	-0.015	0.740	0.292	0.073
23/8/2014	0.045	0.820	0.397	0.090
8/8/2017	0.0000	0.839	0.462	0.105
23/8/2020	-0.121	0.886	0.496	0.116

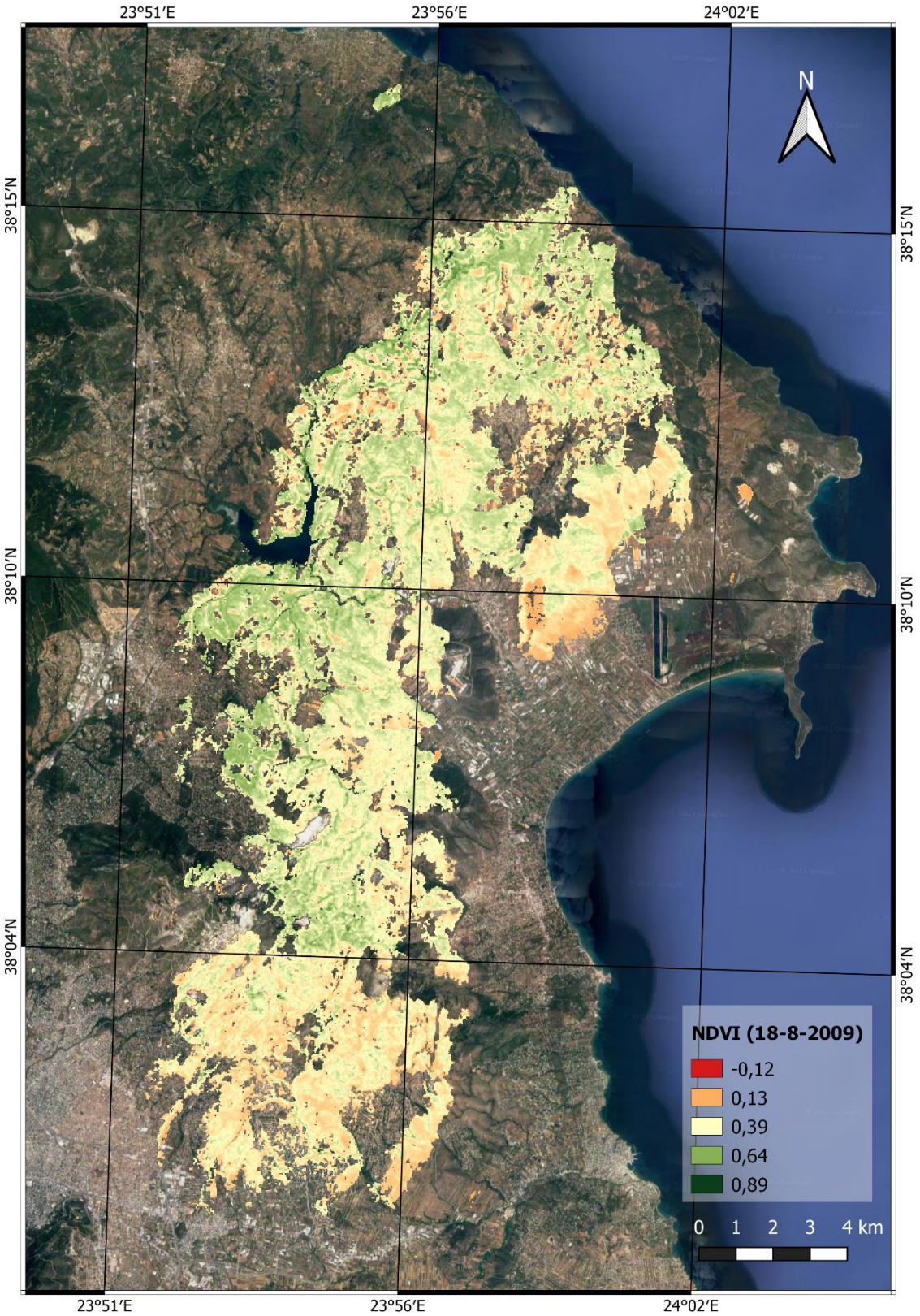

Figure 5-5: Spatial distribution of NDVI within the study area before the fire occurrence

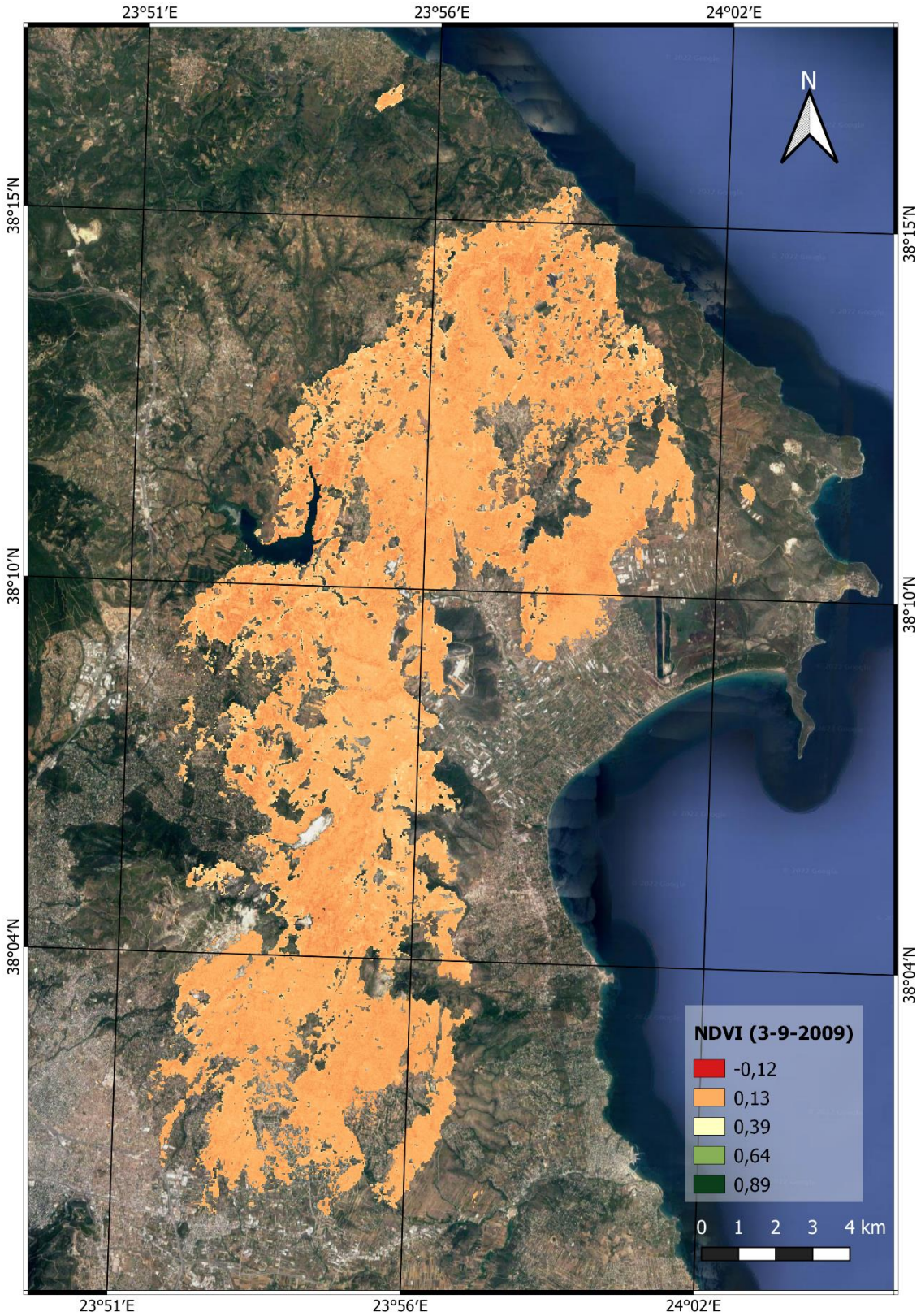

Figure 5-6: Spatial distribution of NDVI within the study area after the fire suppression

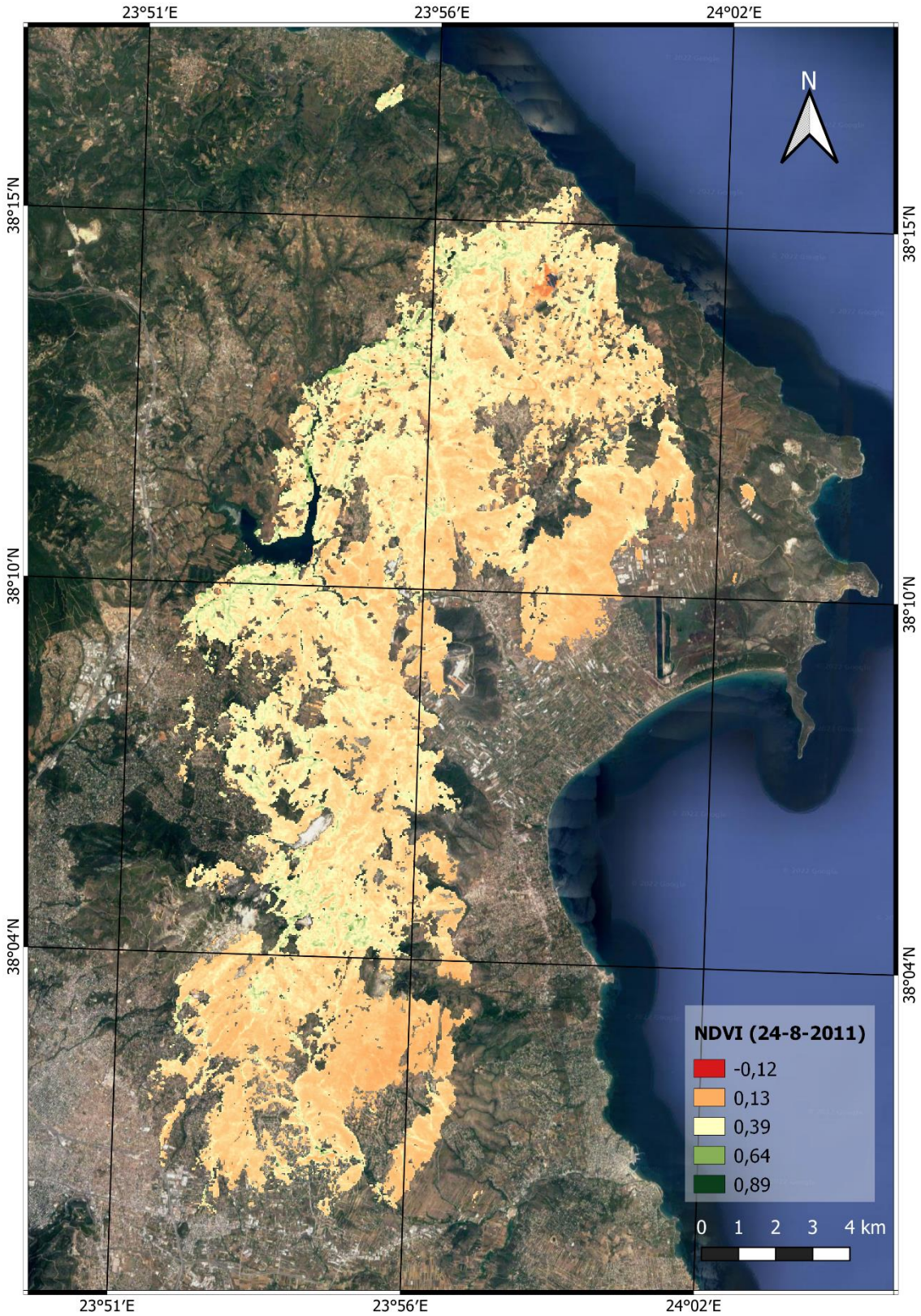

Figure 5-7: Spatial distribution of NDVI after two years from the fire event in the study area

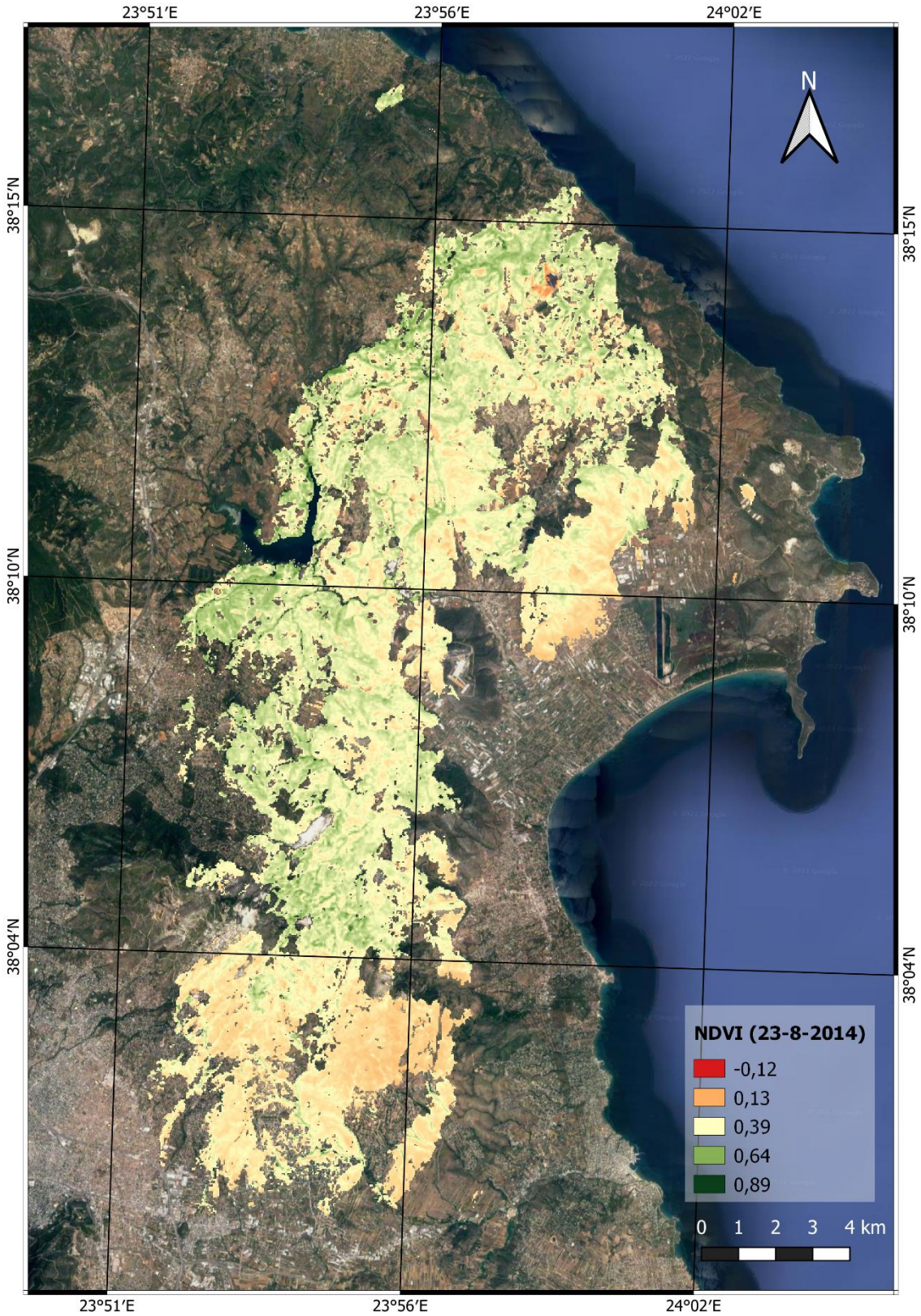

Figure 5-8: Spatial distribution of NDVI after five years from the fire event in the study area

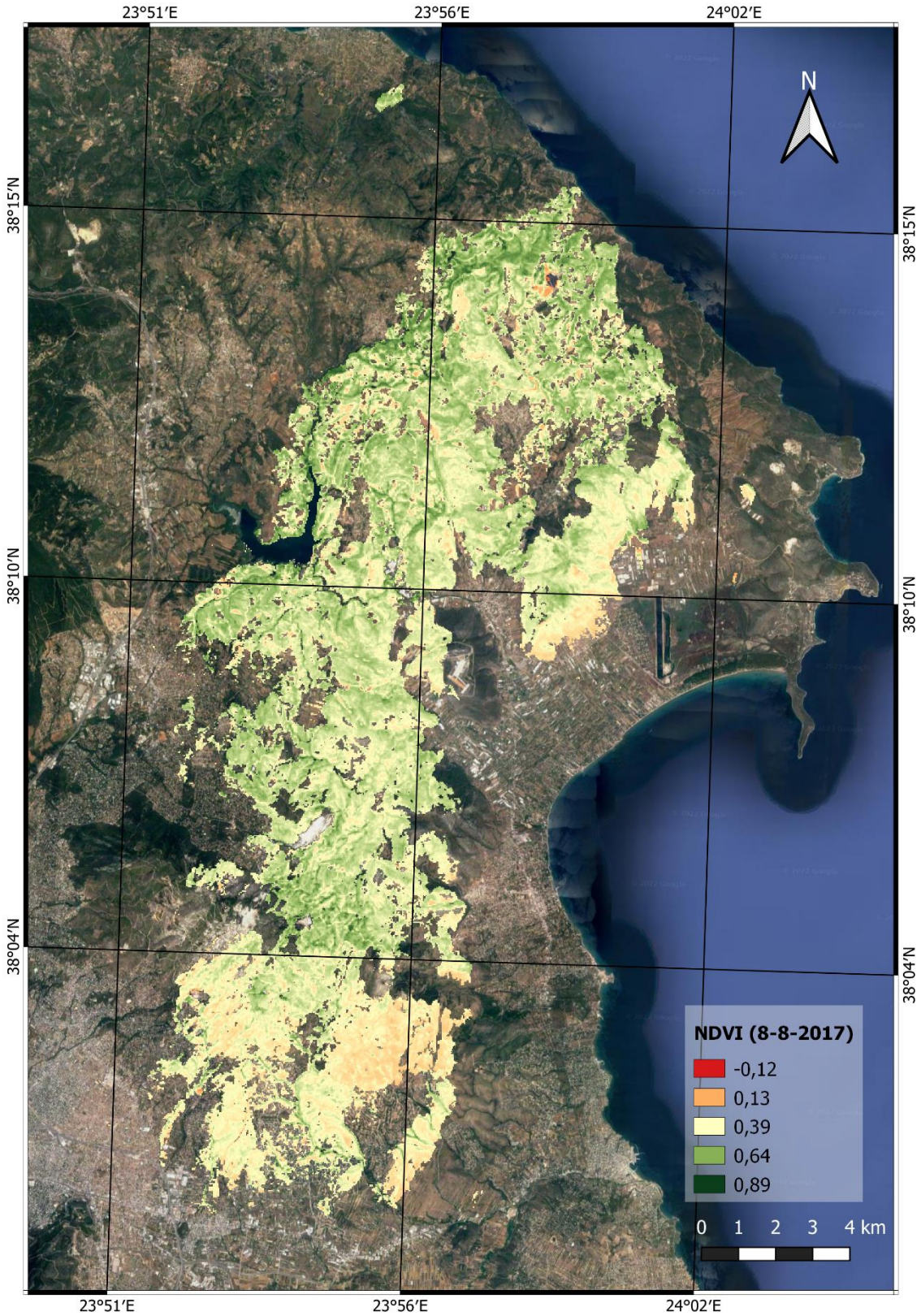

Figure 5-9: Spatial distribution of NDVI after eight years from the fire event in the study area

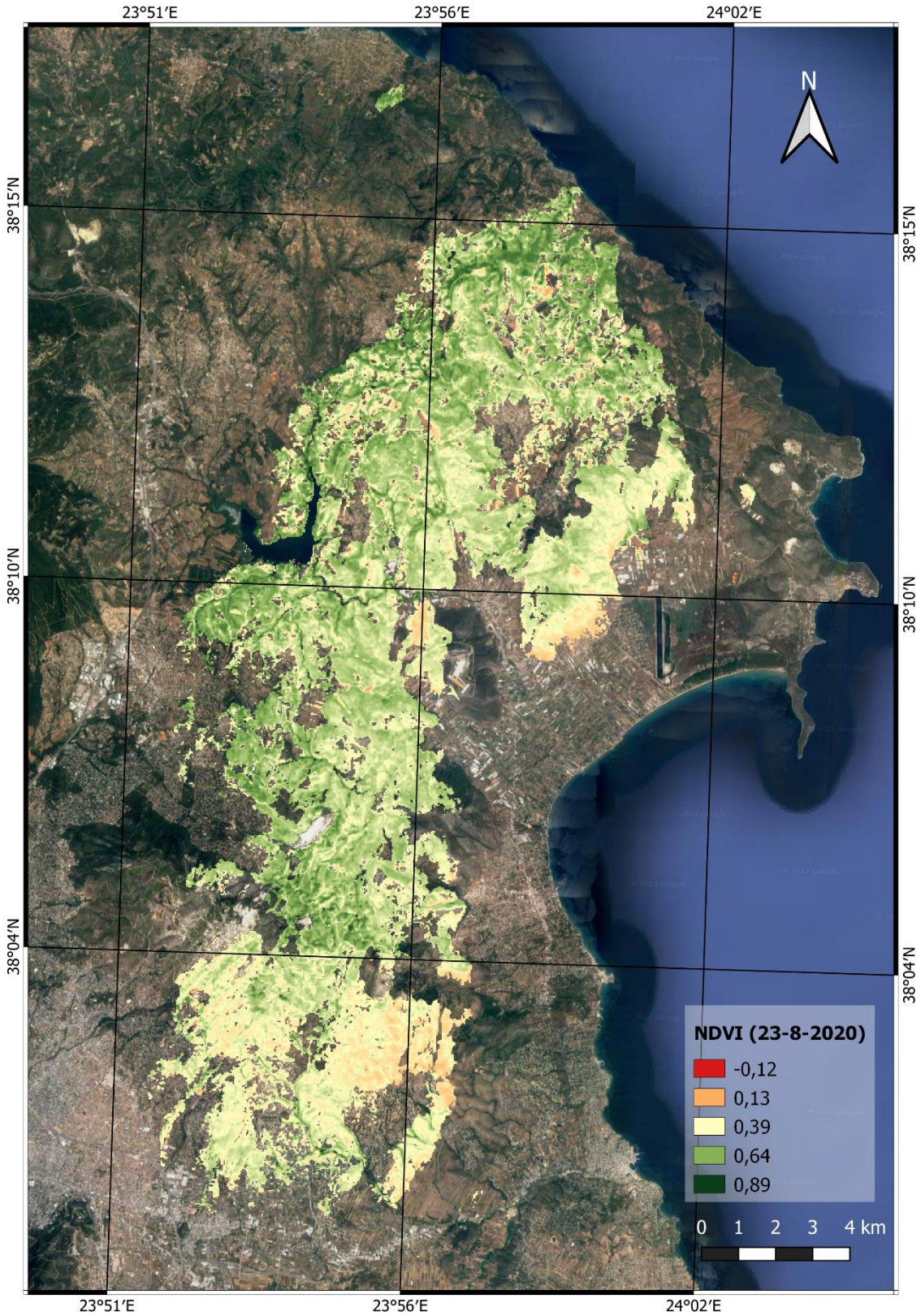

Figure 5-10: Spatial distribution of NDVI after eleven years from the fire event in the study area

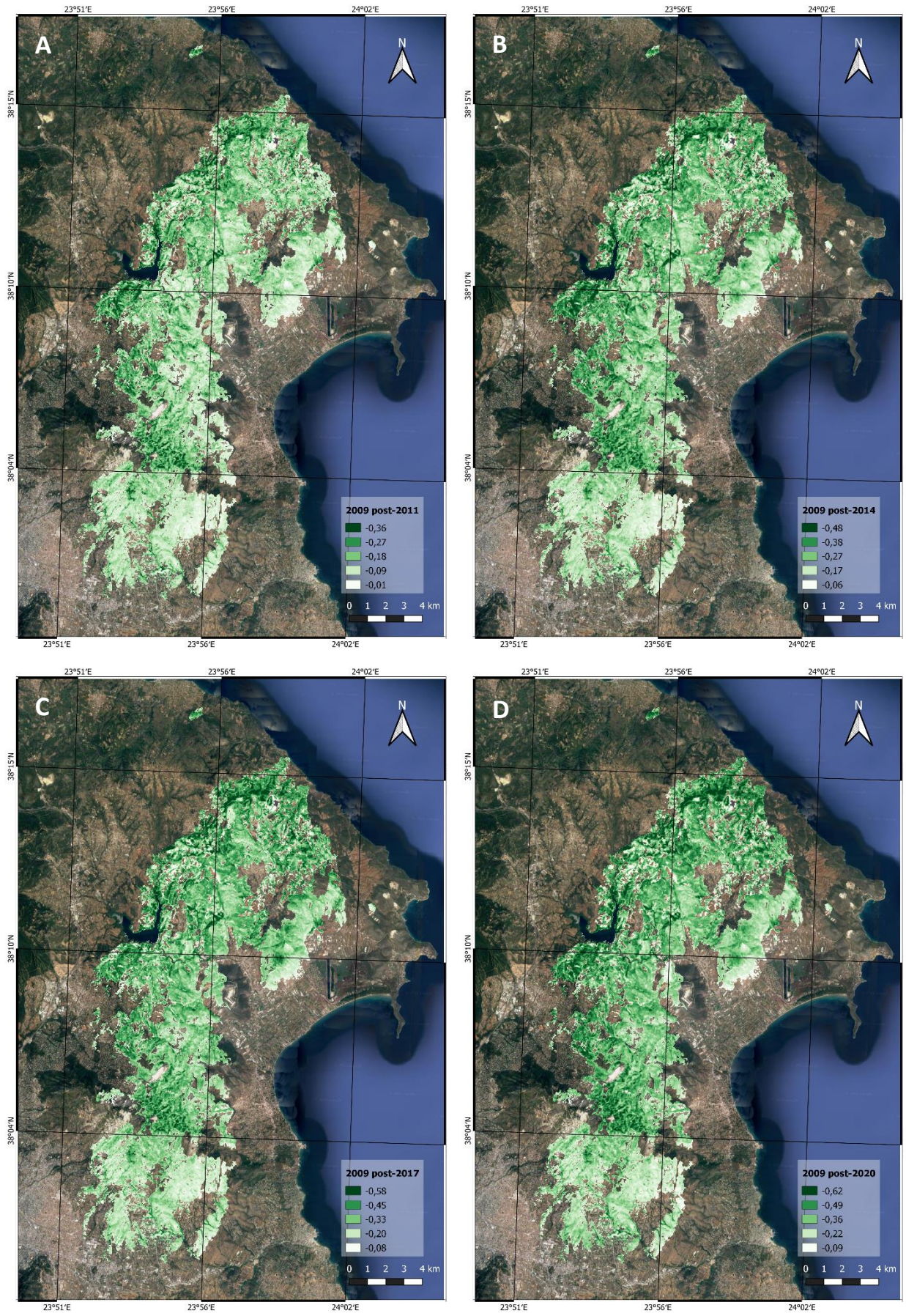

Figure 5-11: Difference maps between the post-fire (just after the fire suppression) distribution of NDVI and the respective after two years from the fire event (A), five years from the fire event (B), eight years from the fire event (C) and eleven years from the fire event (D)

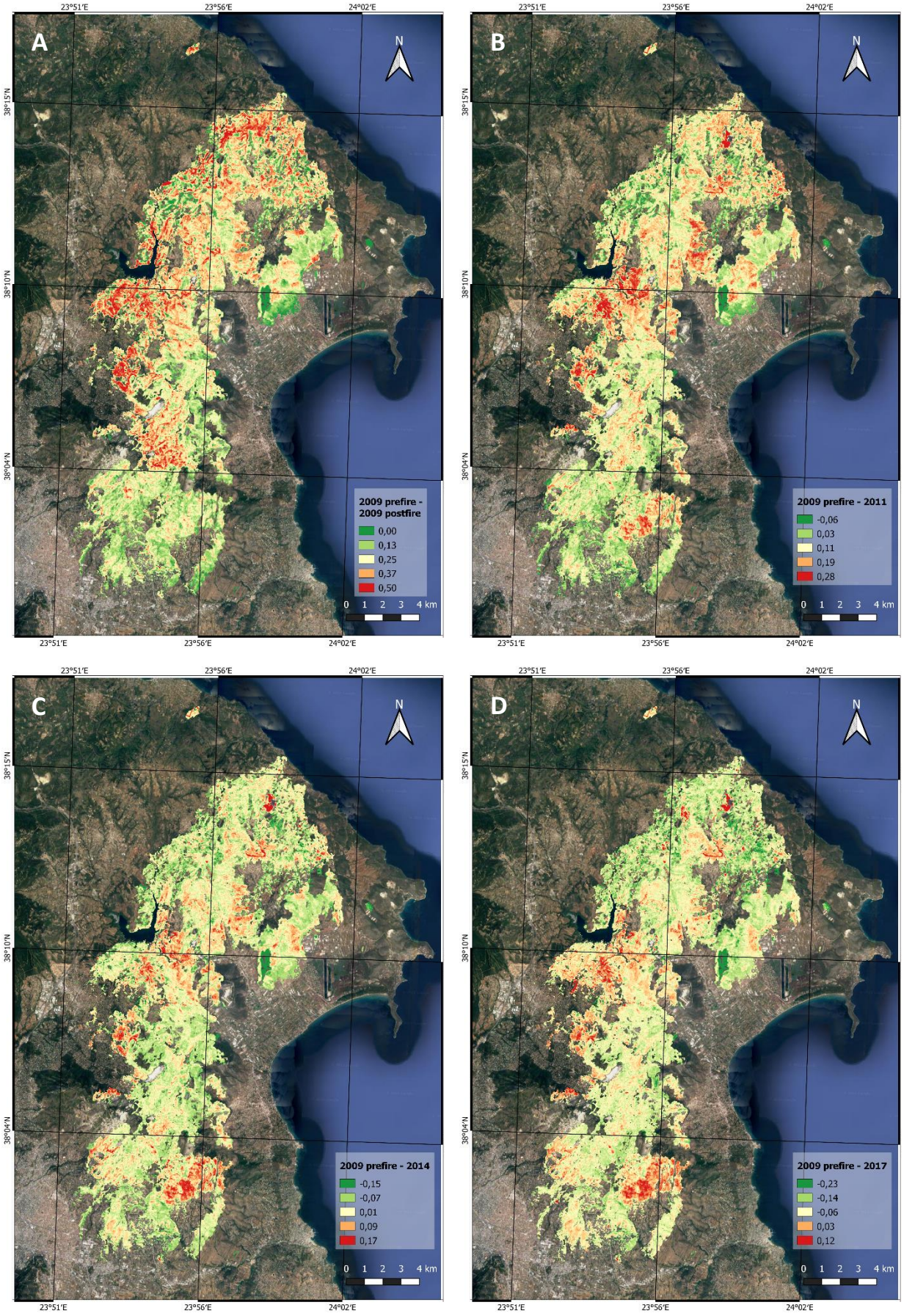
A
B
C
D
N
23°51′E
23°56′E
24°02′E
38°15′N
38°10′N
38°04′N
2009 prefire - 2009 postfire
0,00
0,13
0,25
0,37
0,50
2009 prefire - 2011
-0,06
0,03
0,11
0,19
0,28
2009 prefire - 2014
-0,15
-0,07
0,01
0,09
0,17
2009 prefire - 2017
-0,23
-0,14
-0,06
0,03
0,12
0 1 2 3 4 km

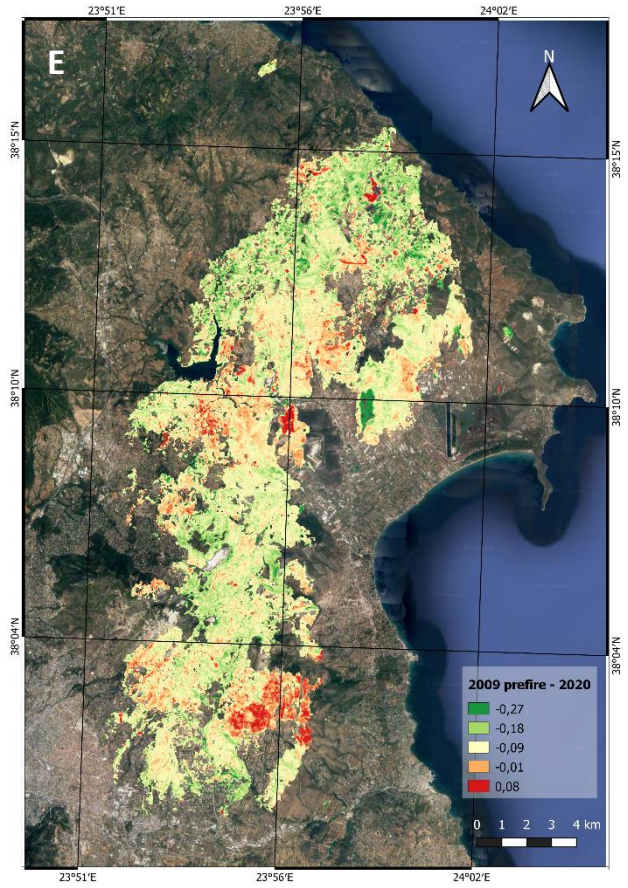

Figure 5-12: Difference maps between the pre-fire distribution of NDVI and the respective post-fire, just after the fire suppression (A), after two years from the fire event (B), five years from the fire event (C), eight years from the fire event (D) and eleven years from the fire event (E)

5.3.1 Regression analysis of post-fire NDVI

To further explore the vegetation regeneration dynamics in the studied burnt area, it is attempted to fit regression models on this process. Based on other studies (Hope et al., 2007; Petropoulos et al., 2014) scatterplots of the NDVI between pre-fire conditions and all subsequent post-fire dates were constructed. With scatterplots, the dynamic of regeneration emerges through the location of the cloud of points relative to the 1:1 line which represents the return of the burn area to pre-fire conditions. Also, slope, intercept and R^2 for the regression line were also computed. Figures 5-13 – 5-17 illustrate the produced scatterplots while Table 5-6 summarizes the regression analysis' statistics relating to those scatterplots. In addition, each scatterplot is accompanied by a corresponding bar chart showing the change rate of pre-fire NDVI pixel values to the respective values of NDVI of each subsequent date.

The results of the analysis of the scatterplots regarding the regeneration dynamics within the study area, clearly mirror the respective of the previous analysis of NDVI. Indeed, the movement

of points towards the 1:1 line is clear after two years of fire suppression (August 2011) indicating the first steps of regeneration while from 2011 until 2014 the regeneration process increases gradually showing high percentage of recovery level of NDVI. From 2014 until 2020, the regression analysis shows that in the majority of the study area NDVI levels has recovered or improved in contrast with the pre-fire levels. More precisely, scatterplot of NDVI pre-fire against post-fire after the fire suppression as well as the respective NDVI change rate of each pixel (Figure 5-13), show that 96% of pixels are below and 4% are on the 1:1 line showing the devastating impacts of fire in the study area. On 2011, 24% of NDVI pixel values are on the 1:1 line, while 74% are below and only 4% of pixels have NDVI values higher than the pre-fire conditions (Figure 5-14). On 2014, 56% of NDVI pixel values are on the 1:1 line, while 20% are below and 24% are above the 1:1 line (Figure 5-15). On August 2017, scatterplot as well as bar plot show that 32% of NDVI pixel values are on the 1:1 line, while 5% are below and 63% are above showing the vegetation improvement in contrast to the pre-fire conditions (Figure 5-16). The improvement is most evident in 2020 where 79% of NDVI pixel values are above the 1:1 line, 18% are on the 1:1 line while only 3% of pixels are below (Figure 5-17).

Table 5-6: Regression analysis statistics between the pre-fire NDVI and the respective NDVI of all subsequent post-fire dates for the area under the burn scar.

Period	Slope	Intercept	R^2
pre-fire August 2009 – post-fire September 2009	-0.066	0.177	0.032
pre-fire August 2009 – post-fire August 2011	0.506	0.093	0.511
pre-fire August 2009 – post-fire August 2014	0.699	0.122	0.642
pre-fire August 2009 – post-fire August 2017	0.815	0.141	0.640
pre-fire August 2009 – post-fire August 2020	0.925	0.132	0.675

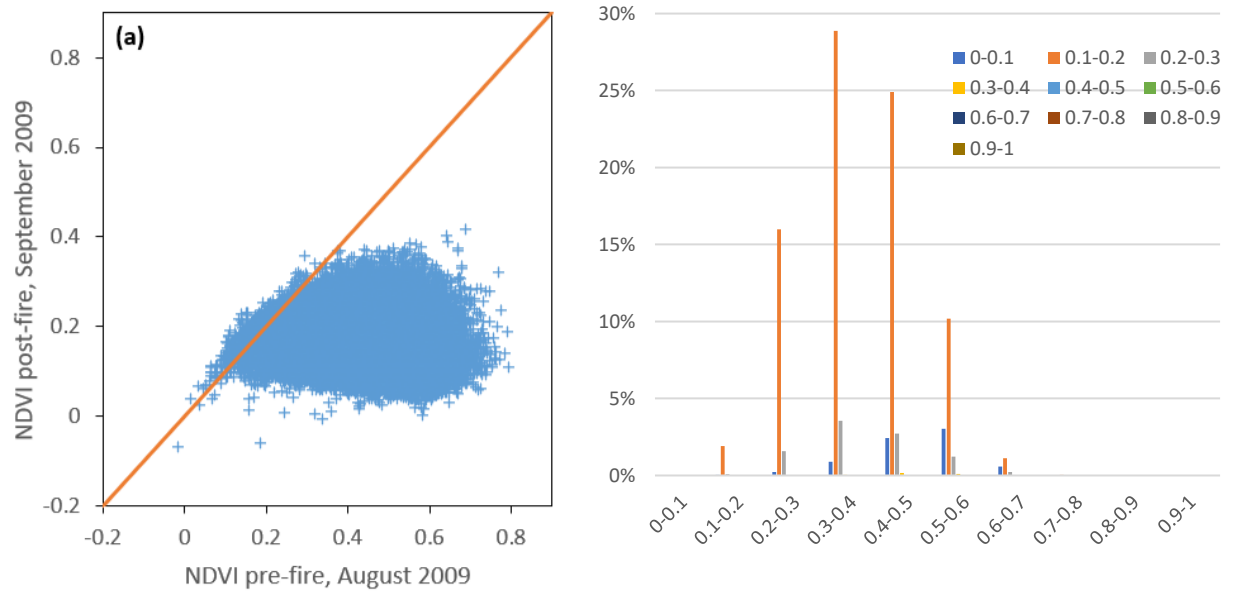

Figure 5-13: Scatterplot of pre-fire (August 2009) NDVI against post-fire after fire suppression (September 2009) and NDVI change rate

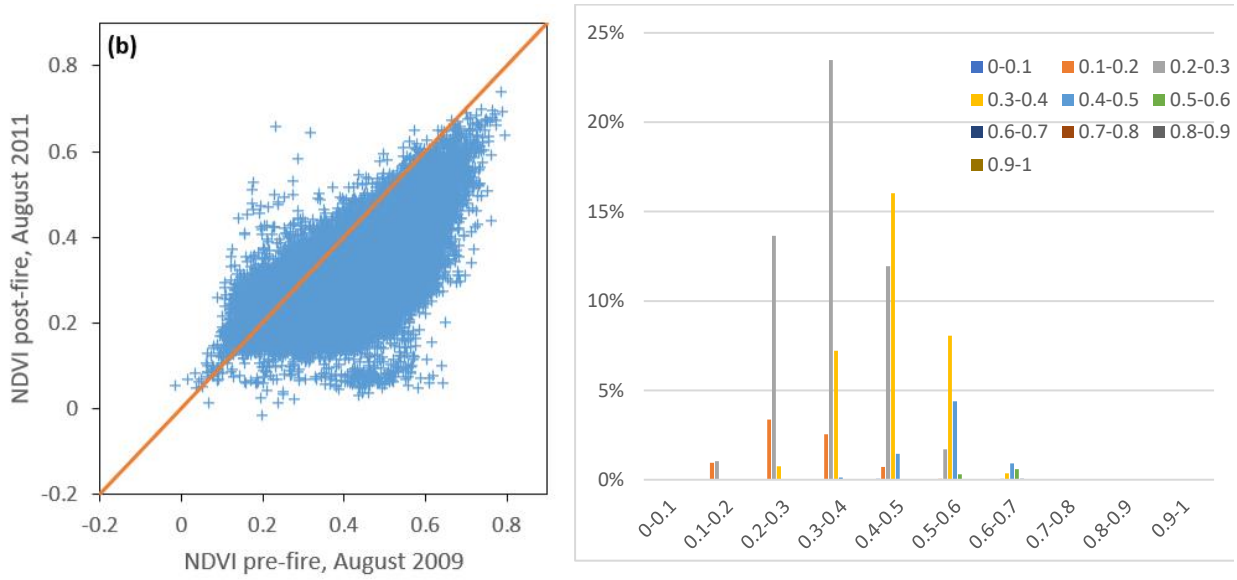

Figure 5-14: Scatterplot of pre-fire (August 2009) NDVI against post-fire after two years of fire suppression (August 2011) and NDVI change rate

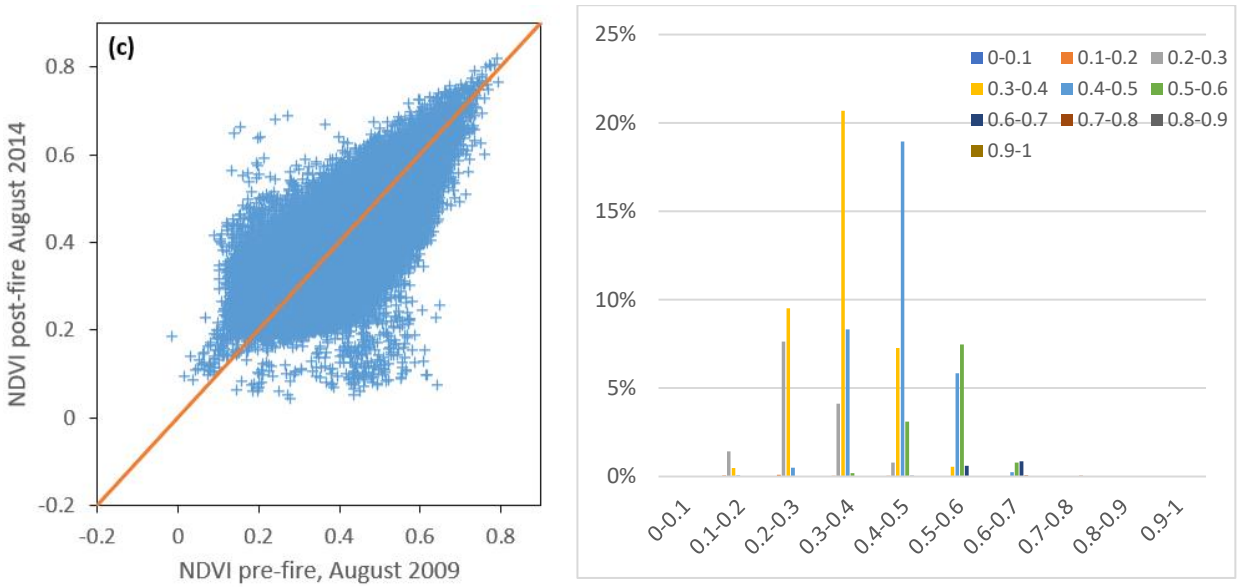

Figure 5-15: Scatterplot of pre-fire (August 2009) NDVI against post-fire after five years of fire suppression (August 2014) and NDVI change rate

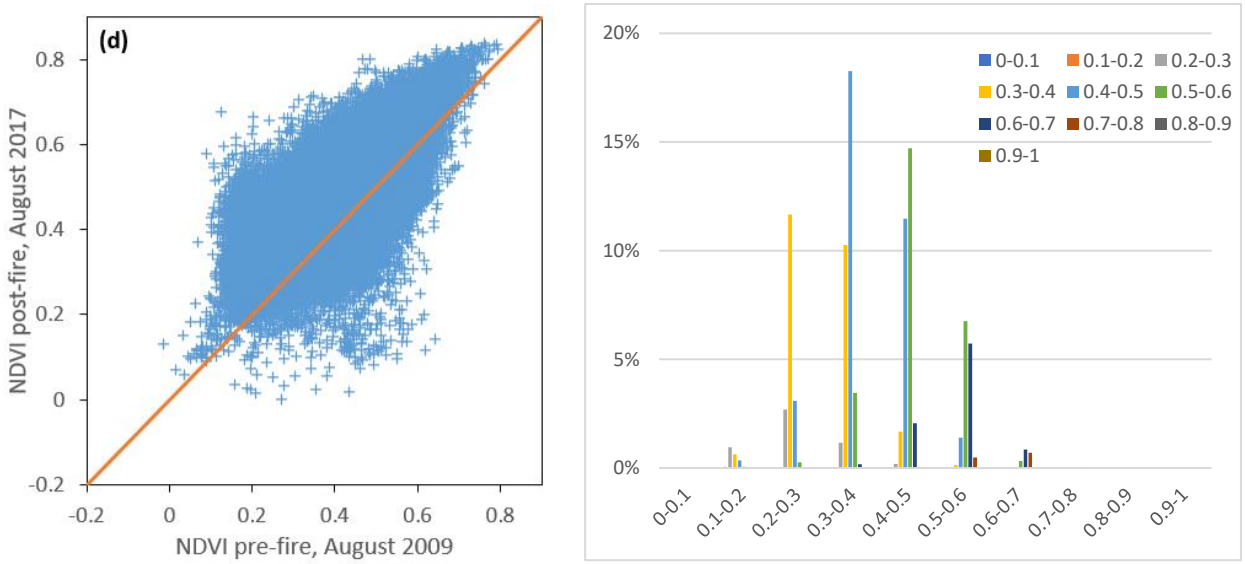

Figure 5-16: Scatterplot of pre-fire (August 2009) NDVI against post-fire after eight years of fire suppression (August 2017) and NDVI change rate

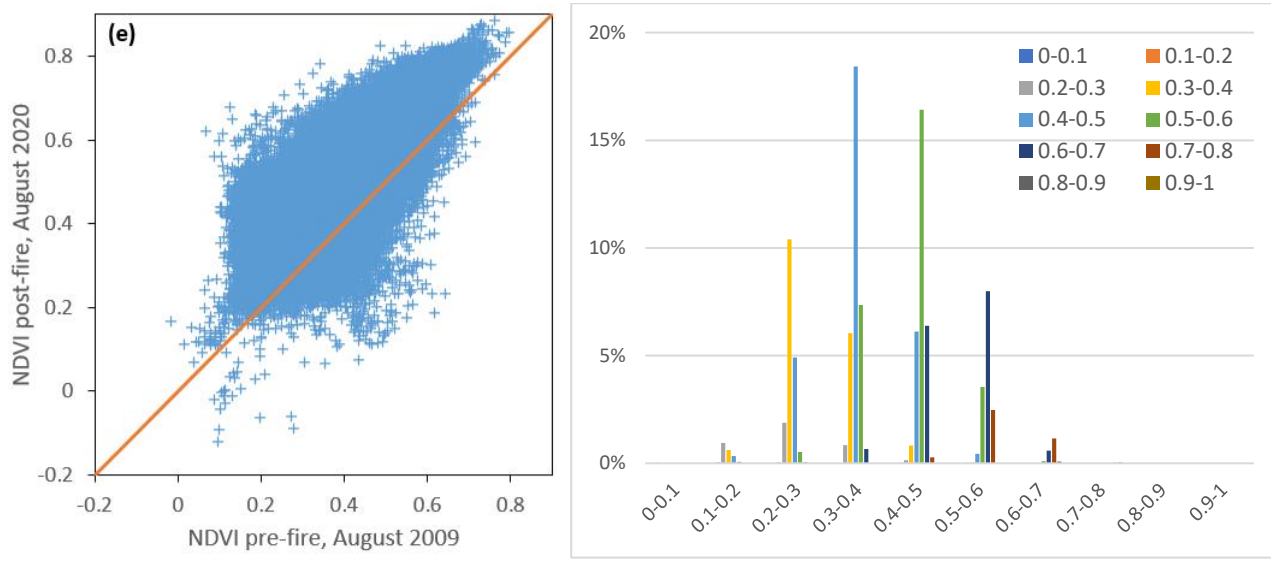

Figure 5-17: Scatterplot of pre-fire (August 2009) NDVI against post-fire after eleven years of fire suppression (August 2020) and NDVI change rate

5.3.2 Vegetation regeneration dynamics and burn severity level

The vegetation regrowth dynamics within the study area under burn scar was also investigated in relation with the burn severity class. Table 5-7 presents the descriptive statistics of the NDVI for each severity class during the study period from August 2009 until August 2020. As expected, the largest change in NDVI values following the devastating impacts of fire on vegetation is presented in highest classes i.e., high severity class as well as moderate-high severity class. Indeed, concerning the high severity class, mean NDVI decreases of about 0.41 after the fire suppression (September 2009) in contract with the pre-fire levels (August 2009), while within the moderate-high class the respective decrease is about 0.29. On the remaining classes, post-fire (September 2009) mean NDVI decreases of about 0.16 and 0.08 in moderate-low and low severity classes respectively. The same pattern between the pre-fire and the immediately after the fire suppression post-fire levels is presented by the maximum NDVI. The highest drop of about 0.42 is shown on high severity class, following by the moderate-high where the decrease is about 0.33, and the moderate-low with a decrease 0.32 as well as low with a decrease of about 0.21.

As far as regeneration process is concerned, it is clear from Table 5-7 that low and moderate-low severity areas present highest regeneration rates in contrast with the other classes. More precisely, mean NDVI values within these classes reaches the pre-fire levels after two to five years after fire event while in other classes, moderate-high and high, pre-fire levels of mean NDVI are reached after five to eight years after fire occurrence. This trend of the mean NDVI values suggest that low severity burn cause less damage to vegetation leading to quicker recovery, while

moderate-high and high severity levels cause extensive vegetation devastation and as a result regrowth process takes longer to reach pre-fire levels.

Table 5-7: Descriptive statistics of NDVI in "anniversary" dates withing the burn scar separately for each burn severity class

	Min	Max	Mean	Stdev
Low				
18/8/2009	0.073	0.582	0.269	0.061
3/9/2009	0.042	0.372	0.183	0.040
24/8/2011	-0.015	0.644	0.253	0.052
23/8/2014	0.051	0.635	0.329	0.065
8/8/2017	0.000	0.734	0.370	0.077
23/8/2020	-0.062	0.733	0.389	0.085
Moderate-Low				
18/8/2009	0.068	0.711	0.327	0.066
3/9/2009	0.008	0.387	0.165	0.038
24/8/2011	0.014	0.607	0.262	0.057
23/8/2014	0.045	0.710	0.353	0.069
8/8/2017	0.024	0.802	0.408	0.081
23/8/2020	-0.089	0.809	0.434	0.090
Moderate-High				
18/8/2009	0.179	0.748	0.423	0.063
3/9/2009	-0.004	0.417	0.144	0.030
24/8/2011	0.032	0.680	0.294	0.064
23/8/2014	0.053	0.767	0.409	0.075
8/8/2017	0.017	0.830	0.480	0.086
23/8/2020	0.074	0.845	0.517	0.092
High				
18/8/2009	0.263	0.794	0.532	0.055
3/9/2009	0.003	0.375	0.121	0.027
24/8/2011	0.049	0.740	0.369	0.074
23/8/2014	0.075	0.820	0.500	0.074
8/8/2017	0.094	0.839	0.580	0.081
23/8/2020	0.113	0.886	0.631	0.081

5.3.3 Relationship of vegetation regrowth dynamics and topography

The relationship between the topographical characteristics such as the aspect and vegetation regeneration dynamics – as captured from NDVI – was also investigated within the study area under burn scar. Table 5-8 presents the descriptive statistics for the NDVI across the study burnt area separately for the north- and south-facing slopes.

Firstly, the results show that fire occurrence in the study area had negative impacts in both aspects. Indeed, mean NDVI as well as max NDVI show a sharp decrease in both aspects immediately after the fire suppression (September 2009), however, the devastating effects of fire are more evident in north-facing slopes where the decrease in mean NDVI is about 0.3 in contrast with the respective decrease of 0.2 in south-facing slopes. Regarding the regeneration

Table 5-8: Descriptive statistics of NDVI in different "anniversary" dates withing the burn scar separately for north facing and south facing slopes

	NDVI			
Landsat image date	Min	Max	Mean	Stdev
	North-facing slopes			
18/8/2009	0.032	0.754	0.432	0.103
3/9/2009	0.003	0.417	0.154	0.046
24/8/2011	0.014	0.680	0.317	0.076
23/8/2014	0.051	0.793	0.436	0.088
8/8/2017	0.000	0.827	0.505	0.102
23/8/2020	-0.062	0.869	0.545	0.113
	South-facing slopes			
18/8/2009	0.037	0.748	0.370	0.098
3/9/2009	-0.004	0.350	0.150	0.032
24/8/2011	0.049	0.700	0.278	0.069
23/8/2014	0.079	0.774	0.372	0.084
8/8/2017	0.059	0.832	0.433	0.100
23/8/2020	-0.044	0.877	0.462	0.108

process withing the burn scar, in both aspects the mean NDVI is gradually increasing though years, however, the mean NDVI of north-facing slopes is higher of about 0.1 than in south-facing slopes. The highest regeneration rate is presented two years after fire (August 2011) where north-facing slopes show an increase of approximately 0.2 in mean NDVI while south-facing slopes show an increase of about 0.1. In the following acquisition images, regrowth process is lower. In north-facing slopes increase in mean NDVI is about 0.12 and 0.07 in years 2014 and 2017 respectively and about 0.04 in 2020. At the same time, in south-facing slopes the respective increase in mean NDVI is about 0.09, 0.06 and 0.03 for the years 2014, 2017 and 2020 respectively.

Regarding the recovery of the burnt area to the pre-fire levels and the relationship of this process with aspect, NDVI difference maps between the pre-fire image and all post-fire images (Figures 5-18 – 5-22) depict that in both slopes, vegetation recovery of the burn scar to the pre-fire level starts from 2014 and continues increasingly until 2020. The distribution of recovery is mainly in center as well as in north areas within the study region.

Table 5-9: Regression analysis of the NDVI before and after the fire occurrence in the study area under the burn scar separately for the north and south facing slopes.

Period	Slope	Intercept	R^2
August 2009 – September 2009			
North facing	-0.099	0.197	0.050
South facing	-0.060	0.172	0.033
August 2009 – August 2011			
North facing	0.518	0.093	0.494
South facing	0.493	0.096	0.452
August 2009 – August 2014			
North facing	0.669	0.148	0.626
South facing	0.678	0.121	0.591
August 2009 – August 2017			
8/8/2017			
North facing	0.768	0.173	0.631
South facing	0.816	0.132	0.601
August 2009 – August 2020			
North facing	0.884	0.163	0.652
South facing	0.907	0.127	0.623

As concerns the comparison of regrowth process between the north- and south-facing slopes, Figures 5-18 – 5-22 show clearly that from 2017 onwards, north-facing slopes present higher levels of regrowth in contrast with south-facing ones.

In common with the analysis conducted earlier, it was also attempted to fit regression models to quantitatively examine the correlation between post-fire regeneration dynamics and aspect. The results of the regression analysis (Table 5-9), show similar trends of the vegetation recovery to both north and south facing slopes, however, north-facing slopes present a higher recovery rate with higher slopes and R^2 values within the study period in contrast with south facing areas.

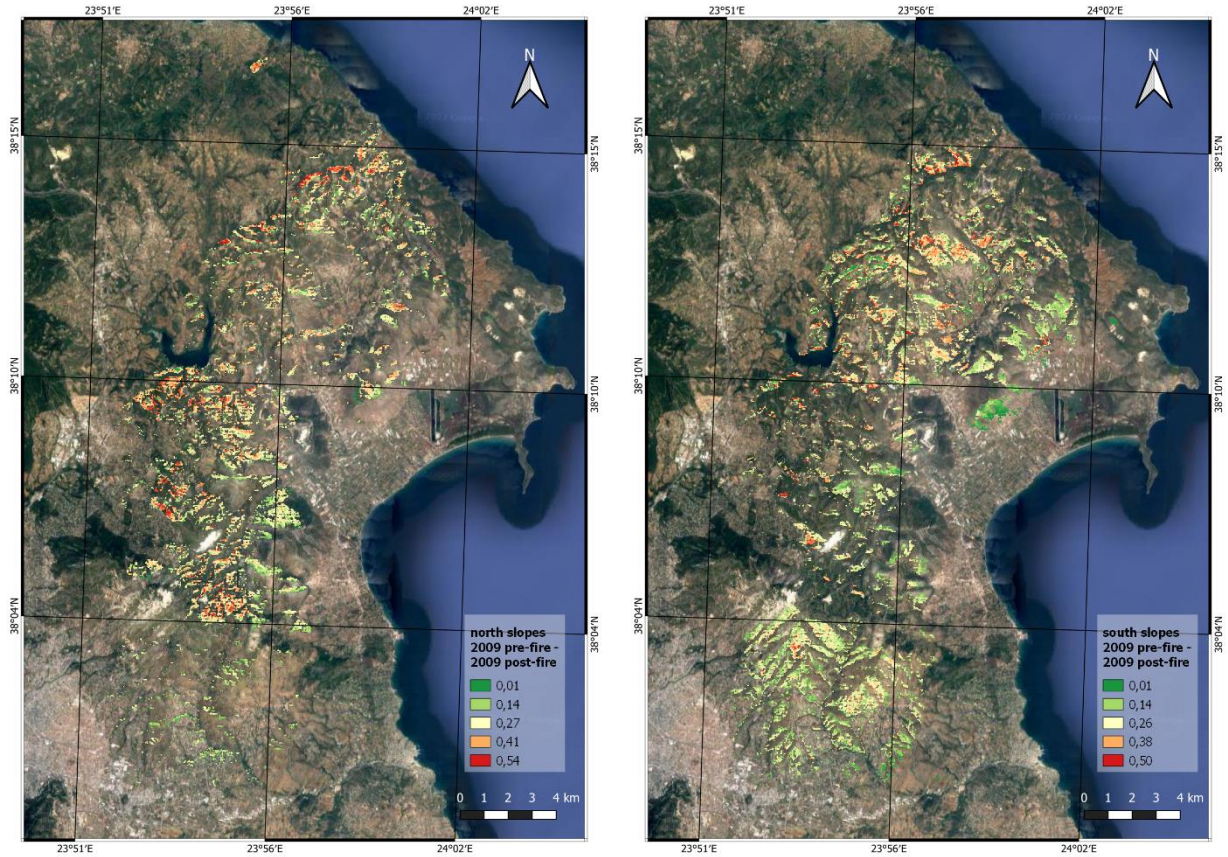

Figure 5-18: NDVI difference maps for the study burnt area between the pre-fire image (August 2009) and the post-fire image immediately after the fire suppression (September 2009) separately for north facing slopes (left) and south-facing slopes (right)

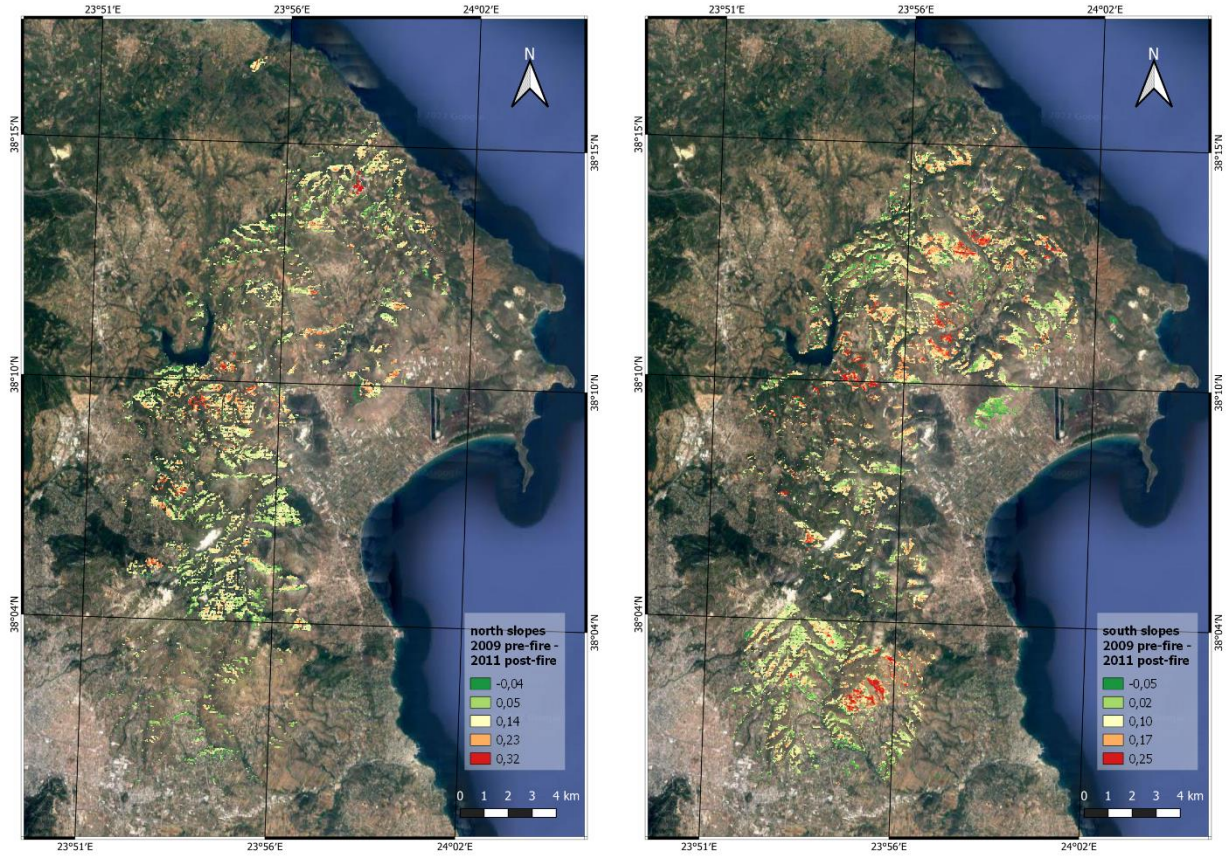

Figure 5-19: NDVI difference maps for the study burnt area between the pre-fire image (August 2009) and the post-fire image two years after the fire event (August 2011) separately for north facing slopes (left) and south-facing slopes (right)

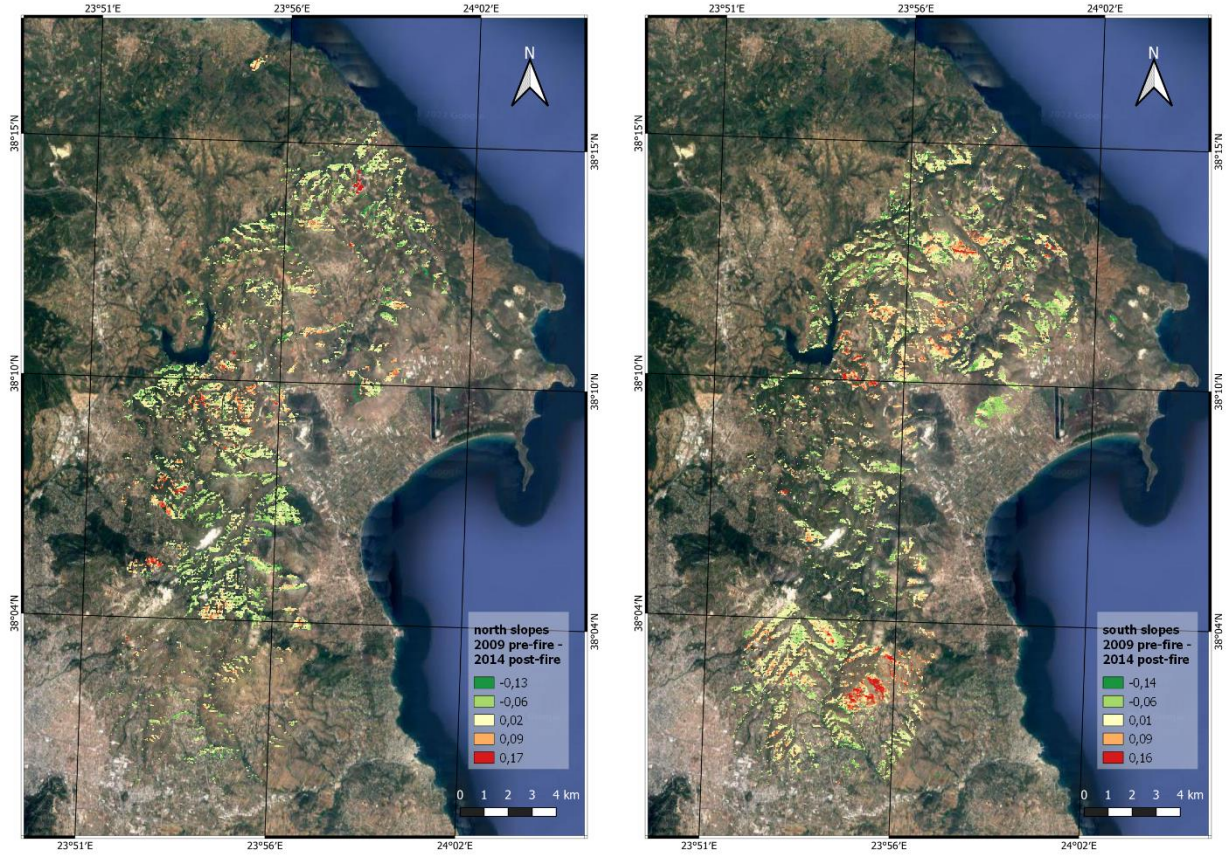

Figure 5-20: NDVI difference maps for the study burnt area between the pre-fire image (August 2009) and the post-fire image five years after the fire event (August 2014) separately for north facing slopes (left) and south-facing slopes (right)

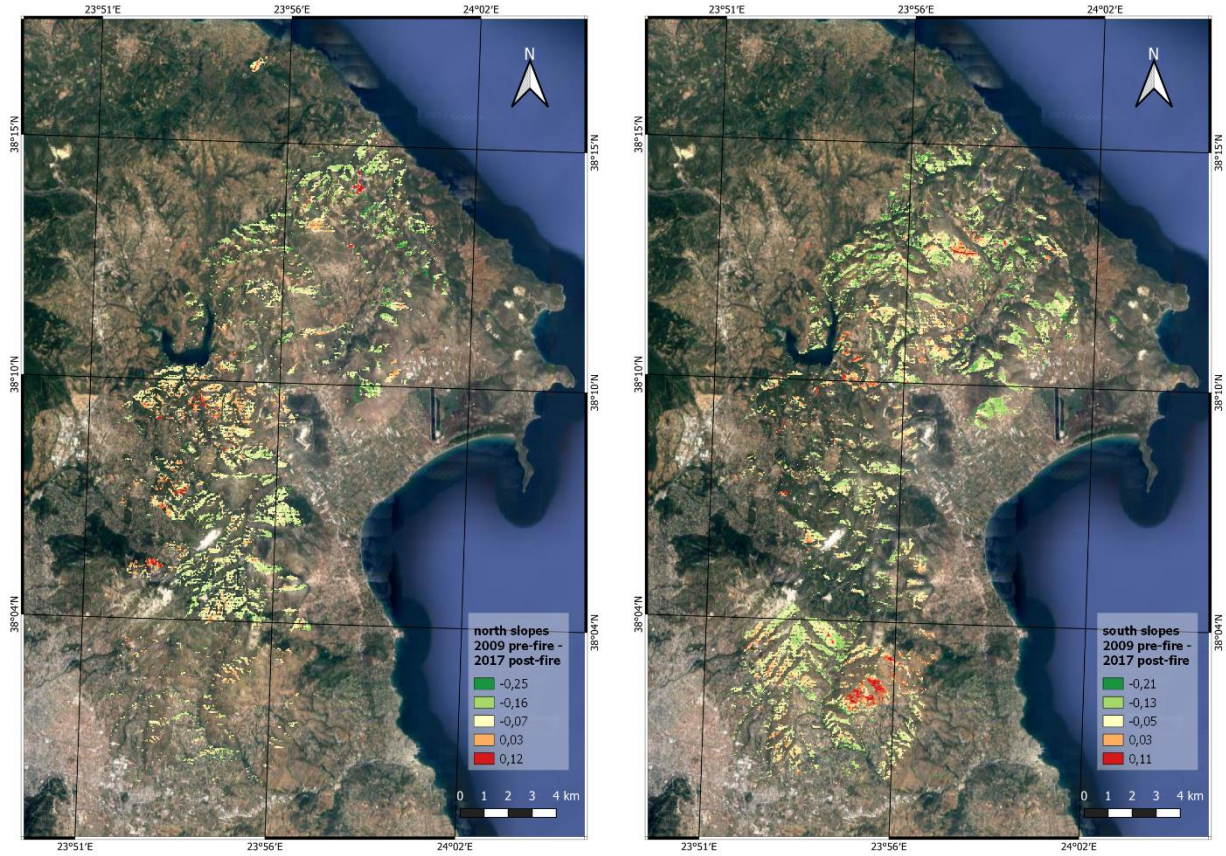

Figure 5-21: NDVI difference maps for the study burnt area between the pre-fire image (August 2009) and the post-fire image eight years after the fire event (August 2017) separately for north facing slopes (left) and south-facing slopes (right)

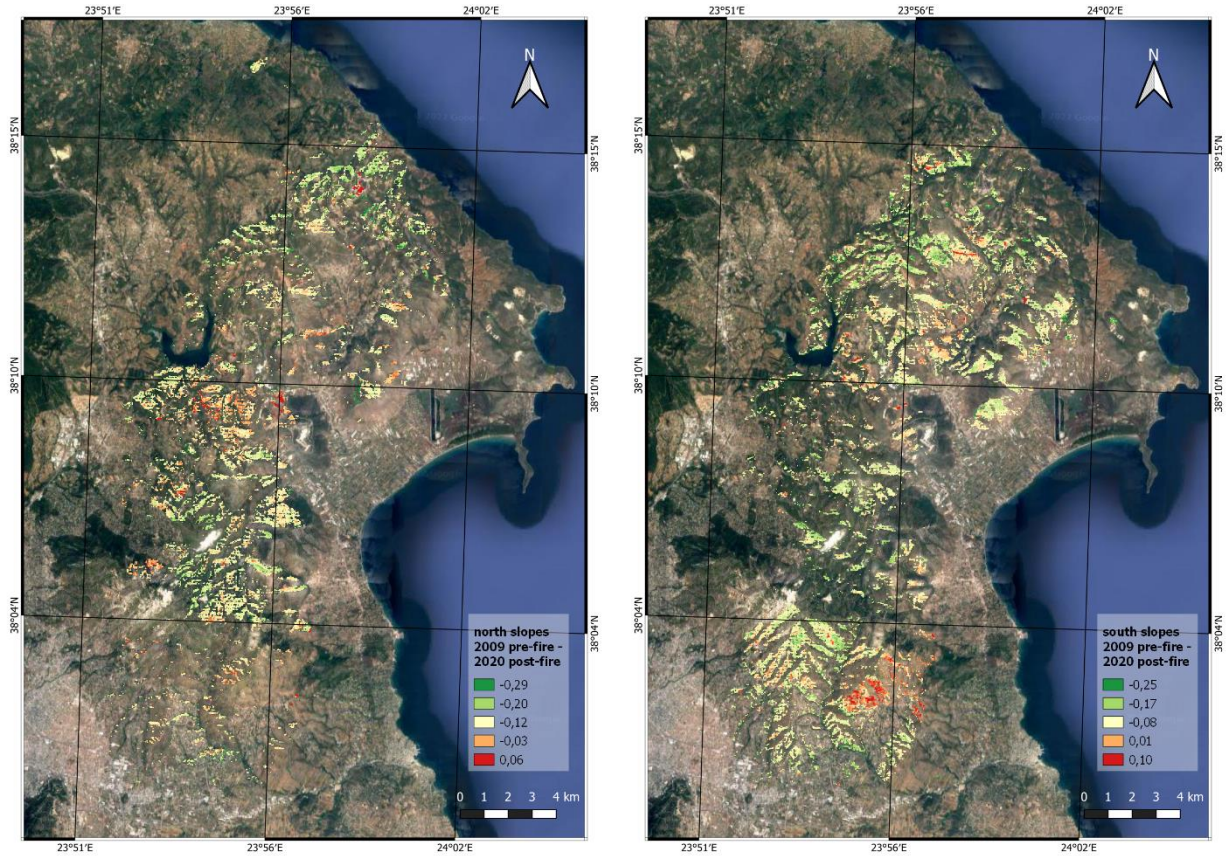

Figure 5-22: NDVI difference maps for the study burnt area between the pre-fire image (August 2009) and the post-fire image eleven years after the fire event (August 2020) separately for north facing slopes (left) and south-facing slopes (right)

5.3.4 Relationship of vegetation regrowth dynamics and topography as well as burn severity level

Finally, the investigation of the relationship of vegetation regeneration with the topography as well as the burn severity was also carried out. The results (Table 5-10 & Figure 5-23) show the previous respective outcomes from each analysis separately. Firstly, the devastating results of the fire are clear in the post-fire image after fire suppression (September 2019), however this is more intense in areas within the high and moderate-high severity classes in both aspects. Regarding the regeneration process, Figure 5-23 depicts that those areas in low and moderate-low severity classes recover faster (August 2011-August 2014) while areas in moderate-high and high severity classes takes more years to recover (August 2014-August 2017). During period 2017-2020, eight to eleven years after the fire suppression, mean NDVI is higher in all areas in contrast with the pre-fire levels, however, those areas in low and moderate-low severity classes present the highest recovery. Additionally, in all severity classes the regeneration process is higher in north-facing slopes (Figure 5-23).

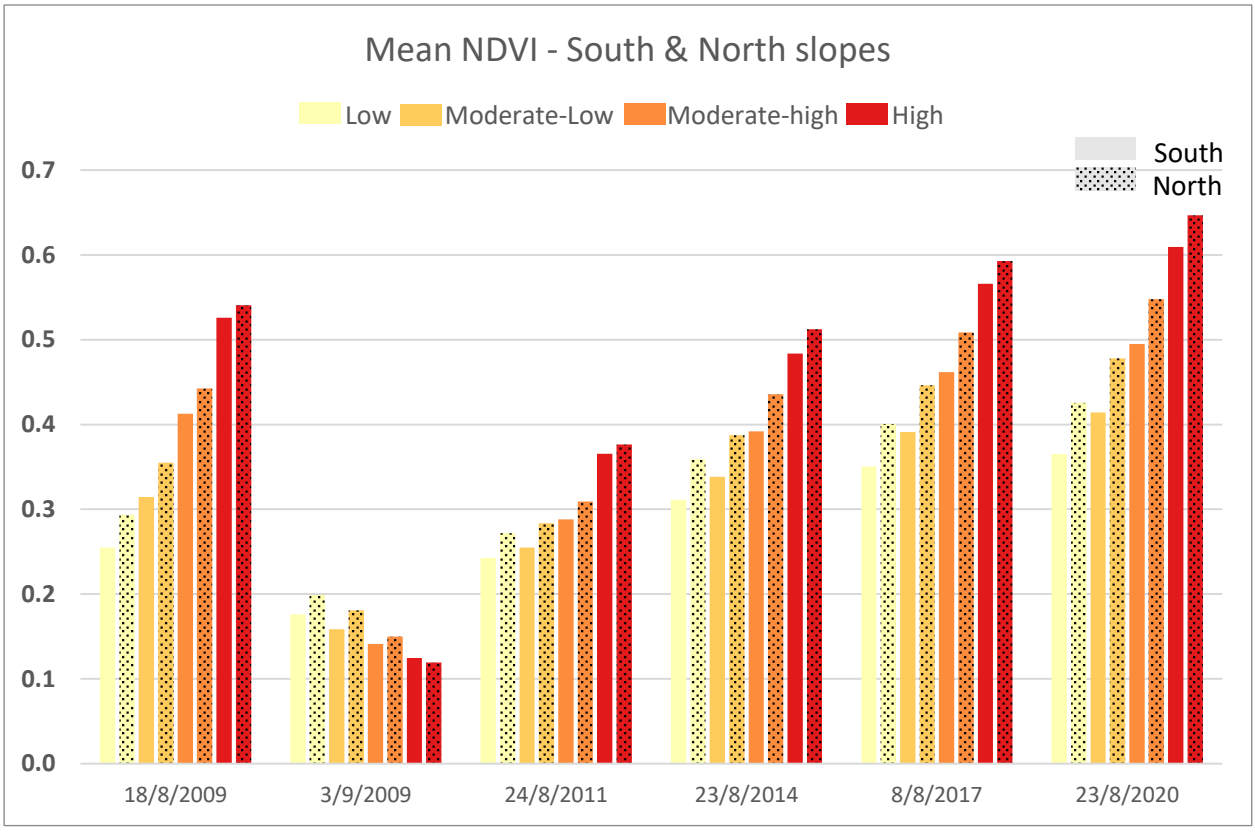

Figure 5-23: Mean NDVI of the burn scar for each severity class separately for north- and south-facing slopes

Table 5-10: Descriptive statistics of NDVI in all "anniversary" dates within study area in each severity class as well as separately for north- and south-facing slopes

	South				North			
	Min	Max	Mean	Stdev	Min	Max	Mean	Stdev
Low								
18/8/2009	0.104	0.539	0.255	0.055	0.118	0.582	0.294	0.067
3/9/2009	0.057	0.349	0.176	0.034	0.053	0.372	0.199	0.047
24/8/2011	0.061	0.644	0.243	0.049	0.026	0.491	0.272	0.056
23/8/2014	0.079	0.635	0.311	0.060	0.051	0.576	0.359	0.068
8/8/2017	0.106	0.734	0.351	0.069	0.000	0.699	0.401	0.081
23/8/2020	0.155	0.707	0.365	0.077	-0.062	0.719	0.425	0.091
Moderate-Low								
18/8/2009	0.135	0.609	0.314	0.060	0.068	0.634	0.355	0.074
3/9/2009	0.038	0.350	0.158	0.032	0.038	0.371	0.181	0.045
24/8/2011	0.074	0.579	0.255	0.052	0.014	0.595	0.283	0.062
23/8/2014	0.113	0.642	0.338	0.062	0.077	0.682	0.387	0.071
8/8/2017	0.113	0.737	0.391	0.072	0.024	0.779	0.446	0.084
23/8/2020	0.139	0.791	0.414	0.079	0.065	0.782	0.478	0.094
Moderate-high								
18/8/2009	0.216	0.691	0.413	0.061	0.179	0.738	0.443	0.062
3/9/2009	-0.004	0.350	0.141	0.026	0.032	0.417	0.150	0.036
24/8/2011	0.121	0.650	0.288	0.064	0.035	0.680	0.309	0.065
23/8/2014	0.148	0.697	0.392	0.074	0.061	0.753	0.436	0.070
8/8/2017	0.129	0.797	0.462	0.086	0.017	0.826	0.508	0.080
23/8/2020	0.183	0.800	0.495	0.090	0.074	0.845	0.548	0.087
High								
18/8/2009	0.292	0.748	0.526	0.056	0.308	0.754	0.541	0.055
3/9/2009	0.030	0.252	0.125	0.023	0.003	0.375	0.119	0.029
24/8/2011	0.150	0.700	0.366	0.077	0.049	0.677	0.376	0.076
23/8/2014	0.223	0.774	0.484	0.080	0.075	0.793	0.512	0.075
8/8/2017	0.244	0.832	0.566	0.088	0.094	0.827	0.593	0.081
23/8/2020	0.244	0.877	0.609	0.086	0.113	0.869	0.647	0.081

5.4 Re-growth dynamics using Regeneration Index

The vegetation regeneration dynamics in the study area was also investigated with the use of Regeneration Index (RI). As already mentioned, for the computation of RI, the mean NDVI of specific areas under burn scar with known types of land cover (before burning) is calculated and divided by the respective mean NDVI of a number of unburnt areas (control areas) with the same land cover. In the framework of this thesis, the calculation of the index was carried out in forest, agricultural areas and areas with shrub vegetation since they constitute the majority of the coverage of the study area. Table 5-11 and Figure 5-24 present the results of the RI computation in the study area concerning the land types of forest, agriculture and shrubs.

Table 5-11: Regeneration Index for each land cover of the study area for the entire study period

	Regeneration Index		
Dates	**Forest**	**Scrubs**	**Agriculture**
18/8/2009	0.902	0.970	1.027
3/9/2009	0.232	0.309	0.391
24/8/2011	0.523	0.561	0.774
23/8/2014	0.618	0.713	0.884
8/8/2017	0.679	0.810	0.971
23/8/2020	0.753	0.922	0.953

Firstly, concerning the selection of areas which was implemented with the use of pre-fire image (18/8/2009) as well as the Copernicus Land Cover of 2006, the results show that for areas covered by scrubs and agriculture the Regeneration Index is near 1 which means that areas within the burn scar and the respective control areas present similar conditions (similar spectral and environmental characteristic) while for forested areas where RI is about 0.902 show slightly different characteristics. Regarding the vegetation regeneration process through years, RI results clearly mirror the patterns shown by the NDVI analysis. More precisely, RI shows the gradual recovery of the burnt area within the study period which is more clear in agricultural areas as well as in areas covered with scrubs and/or herbaceous vegetation and less in forest areas.

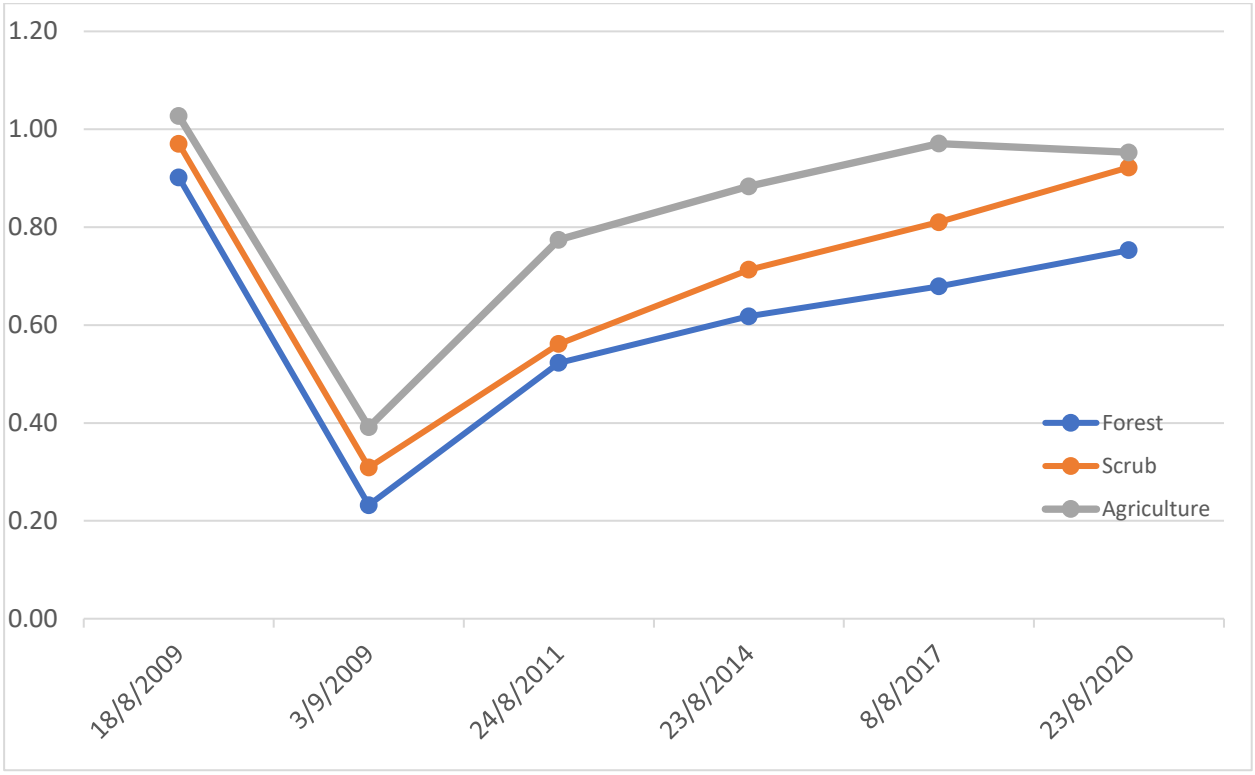

Figure 5-24: Graph showing the values of Regeneration Index for three typical land uses of the study area in each image date.

5 Discussion

Burnt area delineation was implemented with the use of Support Vector Machine supervised classification and the accuracy assessment, based on error matrix, showed that PA and UA of the burnt area class reached approximately 100% and 94% respectively. In addition, the OA and kappa statistic (K_c) of the land cover classification of the Landsat TM, pre-fire satellite image, were 93% and 0,91 respectively. Classification accuracy results reported herein are of similar accuracy compared to other studies deriving burnt area estimates from Landsat TM or other sensors as well as SVM or other classification technics. More precisely, Petropoulos et al., (2012) used satellite images from EO-1 Advanced Land Imager (ALI) radiometer as well as Landsat TM and three different classification methods, i.e. the Maximum Likelihood (ML), the Artificial Neural Networks (ANNs) and the Support Vector Machine for the delineation of the same burnt area studied in the present thesis. Results showed that SVM when applied with either ALI or TM produced the highest classification results in comparison to all other classifiers. Overall accuracy and K_c in the case of Landsat TM and SVM was 93.55 and 0.920 respectively while the PA and UA of the burnt area classification were both 100% which are all in great agreement with the results in the framework of this thesis. Also, Petropoulos et al., (2010) obtained lower overall accuracy and K_c with the use of Landsat TM and Spectral Angle Mapper (SAM) for burnt area mapping. Authors reported an OA and K_c of 83.82% and 0.795 (PA and UA of burnt area 100% and 98.72% respectively) suggesting as previously that SVM can generally produce more accurate classification than other technics. Finally, Petropoulos et al., (2011) used Landsat TM imagery and the SVM classification for the delineation of the burn scar in an area close to the study area of this thesis and the OA and K_c, with the respective parameterization of the SVM used herein (RBF kernel function based on Petropoulos et al., (2012)), were 95.87 and 0.948 (PA and UA of burnt area were both 100%) which although are higher, they are considered in agreement with the results of this study.

Regarding the vegetation regeneration process dynamics within the burn scar during the study period i.e., 2009 – 2020, the results indicate the large degree of spatial variability of the regeneration process within the study area as well as they clearly point out the damaging effects that such wildfires have on the landscape. Although many studies reported that the vegetation regeneration in the affected area is a process that can potentially take a long time (e.g. Arianoutsou et al., 2010; Petropoulos et al., 2014), the results of the vegetation regeneration

analysis conducted for the study area using the NDVI, reveal that two years after the fire event, vegetation of the burnt area shows the first steps of recovery to the pre-fire levels. Indeed, regression analysis of post-fire NDVI showed that after two years from the fire suppression, 24% of the burnt area recovered to pre-fire level. In addition, eleven years after the fire event, the vegetation regrowth analysis pointed out that the majority of the burn area (97%) recovered or improved in contrast to pre-fire NDVI values. These results are in good agreement with other studies, for example, Wittenberg et al., 2007 showed that vegetation had recovered to pre-fire conditions withing five years in Mount Carmel, Israel, even following multiple fires. Additionally, a very recent paper dealing with the issue of sclerophyllous vegetation recovering after fire, reached the same conclusions. More specifically, Smith-Ramírez et al. (2022) using satellite image analysis as well as vegetation sampling, showed that Chilean Mediterranean forested and mixed forest/shrubland cover was reached 10-20 years after the fire if no further intervention occurs. These results are in great agreement with the outcomes of this study, considering that the forest and semi natural area within study region is about 78% (Table 5-2).

As for agricultural land, a large percentage of which is present in the study area, their recovery can be quickly achieved mainly due to human intervention and the replanting of fire-damaged agricultural species. However, some species have the ability to recover such as olives where their recovery depends on the degree of heat damage, tree size and age as well as on moisture stress before and after the event (von Richter et al., 2005). For example in low intensity fire, olive trees with trunks and branches larger than 200mm can recover in contrast with younger trees with stems less than 200mm in diameter (von Richter et al., 2005).

Vegetation regeneration analysis with the use of Regeneration Index (RI) shows the similar regeneration trends as captured by NDVI i.e., the higher regrowth dynamic within the period of 2011-2014 and the slightly lower of the next years until 2020. This strong correlation between the NDVI and RI has also been reported in several studies (e.g. Ireland & Petropoulos, 2015). Additionally, RI results reveal that areas within burn scar covered, before the fire occurrence, with scrubs as well as herbaceous vegetation and agriculture, recovered and reached the NDVI levels of the respective areas outside the burnt area. On the contrary, forested areas (coniferous and mixed forest areas) although they present a gradual increase in regrowth process, they don't reach the NDVI levels of the forested unburned areas. An explanation for this discrepancy could be the difference in the functional characteristics of the vegetation between the two areas (burnt, unburnt). More specifically, for vegetation within the burn scar, although it seems that

the process of its regeneration is being achieved, it has not reached the levels of healthy respective vegetation outside the burnt area. The latter is reflected by the different NDVI values which are affected by the dissimilarities in photosynthetic activity and/or in canopy structural variations of the vegetation between the two areas. These results show that the exclusive use of NDVI for this type of work can lead to incorrect estimates regarding the regeneration dynamics of vegetation and leading to incorrect decision-making for the proper management of the fire-affected area. By adjunctive use of indicators such as RI, more detail and precision can be provided during studies on vegetation regrowth dynamics of burnt areas (Ireland & Petropoulos, 2015).

As far as burn severity analysis is concerned, the results showed that areas of highest severity burn overlapped with the areas of greatest NDVI decrease and the opposite which is in line with several studies (e.g. Miller & Yool, 2002; Ireland & Petropoulos, 2015) showing also the strong correlation between the NDVI and dNBR which was used to estimate burn severity level within burn scar (Ireland & Petropoulos, 2015). Regarding the examination of the relationship between burn severity and vegetation regeneration, the analysis showed that areas with low to moderate-low burn severity presented high regeneration dynamics and recovered within two to five years after fire event. Additionally, in areas with moderate-high and high burn severity covered mainly of sclerophyllous and herbaceous vegetation, shrubs and forested areas (coniferous, mixed forests), regeneration rates were more gradual, and took approximately a decade to revert to pre-fire levels. These results suggest that low severity burn cause less damage to vegetation leading to quicker recovery, while higher severity levels cause extensive vegetation destruction and as a result regrowth process takes longer to reach pre-fire levels. These spatial trends between the burn severity and the vegetation regeneration has also been reported in literature for example in Ireland & Petropoulos (2015).

The examination of the relationship of regeneration process with aspect showed that north facing aspects have a slightly greater regeneration rate compared to south facing exposures which is common with many other studies (e.g. Mouillot et al., 2005; Fox et al., 2008; Ireland & Petropoulos, 2015). This difference in vegetation regeneration reflects the effects of aspect and other topographic elements such as elevation, slope and position on the modification of local environment (Daws et al., 2002; Moeslund et al., 2013; Jucker et al., 2018). Due to the different solar radiation received (Yetemen et al., 2015), the differential environments between north- and south-facing slopes is a global phenomenon at northern hemisphere (Yang et al., 2020).

Especially aspect significantly influences microclimate (e.g. evapotranspiration, air temperature, wind speed) (Burnett et al., 2008), soil property (e.g., soit texture, organic matter content) (Lozano-García et al., 2016) and hydrological processes (e.g., runoff dynamics, soil water retention, hydraulic conductivity) (Casanova et al., 2000; Broxton et al., 2009; L. Wang et al., 2011), elements which are playing an important role in triggering vegetation re-growth (Petropoulos et al., 2014).

6 Conclusions & Future work

In this thesis an analysis of vegetation regeneration dynamics of a burnt Mediterranean ecosystem, in Attica, Greece, with a use of EO and GIS was presented. More specifically, the spatio-temporal variation of vegetation regeneration dynamics within the burn scar, over a period of 11 years after fire, was studied using Landsat TM and OLI satellite images as well as GIS and assessed the degree of the vegetation recovery to pre-fire levels. For this purpose, the widely used NDVI index as well as the Regeneration Index was used. Also, the relationship of vegetation regeneration dynamics with burn severity as well as topographical factors such as aspect was explored.

The results of the vegetation regeneration analysis, revealed that two years after the fire event, vegetation of the burnt area shows the first steps of recovery to the pre-fire levels. Additionally, eleven years after the fire event, the vegetation regrowth analysis showed that the majority of the burn area (97%) recovered or improved in contrast to pre-fire NDVI values. Regarding the analysis conducting with the use of RI, results showed the similar regeneration trends as captured by NDVI as far as scrubs, herbaceous vegetation, woodlands and agricultural areas are concerned. On the contrary, forested areas (coniferous and mixed forest areas) although they presented a gradual increase in regrowth process, they didn't reach the NDVI levels of the forested unburned areas. In addition, the examination of the relationship between burn severity and vegetation regeneration showed that areas with low to moderate-low burn severity presented high regeneration dynamics and recovered within two to five years after fire event. Moreover, areas with moderate-high and high burn severity covered mainly of sclerophyllous and herbaceous vegetation, shrubs and forested areas (coniferous, mixed forests), regeneration rates were more gradual, and took approximately a decade to revert to pre-fire levels. Finally, regarding the relationship between the vegetation regrowth dynamics and aspects, the outcomes of the analysis revealed that north facing aspects have a slightly greater regeneration rate compared to south facing exposures which it might be due to more favourable micro-climatic and hydrological conditions for vegetation growth in these areas.

An understanding of the spatio-temporal patterns of vegetation regeneration dynamics in fire-affected areas can contribute to the better appreciation of post-fire landscape processes. This can subsequently lead to the effective management of post-fire ecosystems, taking the corresponding recovery measures and drawing up prevention policies and strategies.

Additionally, the present study contributes to the understanding of Mediterranean landscape dynamics, and corroborates the usefulness of NDVI and RI in post-fire vegetation regrowth assessment. Last but not least, it confirms that Earth Observation technology and GIS techniques can provide a potentially operational solution to support local studies regarding the assessment of vegetation regeneration, provided that satellite data can be acquired at regular time intervals with the appropriate resolution over a given region.

Regarding future work, this would be the more detailed study of the vegetation such as investigation of species composition since NDVI only provides knowledge of large-scale vegetation coverage without detailed vegetation information. To this end, very high-resolution satellite data and field campaigns would be essential for the validation of the information regarding the regrowth dynamics of the studied area. Last but not least, it will be interesting in future work to explore the spatio-temporal relationships of burn severity and vegetation regeneration with other physical factors, such as the type of the actual fuel burnt, slope angle or soil type.

7 References

Alexandris, N., Gupta, S., & Koutsias, N. (2017). Remote sensing of burned areas via PCA, Part 1; centering, scaling and EVD vs SVD. *Open Geospatial Data, Software and Standards*, *2*(1), 17. https://doi.org/10.1186/s40965-017-0028-1

Al-Rawi, K. R., Casanova, J. L., & Calle, A. (2001). Burned area mapping system and fire detection system, based on neural networks and NOAA-AVHRR imagery. *International Journal of Remote Sensing*, *22*(10), 2015–2032. https://doi.org/10.1080/01431160117531

Arianoutsou, M., Christopoulou, A., Kazanis, D., Tountas, T., Ganou, E., Bazos, I., & Kokkoris, Y. (2010). Effects of fire on high altitude coniferous forests of Greece. *Sixth International Conference of Wildland Fire, Coimbra*, 12.

Barbosa, P. M., Grégoire, J.-M., & Pereira, J. M. C. (1999). An Algorithm for Extracting Burned Areas from Time Series of AVHRR GAC Data Applied at a Continental Scale. *Remote Sensing of Environment*, *69*(3), 253–263. https://doi.org/10.1016/S0034-4257(99)00026-7

Bartalev, S. A., Egorov, V. A., Loupian, E. A., & Uvarov, I. A. (2007). Multi-year circumpolar assessment of the area burnt in boreal ecosystems using SPOT-VEGETATION. *International Journal of Remote Sensing*, *28*(6), 1397–1404. https://doi.org/10.1080/01431160600840978

Bastarrika, A., Chuvieco, E., & Martín, M. P. (2011). Mapping burned areas from Landsat TM/ETM+ data with a two-phase algorithm: Balancing omission and commission errors. *Remote Sensing of Environment*, *115*(4), 1003–1012. https://doi.org/10.1016/j.rse.2010.12.005

Brewer, C. K., Winne, J. C., Redmond, R. L., Opitz, D. W., & Mangrich, M. V. (2005). Classifying and Mapping Wildfire Severity: A Comparison of Methods. *Photogrammetric Engineering & Remote Sensing*, *71*, 1311–1320.

Broxton, P. D., Troch, P. A., & Lyon, S. W. (2009). On the role of aspect to quantify water transit times in small mountainous catchments. *Water Resources Research*, *45*(8). https://doi.org/10.1029/2008WR007438

Burnett, B. N., Meyer, G. A., & McFadden, L. D. (2008). Aspect-related microclimatic influences on slope forms and processes, northeastern Arizona. *Journal of Geophysical Research: Earth Surface*, *113*(F3). https://doi.org/10.1029/2007JF000789

Cai, L., & Wang, M. (2022). Is the RdNBR a better estimator of wildfire burn severity than the dNBR? A discussion and case study in southeast China. *Geocarto International*, *37*(3), 758–772. https://doi.org/10.1080/10106049.2020.1737973

Caldararo, N. (2002). Human ecological intervention and the role of forest fires in human ecology. *Science of The Total Environment*, *292*(3), 141–165. https://doi.org/10.1016/S0048-9697(01)01067-1

Cao, X., Chen, J., Matsushita, B., Imura, H., & Wang, L. (2009). An automatic method for burn scar mapping using support vector machines. *International Journal of Remote Sensing*, *30*(3), 577–594. https://doi.org/10.1080/01431160802220219

Capitanio, R., & Carcaillet, C. (2008). Post-fire Mediterranean vegetation dynamics and diversity: A discussion of succession models. *Forest Ecology and Management*, *255*(3), 431–439. https://doi.org/10.1016/j.foreco.2007.09.010

Casady, G. M., van Leeuwen, W. J. D., & Marsh, S. E. (2010). Evaluating Post-wildfire Vegetation Regeneration as a Response to Multiple Environmental Determinants. *Environmental Modeling & Assessment*, *15*(5), 295–307. https://doi.org/10.1007/s10666-009-9210-x

Casanova, M., Messing, I., & Joel, A. (2000). Influence of aspect and slope gradient on hydraulic conductivity measured by tension infiltrometer. *Hydrological Processes*, *14*(1), 155–164. https://doi.org/10.1002/(SICI)1099-1085(200001)14:1<155::AID-HYP917>3.0.CO;2-J

Chen, D., Fu, C., Hall, J. V., Hoy, E. E., & Loboda, T. V. (2021). Spatio-temporal patterns of optimal Landsat data for burn severity index calculations: Implications for high northern latitudes wildfire research. *Remote Sensing of Environment*, *258*, 112393. https://doi.org/10.1016/j.rse.2021.112393

Chen, D., Loboda, T. V., & Hall, J. V. (2020). A systematic evaluation of influence of image selection process on remote sensing-based burn severity indices in North American boreal forest and tundra ecosystems. *ISPRS Journal of Photogrammetry and Remote Sensing*, *159*, 63–77. https://doi.org/10.1016/j.isprsjprs.2019.11.011

Chen, S., Chen, L., Liu, Q., Li, X., & Tan, Q. (2005). Remote sensing and GIS-based integrated analysis of coastal changes and their environmental impacts in Lingding Bay, Pearl River Estuary, South China. *Ocean & Coastal Management*, *48*(1), 65–83. https://doi.org/10.1016/j.ocecoaman.2004.11.004

Chen, X., Vogelmann, J. E., Rollins, M., Ohlen, D., Key, C. H., Yang, L., Huang, C., & Shi, H. (2011). Detecting post-fire burn severity and vegetation recovery using multitemporal remote sensing spectral indices and field-collected composite burn index data in a ponderosa pine forest. *International Journal of Remote Sensing*, *32*(23), 7905–7927. https://doi.org/10.1080/01431161.2010.524678

Chompuchan, C., & Lin, C.-Y. (2017). Assessment of forest recovery at Wu-Ling fire scars in Taiwan using multi-temporal Landsat imagery. *Ecological Indicators*, *79*, 196–206. https://doi.org/10.1016/j.ecolind.2017.04.038

Chu, T., Guo, X., & Takeda, K. (2017). Effects of Burn Severity and Environmental Conditions on Post-Fire Regeneration in Siberian Larch Forest. *Forests*, *8*(3), 76. https://doi.org/10.3390/f8030076

Chuvieco, E., & Congalton, R. G. (1988). Mapping and inventory of forest fires from digital processing of tm data. *Geocarto International*, *3*(4), 41–53. https://doi.org/10.1080/10106048809354180

Chuvieco, E., Riaño, D., Aguado, I., & Cocero, D. (2002). Estimation of fuel moisture content from multitemporal analysis of Landsat Thematic Mapper reflectance data: Applications in fire danger assessment. *International Journal of Remote Sensing*, *23*(11), 2145–2162. https://doi.org/10.1080/01431160110069818

Chuvieco, E., Ventura, G., Martín, M. P., & Gómez, I. (2005). Assessment of multitemporal compositing techniques of MODIS and AVHRR images for burned land mapping. *Remote Sensing of Environment*, *94*(4), 450–462. https://doi.org/10.1016/j.rse.2004.11.006

Climate change, impacts and vulnerability in Europe 2016—European Environment Agency. (n.d.). [Publication]. Retrieved 27 August 2022, from https://www.eea.europa.eu/publications/climate-change-impacts-and-vulnerability-2016

Congalton, R. G., & Green, K. (2019). *Assessing the Accuracy of Remotely Sensed Data: Principles and Practices, Third Edition* (3rd ed.). CRC Press. https://doi.org/10.1201/9780429052729

Daws, M. I., Mullins, C. E., Burslem, D. F. R. P., Paton, S. R., & Dalling, J. W. (2002). Topographic position affects the water regime in a semideciduous tropical forest in Panamá. *Plant and Soil*, *238*(1), 79–89. https://doi.org/10.1023/A:1014289930621

Dimitrakopoulos, A. P., Vlahou, M., Anagnostopoulou, Ch. G., & Mitsopoulos, I. D. (2011). Impact of drought on wildland fires in Greece: Implications of climatic change? *Climatic Change*, *109*(3), 331–347. https://doi.org/10.1007/s10584-011-0026-8

Dragozi, E., Gitas, I. Z., Stavrakoudis, D. G., & Theocharis, J. B. (2014). Burned Area Mapping Using Support Vector Machines and the FuzCoC Feature Selection Method on VHR IKONOS Imagery. *Remote Sensing*, *6*(12), 12005–12036. https://doi.org/10.3390/rs61212005

Duncan, B. W., Shao, G., & Adrian, F. W. (2009). Delineating a managed fire regime and exploring its relationship to the natural fire regime in East Central Florida, USA: A remote sensing and GIS approach. *Forest Ecology and Management*, *258*(2), 132–145. https://doi.org/10.1016/j.foreco.2009.03.053

Dupuy, J., Fargeon, H., Martin-StPaul, N., Pimont, F., Ruffault, J., Guijarro, M., Hernando, C., Madrigal, J., & Fernandes, P. (2020). Climate change impact on future wildfire danger and activity in southern Europe: A review. *Annals of Forest Science*, *77*(2), 1–24. https://doi.org/10.1007/s13595-020-00933-5

Durduran, S. S. (2010). Coastline change assessment on water reservoirs located in the Konya Basin Area, Turkey, using multitemporal landsat imagery. *Environmental Monitoring and Assessment*, *164*(1), 453–461. https://doi.org/10.1007/s10661-009-0906-9

Escuin, S., Navarro, R., & Fernández, P. (2008). Fire severity assessment by using NBR (Normalized Burn Ratio) and NDVI (Normalized Difference Vegetation Index) derived from LANDSAT TM/ETM images. *International Journal of Remote Sensing*, *29*(4), 1053–1073. https://doi.org/10.1080/01431160701281072

Eva, H., & Lambin, E. F. (1998). Burnt area mapping in Central Africa using ATSR data. *International Journal of Remote Sensing*, *19*(18), 3473–3497. https://doi.org/10.1080/014311698213768

Fernandez-Manso, A., Quintano, C., & Roberts, D. A. (2016). Burn severity influence on post-fire vegetation cover resilience from Landsat MESMA fraction images time series in Mediterranean forest ecosystems. *Remote Sensing of Environment*, *184*, 112–123. https://doi.org/10.1016/j.rse.2016.06.015

Fernandez-Manso, A., Quintano, C., & Roberts, D. A. (2019). Burn severity analysis in Mediterranean forests using maximum entropy model trained with EO-1 Hyperion and LiDAR data. *ISPRS Journal of Photogrammetry and Remote Sensing*, *155*, 102–118. https://doi.org/10.1016/j.isprsjprs.2019.07.003

Ferran, A., Delitti, W., & Vallejo, V. R. (2005). Effects of fire recurrence in Quercus coccifera L. shrublands of the Valencia Region (Spain): II. plant and soil nutrients. *Plant Ecology*, *177*(1), 71–83. https://doi.org/10.1007/s11258-005-2141-y

Fornacca, D., Ren, G., & Xiao, W. (2018). Evaluating the Best Spectral Indices for the Detection of Burn Scars at Several Post-Fire Dates in a Mountainous Region of Northwest Yunnan, China. *Remote Sensing*, *10*(8), 1196. https://doi.org/10.3390/rs10081196

Fox, D. M., Maselli, F., & Carrega, P. (2008). Using SPOT images and field sampling to map burn severity and vegetation factors affecting post forest fire erosion risk. *CATENA*, *75*(3), 326–335. https://doi.org/10.1016/j.catena.2008.08.001

Fraser, R. H., Li, Z., & Cihlar, J. (2000). Hotspot and NDVI Differencing Synergy (HANDS): A New Technique for Burned Area Mapping over Boreal Forest. *Remote Sensing of Environment*, *74*(3), 362–376. https://doi.org/10.1016/S0034-4257(00)00078-X

Frazier, R. J., Coops, N. C., Wulder, M. A., Hermosilla, T., & White, J. C. (2018). Analyzing spatial and temporal variability in short-term rates of post-fire vegetation return from Landsat time series. *Remote Sensing of Environment*, *205*, 32–45. https://doi.org/10.1016/j.rse.2017.11.007

French, N. H. F., Kasischke, E. S., Hall, R. J., Murphy, K. A., Verbyla, D. L., Hoy, E. E., Allen, J. L., French, N. H. F., Kasischke, E. S., Hall, R. J., Murphy, K. A., Verbyla, D. L., Hoy, E. E., & Allen, J. L. (2008). Using Landsat data to assess fire and burn severity in the North American boreal forest region: An overview and summary of results. *International Journal of Wildland Fire*, *17*(4), 443–462. https://doi.org/10.1071/WF08007

García-Llamas, P., Suárez-Seoane, S., Fernández-Guisuraga, J. M., Fernández-García, V., Fernández-Manso, A., Quintano, C., Taboada, A., Marcos, E., & Calvo, L. (2019). Evaluation and comparison of Landsat 8, Sentinel-2 and Deimos-1 remote sensing indices for assessing burn severity in Mediterranean fire-prone ecosystems. *International Journal of Applied Earth Observation and Geoinformation*, *80*, 137–144. https://doi.org/10.1016/j.jag.2019.04.006

Gens, R. (2010). Remote sensing of coastlines: Detection, extraction and monitoring. *International Journal of Remote Sensing*, *31*(7), 1819–1836. https://doi.org/10.1080/01431160902926673

Gibson, R., Danaher, T., Hehir, W., & Collins, L. (2020). A remote sensing approach to mapping fire severity in south-eastern Australia using sentinel 2 and random forest. *Remote Sensing of Environment*, *240*, 111702. https://doi.org/10.1016/j.rse.2020.111702

Giddey, B. L., Baard, J. A., & Kraaij, T. (2022). Verification of the differenced Normalised Burn Ratio (dNBR) as an index of fire severity in Afrotemperate Forest. *South African Journal of Botany*, *146*, 348–353. https://doi.org/10.1016/j.sajb.2021.11.005

Giglio, L., Loboda, T., Roy, D. P., Quayle, B., & Justice, C. O. (2009). An active-fire based burned area mapping algorithm for the MODIS sensor. *Remote Sensing of Environment*, *113*(2), 408–420. https://doi.org/10.1016/j.rse.2008.10.006

Gitas, I., Mitri, G., Veraverbeke, S., & Polychronaki, A. (2012). Advances in Remote Sensing of Post-Fire Vegetation Recovery Monitoring—A Review. In L. Fatoyinbo (Ed.), *Remote Sensing of Biomass—Principles and Applications*. InTech. https://doi.org/10.5772/20571

Gitas, I., Polychronaki, A., Katagis, T., & Mallinis, G. (2008). Contribution of remote sensing to disaster management activities: A case study of the large fires in the Peloponnese, Greece. *International Journal of Remote Sensing*, *29*(6), 1847–1853. https://doi.org/10.1080/01431160701874553

Gitas, I. Z., Mitri, G. H., & Ventura, G. (2004). Object-based image classification for burned area mapping of Creus Cape, Spain, using NOAA-AVHRR imagery. *Remote Sensing of Environment*, *92*(3), 409–413. https://doi.org/10.1016/j.rse.2004.06.006

Gong, X., Brueck, H., Giese, K. M., Zhang, L., Sattelmacher, B., & Lin, S. (2008). Slope aspect has effects on productivity and species composition of hilly grassland in the Xilin River Basin, Inner Mongolia, China. *Journal of Arid Environments*, *72*(4), 483–493. https://doi.org/10.1016/j.jaridenv.2007.07.001

Gouveia, C., DaCamara, C. C., & Trigo, R. M. (2010). Post-fire vegetation recovery in Portugal based on spot/vegetation data. *Natural Hazards and Earth System Sciences*, *10*(4), 673–684. https://doi.org/10.5194/nhess-10-673-2010

Hall, R. J., Freeburn, J. T., Groot, W. J. de, Pritchard, J. M., Lynham, T. J., Landry, R., Hall, R. J., Freeburn, J. T., Groot, W. J. de, Pritchard, J. M., Lynham, T. J., & Landry, R. (2008). Remote sensing of burn severity: Experience from western Canada boreal fires*. *International Journal of Wildland Fire*, *17*(4), 476–489. https://doi.org/10.1071/WF08013

He, Y., Chen, G., De Santis, A., Roberts, D. A., Zhou, Y., & Meentemeyer, R. K. (2019). A disturbance weighting analysis model (DWAM) for mapping wildfire burn severity in the presence of forest disease. *Remote Sensing of Environment*, *221*, 108–121. https://doi.org/10.1016/j.rse.2018.11.015

Hope, A., Tague, C., & Clark, R. (2007). Characterizing post-fire vegetation recovery of California chaparral using TM/ETM+ time-series data. *International Journal of Remote Sensing*, *28*(6), 1339–1354. https://doi.org/10.1080/01431160600908924

Hultquist, C., Chen, G., & Zhao, K. (2014). A comparison of Gaussian process regression, random forests and support vector regression for burn severity assessment in diseased forests. *Remote Sensing Letters*, *5*(8), 723–732. https://doi.org/10.1080/2150704X.2014.963733

Ireland, G., & Petropoulos, G. P. (2015). Exploring the relationships between post-fire vegetation regeneration dynamics, topography and burn severity: A case study from the Montane Cordillera Ecozones of Western Canada. *Applied Geography*, *56*, 232–248. https://doi.org/10.1016/j.apgeog.2014.11.016

Joint Research Centre (European Commission), Ciscar, J. C., Feyen, L., Ibarreta, D., & Soria, A. (2018). *Climate impacts in Europe: Final report of the JRC PESETA III project*. Publications Office of the European Union. https://data.europa.eu/doi/10.2760/93257

Joint Research Centre (European Commission), Costa, H., Rigo, D. de, Libertà, G., Houston Durrant, T., & San-Miguel-Ayanz, J. (2020). *European wildfire danger and vulnerability in a changing climate: Towards integrating risk dimensions : JRC PESETA IV project : Task 9 forest fires*. Publications Office of the European Union. https://data.europa.eu/doi/10.2760/46951

Jucker, T., Bongalov, B., Burslem, D. F. R. P., Nilus, R., Dalponte, M., Lewis, S. L., Phillips, O. L., Qie, L., & Coomes, D. A. (2018). Topography shapes the structure, composition and function of tropical forest landscapes. *Ecology Letters*, *21*(7), 989–1000. https://doi.org/10.1111/ele.12964

Kalivas, D. P., Petropoulos, G. P., Athanasiou, I. M., & Kollias, V. J. (2013). An intercomparison of burnt area estimates derived from key operational products: The Greek wildland fires of 2005–2007. *Nonlinear Processes in Geophysics*, *20*(3), 397–409. https://doi.org/10.5194/npg-20-397-2013

Keeley, J. E. (2009). Fire intensity, fire severity and burn severity: A brief review and suggested usage. *International Journal of Wildland Fire*, *18*(1), 116–126. https://doi.org/10.1071/WF07049

Keeley, J. E., Bond, W. J., Bradstock, R. A., Pausas, J. G., & Rundel, P. W. (2011). *Fire in Mediterranean Ecosystems: Ecology, Evolution and Management*. Cambridge University Press. https://doi.org/10.1017/CBO9781139033091

Kokaly, R. F., Rockwell, B. W., Haire, S. L., & King, T. V. V. (2007). Characterization of post-fire surface cover, soils, and burn severity at the Cerro Grande Fire, New Mexico, using hyperspectral and multispectral remote sensing. *Remote Sensing of Environment*, *106*(3), 305–325. https://doi.org/10.1016/j.rse.2006.08.006

Kontoes, C. C., Poilvé, H., Florsch, G., Keramitsoglou, I., & Paralikidis, S. (2009). A comparative analysis of a fixed thresholding vs. A classification tree approach for operational burn scar detection and mapping. *International Journal of Applied Earth Observation and Geoinformation*, *11*(5), 299–316. https://doi.org/10.1016/j.jag.2009.04.001

Koutsias, N., Arianoutsou, M., Kallimanis, A. S., Mallinis, G., Halley, J. M., & Dimopoulos, P. (2012). Where did the fires burn in Peloponnisos, Greece the summer of 2007? Evidence for a synergy of fuel and weather. *Agricultural and Forest Meteorology*, *156*, 41–53. https://doi.org/10.1016/j.agrformet.2011.12.006

Koutsias, N., & Karteris, M. (2000). Burned area mapping using logistic regression modeling of a single post-fire Landsat-5 Thematic Mapper image. *International Journal of Remote Sensing*, *21*(4), 673–687. https://doi.org/10.1080/014311600210506

Lazzeri, G., Frodella, W., Rossi, G., & Moretti, S. (2021). Multitemporal Mapping of Post-Fire Land Cover Using Multiplatform PRISMA Hyperspectral and Sentinel-UAV Multispectral Data: Insights from Case Studies in Portugal and Italy. *Sensors*, *21*(12), 3982. https://doi.org/10.3390/s21123982

Lentile, L. B., Holden, Z. A., Smith, A. M. S., Falkowski, M. J., Hudak, A. T., Morgan, P., Lewis, S. A., Gessler, P. E., Benson, N. C., Lentile*, L. B., Holden*, Z. A., Smith*, A. M. S., Falkowski, M. J., Hudak, A. T., Morgan, P., Lewis, S. A., Gessler, P. E., & Benson, N. C. (2006). Remote

sensing techniques to assess active fire characteristics and post-fire effects. *International Journal of Wildland Fire*, *15*(3), 319–345. https://doi.org/10.1071/WF05097

Lillesand, T., Kiefer, R. W., & Chipman, J. (2015). *Remote Sensing and Image Interpretation*. John Wiley & Sons.

Liu, C., Frazier, P., & Kumar, L. (2007). Comparative assessment of the measures of thematic classification accuracy. *Remote Sensing of Environment*, *107*(4), 606–616. https://doi.org/10.1016/j.rse.2006.10.010

Llorens, R., Sobrino, J. A., Fernández, C., Fernández-Alonso, J. M., & Vega, J. A. (2021). A methodology to estimate forest fires burned areas and burn severity degrees using Sentinel-2 data. Application to the October 2017 fires in the Iberian Peninsula. *International Journal of Applied Earth Observation and Geoinformation*, *95*, 102243. https://doi.org/10.1016/j.jag.2020.102243

Loboda, T., O'Neal, K. J., & Csiszar, I. (2007). Regionally adaptable dNBR-based algorithm for burned area mapping from MODIS data. *Remote Sensing of Environment*, *109*(4), 429–442. https://doi.org/10.1016/j.rse.2007.01.017

Loboda, T. V., French, N. H. F., Hight-Harf, C., Jenkins, L., & Miller, M. E. (2013). Mapping fire extent and burn severity in Alaskan tussock tundra: An analysis of the spectral response of tundra vegetation to wildland fire. *Remote Sensing of Environment*, *134*, 194–209. https://doi.org/10.1016/j.rse.2013.03.003

Louhaichi, M., Toshpulot, R., Moyo, H. P., & Belgacem, A. O. (2021). Effect of slope aspect on vegetation characteristics in mountain rangelands of Tajikistan: Considerations for future ecological management and restoration. *African Journal of Range & Forage Science*, *0*(0), 1–9. https://doi.org/10.2989/10220119.2021.1951840

Lozano-García, B., Parras-Alcántara, L., & Brevik, E. C. (2016). Impact of topographic aspect and vegetation (native and reforested areas) on soil organic carbon and nitrogen budgets in

Mediterranean natural areas. *Science of The Total Environment*, *544*, 963–970. https://doi.org/10.1016/j.scitotenv.2015.12.022

Mather, P. M., & Koch, M. (2011). *Computer Processing of Remotely-Sensed Images: An Introduction*. John Wiley & Sons.

Meng, R., Wu, J., Schwager, K. L., Zhao, F., Dennison, P. E., Cook, B. D., Brewster, K., Green, T. M., & Serbin, S. P. (2017). Using high spatial resolution satellite imagery to map forest burn severity across spatial scales in a Pine Barrens ecosystem. *Remote Sensing of Environment*, *191*, 95–109. https://doi.org/10.1016/j.rse.2017.01.016

Miller, J. D., Knapp, E. E., Key, C. H., Skinner, C. N., Isbell, C. J., Creasy, R. M., & Sherlock, J. W. (2009). Calibration and validation of the relative differenced Normalized Burn Ratio (RdNBR) to three measures of fire severity in the Sierra Nevada and Klamath Mountains, California, USA. *Remote Sensing of Environment*, *113*(3), 645–656. https://doi.org/10.1016/j.rse.2008.11.009

Miller, J. D., & Thode, A. E. (2007). Quantifying burn severity in a heterogeneous landscape with a relative version of the delta Normalized Burn Ratio (dNBR). *Remote Sensing of Environment*, *109*(1), 66–80. https://doi.org/10.1016/j.rse.2006.12.006

Miller, J. D., & Yool, S. R. (2002). Mapping forest post-fire canopy consumption in several overstory types using multi-temporal Landsat TM and ETM data. *Remote Sensing of Environment*, *82*(2), 481–496. https://doi.org/10.1016/S0034-4257(02)00071-8

Mitri, G. H., & Gitas, I. Z. (2013). Mapping post-fire forest regeneration and vegetation recovery using a combination of very high spatial resolution and hyperspectral satellite imagery. *International Journal of Applied Earth Observation and Geoinformation*, *20*, 60–66. https://doi.org/10.1016/j.jag.2011.09.001

Moeslund, J. E., Arge, L., Bøcher, P. K., Dalgaard, T., & Svenning, J.-C. (2013). Topography as a driver of local terrestrial vascular plant diversity patterns. *Nordic Journal of Botany*, *31*(2), 129–144. https://doi.org/10.1111/j.1756-1051.2013.00082.x

Moreira, F., Ascoli, D., Safford, H., Adams, M. A., Moreno, J. M., Pereira, J. M. C., Catry, F. X., Armesto, J., Bond, W., González, M. E., Curt, T., Koutsias, N., McCaw, L., Price, O., Pausas, J. G., Rigolot, E., Stephens, S., Tavsanoglu, C., Vallejo, V. R., … Fernandes, P. M. (2020). Wildfire management in Mediterranean-type regions: Paradigm change needed. *Environmental Research Letters*, *15*(1), 011001. https://doi.org/10.1088/1748-9326/ab541e

Moreira, F., Catry, F., Duarte, I., Acácio, V., & Silva, J. S. (2009). A conceptual model of sprouting responses in relation to fire damage: An example with cork oak (Quercus suber L.) trees in Southern Portugal. In A. G. Van der Valk (Ed.), *Forest Ecology: Recent Advances in Plant Ecology* (pp. 77–85). Springer Netherlands. https://doi.org/10.1007/978-90-481-2795-5_7

Morresi, D., Marzano, R., Lingua, E., Motta, R., & Garbarino, M. (2022). Mapping burn severity in the western Italian Alps through phenologically coherent reflectance composites derived from Sentinel-2 imagery. *Remote Sensing of Environment*, *269*, 112800. https://doi.org/10.1016/j.rse.2021.112800

Mouillot, F., Ratte, J.-P., Joffre, R., Mouillot, D., & Serge Rambal, and. (2005). Long-term forest dynamic after land abandonment in a fire prone Mediterranean landscape (central Corsica, France). *Landscape Ecology*, *20*(1), 101–112. https://doi.org/10.1007/s10980-004-1297-5

Oliveira, S. L. J., Pereira, J. M. C., Carreiras, J. M. B., Oliveira, S. L. J., Pereira, J. M. C., & Carreiras, J. M. B. (2011). Fire frequency analysis in Portugal (1975–2005), using Landsat-based

burnt area maps. *International Journal of Wildland Fire*, *21*(1), 48–60. https://doi.org/10.1071/WF10131

Ozelkan, E., Ormeci, C., & Karaman, M. (2011). *Determination of the Forest Fire Potential by Using Remote Sensing and Geographical Information System, Case Study-Bodrum/Turkey*. https://bit.ly/3eGklum

Pal, M., & Mather, P. M. (2006). Some issues in the classification of DAIS hyperspectral data. *International Journal of Remote Sensing*, *27*(14), 2895–2916. https://doi.org/10.1080/01431160500185227

Parks, S. A., Dillon, G. K., & Miller, C. (2014). A New Metric for Quantifying Burn Severity: The Relativized Burn Ratio. *Remote Sensing*, *6*(3), 1827–1844. https://doi.org/10.3390/rs6031827

Pausas, J. G., & Fernández-Muñoz, S. (2012). Fire regime changes in the Western Mediterranean Basin: From fuel-limited to drought-driven fire regime. *Climatic Change*, *110*(1), 215–226. https://doi.org/10.1007/s10584-011-0060-6

Pausas, J. G., Llovet, J., Rodrigo, A., Vallejo, R., Pausas, J. G., Llovet, J., Rodrigo, A., & Vallejo, R. (2008). Are wildfires a disaster in the Mediterranean basin? – A review. *International Journal of Wildland Fire*, *17*(6), 713–723. https://doi.org/10.1071/WF07151

Pausas, J. G., & Vallejo, V. R. (1999). The role of fire in European Mediterranean ecosystems. In E. Chuvieco (Ed.), *Remote Sensing of Large Wildfires: In the European Mediterranean Basin* (pp. 3–16). Springer. https://doi.org/10.1007/978-3-642-60164-4_2

Pereira, J. M. C. (1999). A comparative evaluation of NOAA/AVHRR vegetation indexes for burned surface detection and mapping. *IEEE Transactions on Geoscience and Remote Sensing*, *37*(1), 217–226. https://doi.org/10.1109/36.739156

Pérez-Cabello, F., de la Riva Fernández, J., Montorio Llovería, R., & García-Martín, A. (2006). Mapping erosion-sensitive areas after wildfires using fieldwork, remote sensing, and

geographic information systems techniques on a regional scale. *Journal of Geophysical Research: Biogeosciences*, *111*(G4). https://doi.org/10.1029/2005JG000148

Petropoulos, G. P., Griffiths, H. M., & Kalivas, D. P. (2014a). Quantifying spatial and temporal vegetation recovery dynamics following a wildfire event in a Mediterranean landscape using EO data and GIS. *Applied Geography*, *50*, 120–131. https://doi.org/10.1016/j.apgeog.2014.02.006

Petropoulos, G. P., Griffiths, H. M., & Kalivas, D. P. (2014b). Quantifying spatial and temporal vegetation recovery dynamics following a wildfire event in a Mediterranean landscape using EO data and GIS. *Applied Geography*, *50*, 120–131. https://doi.org/10.1016/j.apgeog.2014.02.006

Petropoulos, G. P., Kontoes, C. C., & Keramitsoglou, I. (2012). Land cover mapping with emphasis to burnt area delineation using co-orbital ALI and Landsat TM imagery. *International Journal of Applied Earth Observation and Geoinformation*, *18*, 344–355. https://doi.org/10.1016/j.jag.2012.02.004

Petropoulos, G. P., Kontoes, C., & Keramitsoglou, I. (2011). Burnt area delineation from a uni-temporal perspective based on Landsat TM imagery classification using Support Vector Machines. *International Journal of Applied Earth Observation and Geoinformation*, *13*(1), 70–80. https://doi.org/10.1016/j.jag.2010.06.008

Petropoulos, G. P., Vadrevu, K. P., Xanthopoulos, G., Karantounias, G., & Scholze, M. (2010). A Comparison of Spectral Angle Mapper and Artificial Neural Network Classifiers Combined with Landsat TM Imagery Analysis for Obtaining Burnt Area Mapping. *Sensors*, *10*(3), 1967–1985. https://doi.org/10.3390/s100301967

Picotte, J. J., Cansler, C. A., Kolden, C. A., Lutz, J. A., Key, C., Benson, N. C., & Robertson, K. M. (2021). Determination of burn severity models ranging from regional to national scales

for the conterminous United States. *Remote Sensing of Environment*, *263*, 112569. https://doi.org/10.1016/j.rse.2021.112569

Piper, J. (1992). Variability and bias in experimentally measured classifier error rates. *Pattern Recognition Letters*, *13*(10), 685–692. https://doi.org/10.1016/0167-8655(92)90097-J

Polychronaki, A., & Gitas, I. Z. (2012). Burned Area Mapping in Greece Using SPOT-4 HRVIR Images and Object-Based Image Analysis. *Remote Sensing*, *4*(2), 424–438. https://doi.org/10.3390/rs4020424

Quintano, C., Fernández-Manso, A., & Fernández-Manso, O. (2018). Combination of Landsat and Sentinel-2 MSI data for initial assessing of burn severity. *International Journal of Applied Earth Observation and Geoinformation*, *64*, 221–225. https://doi.org/10.1016/j.jag.2017.09.014

Quintano, C., Fernández-Manso, A., Fernández-Manso, O., & Shimabukuro, Y. E. (2006). Mapping burned areas in Mediterranean countries using spectral mixture analysis from a uni-temporal perspective. *International Journal of Remote Sensing*, *27*(4), 645–662. https://doi.org/10.1080/01431160500212195

Quintano, C., Fernández-Manso, A., & Roberts, D. A. (2013). Multiple Endmember Spectral Mixture Analysis (MESMA) to map burn severity levels from Landsat images in Mediterranean countries. *Remote Sensing of Environment*, *136*, 76–88. https://doi.org/10.1016/j.rse.2013.04.017

Quintano, C., Fernandez-Manso, A., & Roberts, D. A. (2017). Burn severity mapping from Landsat MESMA fraction images and Land Surface Temperature. *Remote Sensing of Environment*, *190*, 83–95. https://doi.org/10.1016/j.rse.2016.12.009

Quintano, C., Fernández-Manso, A., & Roberts, D. A. (2020). Enhanced burn severity estimation using fine resolution ET and MESMA fraction images with machine learning algorithm. *Remote Sensing of Environment*, *244*, 111815. https://doi.org/10.1016/j.rse.2020.111815

Riaño, D., Chuvieco, E., Salas, J., Palacios-Orueta, A., & Bastarrika, A. (2002). Generation of fuel type maps from Landsat TM images and ancillary data in Mediterranean ecosystems. *Canadian Journal of Forest Research*, *32*(8), 1301–1315. https://doi.org/10.1139/x02-052

Riaño, D., Chuvieco, E., Ustin, S., Zomer, R., Dennison, P., Roberts, D., & Salas, J. (2002). Assessment of vegetation regeneration after fire through multitemporal analysis of AVIRIS images in the Santa Monica Mountains. *Remote Sensing of Environment*, *79*(1), 60–71. https://doi.org/10.1016/S0034-4257(01)00239-5

Ribeiro, L. M., Viegas, D. X., Almeida, M., McGee, T. K., Pereira, M. G., Parente, J., Xanthopoulos, G., Leone, V., Delogu, G. M., & Hardin, H. (2020). 2 - Extreme wildfires and disasters around the world: Lessons to be learned. In F. Tedim, V. Leone, & T. K. McGee (Eds.), *Extreme Wildfire Events and Disasters* (pp. 31–51). Elsevier. https://doi.org/10.1016/B978-0-12-815721-3.00002-3

Röder, A., Hill, J., Duguy, B., Alloza, J. A., & Vallejo, R. (2008). Using long time series of Landsat data to monitor fire events and post-fire dynamics and identify driving factors. A case study in the Ayora region (eastern Spain). *Remote Sensing of Environment*, *112*(1), 259–273. https://doi.org/10.1016/j.rse.2007.05.001

Roy, D. P., Boschetti, L., Justice, C. O., & Ju, J. (2008). The collection 5 MODIS burned area product—Global evaluation by comparison with the MODIS active fire product. *Remote Sensing of Environment*, *112*(9), 3690–3707. https://doi.org/10.1016/j.rse.2008.05.013

Rupasinghe, P. A., & Chow-Fraser, P. (2021). Relating pre-fire canopy species, fire season, and proximity to surface waters to burn severity of boreal wildfires in Alberta, Canada. *Forest Ecology and Management*, *496*, 119386. https://doi.org/10.1016/j.foreco.2021.119386

Schmidt, H., & Glaesser, C. (1998). Multitemporal analysis of satellite data and their use in the monitoring of the environmental impacts of open cast lignite mining areas in Eastern

Germany. *International Journal of Remote Sensing*, *19*(12), 2245–2260. https://doi.org/10.1080/014311698214695

Simone, W. D., Musciano, M. D., Cecco, V. D., Ferella, G., & Frattaroli, A. R. (2020). The potentiality of Sentinel-2 to assess the effect of fire events on Mediterranean mountain vegetation. *Plant Sociology*, *57*, 11–22. https://doi.org/10.3897/pls2020571/02

Smith-Ramírez, C., Castillo-Mandujano, J., Becerra, P., Sandoval, N., Fuentes, R., Allende, R., & Paz Acuña, M. (2022). Combining remote sensing and field data to assess recovery of the Chilean Mediterranean vegetation after fire: Effect of time elapsed and burn severity. *Forest Ecology and Management*, *503*, 119800. https://doi.org/10.1016/j.foreco.2021.119800

Soverel, N. O., Perrakis, D. D. B., & Coops, N. C. (2010). Estimating burn severity from Landsat dNBR and RdNBR indices across western Canada. *Remote Sensing of Environment*, *114*(9), 1896–1909. https://doi.org/10.1016/j.rse.2010.03.013

Stroppiana, D., Pinnock, S., Pereira, J. M. C., & Grégoire, J.-M. (2002). Radiometric analysis of SPOT-VEGETATION images for burnt area detection in Northern Australia. *Remote Sensing of Environment*, *82*(1), 21–37. https://doi.org/10.1016/S0034-4257(02)00021-4

Stueve, K. M., Cerney, D. L., Rochefort, R. M., & Kurth, L. L. (2009). Post-fire tree establishment patterns at the alpine treeline ecotone: Mount Rainier National Park, Washington, USA. *Journal of Vegetation Science*, *20*(1), 107–120. https://doi.org/10.1111/j.1654-1103.2009.05437.x

Tedim, F., Leone, V., Amraoui, M., Bouillon, C., Coughlan, M. R., Delogu, G. M., Fernandes, P. M., Ferreira, C., McCaffrey, S., McGee, T. K., Parente, J., Paton, D., Pereira, M. G., Ribeiro, L. M., Viegas, D. X., & Xanthopoulos, G. (2018). Defining Extreme Wildfire Events: Difficulties, Challenges, and Impacts. *Fire*, *1*(1), 9. https://doi.org/10.3390/fire1010009

Tedim, F., Xanthopoulos, G., & Leone, V. (2015). Chapter 5 - Forest Fires in Europe: Facts and Challenges. In J. F. Shroder & D. Paton (Eds.), *Wildfire Hazards, Risks and Disasters* (pp. 77–99). Elsevier. https://doi.org/10.1016/B978-0-12-410434-1.00005-1

Tonbul, H., Colkesen, I., & Kavzoglu, T. (2022). Pixel- and Object-Based ensemble learning for forest burn severity using USGS FIREMON and Mediterranean condition dNBRs in Aegean ecosystem (Turkey). *Advances in Space Research*, *69*(10), 3609–3632. https://doi.org/10.1016/j.asr.2022.02.051

Turco, M., Bedia, J., Liberto, F. D., Fiorucci, P., Hardenberg, J. von, Koutsias, N., Llasat, M.-C., Xystrakis, F., & Provenzale, A. (2016). Decreasing Fires in Mediterranean Europe. *PLOS ONE*, *11*(3), e0150663. https://doi.org/10.1371/journal.pone.0150663

UN-SPYDER Knowledge Portal (2022). Normalized Burn Ratio (NBR). Available at: https://tinyurl.com/5fabkfxr

Van Niel, T. G., McVicar, T. R., & Datt, B. (2005). On the relationship between training sample size and data dimensionality: Monte Carlo analysis of broadband multi-temporal classification. *Remote Sensing of Environment*, *98*(4), 468–480. https://doi.org/10.1016/j.rse.2005.08.011

Varela, V., Vlachogiannis, D., Sfetsos, A., Karozis, S., Politi, N., & Giroud, F. (2019). Projection of Forest Fire Danger due to Climate Change in the French Mediterranean Region. *Sustainability*, *11*(16), 4284. https://doi.org/10.3390/su11164284

Venäläinen, A., Lehtonen, I., Laapas, M., Ruosteenoja, K., Tikkanen, O.-P., Viiri, H., Ikonen, V.-P., & Peltola, H. (2020). Climate change induces multiple risks to boreal forests and forestry in Finland: A literature review. *Global Change Biology*, *26*(8), 4178–4196. https://doi.org/10.1111/gcb.15183

Veraverbeke, S., Gitas, I., Katagis, T., Polychronaki, A., Somers, B., & Goossens, R. (2012). Assessing post-fire vegetation recovery using red–near infrared vegetation indices:

Accounting for background and vegetation variability. *ISPRS Journal of Photogrammetry and Remote Sensing*, *68*, 28–39. https://doi.org/10.1016/j.isprsjprs.2011.12.007

Veraverbeke, S., Lhermitte, S., Verstraeten, W. W., & Goossens, R. (2010). The temporal dimension of differenced Normalized Burn Ratio (dNBR) fire/burn severity studies: The case of the large 2007 Peloponnese wildfires in Greece. *Remote Sensing of Environment*, *114*(11), 2548–2563. https://doi.org/10.1016/j.rse.2010.05.029

Viana-Soto, A., Aguado, I., & Martínez, S. (2017). Assessment of Post-Fire Vegetation Recovery Using Fire Severity and Geographical Data in the Mediterranean Region (Spain). *Environments*, *4*(4), 90. https://doi.org/10.3390/environments4040090

von Richter, L., Little, D., & Benson, D. (2005). Effects of low intensity fire on the resprouting of the weed African Olive (Olea europaea subsp. Cuspidata) in Cumberland Plain Woodland, western Sydney. *Ecological Management & Restoration*, *6*(3), 230–233. https://doi.org/10.1111/j.1442-8903.2005.239-6.x

Wang, C., Wang, A., Guo, D., Li, H., & Zang, S. (2022). Off-peak NDVI correction to reconstruct Landsat time series for post-fire recovery in high-latitude forests. *International Journal of Applied Earth Observation and Geoinformation*, *107*, 102704. https://doi.org/10.1016/j.jag.2022.102704

Wang, L., Wei, S., Horton, R., & Shao, M. (2011). Effects of vegetation and slope aspect on water budget in the hill and gully region of the Loess Plateau of China. *CATENA*, *87*(1), 90–100. https://doi.org/10.1016/j.catena.2011.05.010

Warner, T. A., Skowronski, N. S., & Gallagher, M. R. (2017). High spatial resolution burn severity mapping of the New Jersey Pine Barrens with WorldView-3 near-infrared and shortwave infrared imagery. *International Journal of Remote Sensing*, *38*(2), 598–616. https://doi.org/10.1080/01431161.2016.1268739

Whitman, E., Parisien, M.-A., Holsinger, L. M., Park, J., Parks, S. A., Whitman, E., Parisien, M.-A., Holsinger, L. M., Park, J., & Parks, S. A. (2020). A method for creating a burn severity atlas: An example from Alberta, Canada. *International Journal of Wildland Fire*, *29*(11), 995–1008. https://doi.org/10.1071/WF19177

Whitman, E., Parisien, M.-A., Thompson, D. K., Hall, R. J., Skakun, R. S., & Flannigan, M. D. (2018). Variability and drivers of burn severity in the northwestern Canadian boreal forest. *Ecosphere*, *9*(2), e02128. https://doi.org/10.1002/ecs2.2128

Wittenberg, L., Malkinson, D., Beeri, O., Halutzy, A., & Tesler, N. (2007). Spatial and temporal patterns of vegetation recovery following sequences of forest fires in a Mediterranean landscape, Mt. Carmel Israel. *CATENA*, *71*(1), 76–83. https://doi.org/10.1016/j.catena.2006.10.007

Xanthopoulos, G., Athanasiou, M., Nikiforaki, A., Kaoukis, K., Mantakas, G., Xanthopoulos, P., Papoutsakis, C., Christopoulou, A., Sofronas, S., Gletsos, M., & Varela, V. (2022). Innovative Action for Forest Fire Prevention in Kythira Island, Greece, through Mobilization and Cooperation of the Population: Methodology and Challenges. *Sustainability*, *14*(2), 594. https://doi.org/10.3390/su14020594

Yang, J., El-Kassaby, Y. A., & Guan, W. (2020). The effect of slope aspect on vegetation attributes in a mountainous dry valley, Southwest China. *Scientific Reports*, *10*(1), 16465. https://doi.org/10.1038/s41598-020-73496-0

Yetemen, O., Istanbulluoglu, E., & Duvall, A. R. (2015). Solar radiation as a global driver of hillslope asymmetry: Insights from an ecogeomorphic landscape evolution model. *Water Resources Research*, *51*(12), 9843–9861. https://doi.org/10.1002/2015WR017103

Zheng, Z., Zeng, Y., Li, S., & Huang, W. (2018). Mapping Burn Severity of Forest Fires in Small Sample Size Scenarios. *Forests*, *9*(10), 608. https://doi.org/10.3390/f9100608